The Hong Kong Polytechnic University

Institute of Textiles and Clothing

Study of Photocatalytic Activities of Nanoscaled Metal Oxides on Textiles

Qi Kaihong

A thesis submitted in partial fulfillment of the requirements

for the degree of

Doctor of Philosophy

October 2008

CERTIFICATE OF ORIGINALITY

I hereby declare that this thesis is my own work and that, to the best of my knowledge and belief, it reproduces no material previously published or written, nor material that has been accepted for the award of any other degree or diploma, except where due acknowledgement has been made in the text.

______________________________(Signed)

Qi Kaihong ____________________(Name of student)

Abstract

A systematic study of the synthesis and application of nanoscaled metal oxides with photocatalytic activity was conducted. The synthesis was based on sol-gel nanotechnology at low temperatures and atmospheric pressure. The metal oxide sols were then applied to textile materials to form photocatalytic self-cleaning thin films by a dip-pad–dry-cure process. The main research work was focused on the synthesis, characterization, and application of pure anatase titanium dioxide (TiO_2) and anatase titanium dioxide doped with other materials. The results showed that the anatase titania and its doped forms possess high photocatalytic activity, which was demonstrated by the complete decomposition of bacteria, colorants, red wine and coffee stains.

Nanocrystalline anatase TiO_2 sols were prepared under ambient pressure and at temperatures close to or approaching to room temperature using hydrolysis of titanium tetraisopropoxide in an acidic aqueous solution. A comprehensive study was carried out on the surface morphology, crystal phase and particle size of nanocrystalline TiO_2 using field-emission scanning electron microscopy (FESEM), X-ray diffraction spectroscopy (XRD), and high resolution transmission electron microscopy (HRTEM). The effect of catalysts and different temperatures on the formation of anatase TiO_2 and the self-cleaning performance of TiO_2 treated cotton fabrics under UV irradiation were evaluated.

These TiO_2 treated cotton fabrics possess significant photocatalytic self-cleaning properties, such as bactericidal activity, colorant decomposition and degradation of red wine and coffee stains. The UV absorption, the mechanical properties and durability of TiO_2 treated cotton fabrics were investigated.

Anatase TiO_2 prepared by an aqueous sol-gel process at 60 °C was applied to polyester fabric since polyester is the most widely applied synthetic fibre in textile and clothing. Due to the poor adhesion between the TiO_2 and polyester fibres, low temperature plasma (LTP) pretreatment of polyester fibres using oxygen gas was performed. The wettability of polyester towards the titania sol and the adhesion of titania layers to polyester fibres were improved as a result of the introduction of negative groups COO-,-O-O- onto polyester surface. The self-cleaning properties, such as bactericidal activities, colorant decomposition and degradation of red wine and coffee stains, of the anatase functionalized polyester fibers were studied. The surface morphological changes of polyester fibers before and after plasma treatment, and of plasma-treated fibers before and after applying anatase titania film were characterized by SEM. The adhesion between the anatase titania and polyester fibers was investigated.

To improve the photocatalytic activity of TiO_2 films, the anatase TiO_2/SiO_2 nanocomposites were investigated. Anatase TiO_2/SiO_2 nanocomposites were

developed in an aqueous solution by a sol–gel process at a low temperature. The morphology of these nanocomposites was characterized by SEM, showing that TiO_2 nanoparticles were deposited on the surface of SiO_2 spheres. The spherical TiO_2/SiO_2 nanocomposites treated cotton fabrics demonstrated higher photocatalytic activity in comparison to pure TiO_2 treated cotton fabrics in a typical photocatalytic test using a model compound of Neolan Blue 2G dye. The enhanced photocatalytic activities of the TiO_2/SiO_2 treated cotton fabrics was considered attributable to the increased specific surface area and the enhanced surface acidity of nanocomposites.

To eliminate the need for high temperature operations and the use of corrosive chemicals such as nitric acid and hydrochloric acid in synthesizing anatase TiO_2, a new synthesis method for single-phase anatase TiO_2 was developed using a sol-gel process in aqueous media followed by aging at room temperature. The self-cleaning activities of the as-prepared TiO_2 thin films deposited on cotton fabrics were evaluated by the photodegradation of Neolan Blue 2G and the decomposition of red wine and coffee stains. The UV absorption, tensile strength and durability to laundering of the TiO_2 treated cotton were also studied. This study further optimizes the synthesis conditions for anatase TiO_2 which could contribute to the large scale fabrication of self-cleaning textiles.

To extend the absorption of TiO_2 into visible region of the spectrum and to reduce electron-hole recombination to further improve photocatalytic activity of TiO_2 in UV-Visible region, Fe^{3+} doped TiO_2 photocatalytic self-cleaning system was investigated. The synthesis was based on a sol-gel process in an aqueous solution at a temperature of 60 °C with the addition of Fe^{3+} dopant. The doping reduces the band gap energy and increases the wavelength response range extending to visible region. The Fe^{3+} dopant with various doping level was also studied. It was found that higher photocatalytic activity was achieved at optimum doping level compared to that of the pure TiO_2 system under both UV irradiation and a visible light source without UV.

The study revealed that anatase TiO_2-based self-cleaning system is one of the most promising systems for the development of self-cleaning textiles that would have high potential in commercialization with the advantages of being environmentally friendly, low cost, energy and water saving due to the reduced laundry requirements of the treated items.

Prizes and Publications

Award

John H. Xin, Walid A. Daoud, Liu Yuyang, **Qi Kaihong**, Chen Xianqiong, Self-cleaning garment, the Gold Medal in the 34th International Exhibition of Inventions, New Techniques and Products, Geneva, Switzerland, 5-9 April, 2006.

Patents

1. Daoud Walid Abdelhamid, Xin, John Haozhong and **Qi Kaihong**, Method for making single-phase nanocrystalline anatase, United States Patent 7255847.
2. Walid Abdelhamid Daoud, Sze Kar Leung, Wing Sze Tung, Hao Zhong John Xin, Ka Leung Kevin Cheuk, Xiaowen Wang, Yee Yee Kong, **Kaihong Qi**, Formulation coated self-cleaning wool, United States Patent Application Publication 20080241405.

Refereed journal papers

1. **Kaihong Qi**, Walid A. Daoud, John H. Xin, C. L. Mak, Waisze Tang and W. P. Cheung, Self-cleaning cotton, Journal of Materials Chemistry, 2006, 16 [47], 4567-4574.
2. **Kaihong Qi**, Xianqiong Chen, Yuyang Liu, John H. Xin, C. L. Mak

and Walid A. Daoud, Facile preparation of anatase /SiO_2 spherical nanocomposites and their application in self-cleaning textiles, Journal of Materials Chemistry, 2007, 17 [33], 3504–3508.

3. **Kaihong Qi**, John H. Xin, Walid A. Daoud and C. L. Mak, Functionalizing polyester fibre with a self-cleaning property using anatase TiO_2 and low temperature plasma treatment, International Journal of Applied Ceramic Technology, 2007, 4 [6], 554–563.
4. Walid A. Daoud, S. K. Leung, W. S. Tung, J. H. Xin, K. Cheuk and **Kaihong Qi**, Self-cleaning keratins, Chemistry of Materials**,** 2008**,** 20 [4], 1242–1244.
5. Xianqiong Chen, Yuyang Liu, **Kaihong Qi**, Xiang Zhou and John H. Xin, A direct route to active silica nanoparticles, Diffusion and Defect Data--Solid State Data, Part B: Solid State Phenomena, 2007, 121-123 [23], 65-68.
6. Bin Fei, Haifeng Lu, **Kaihong Qi**, Haifeng Shi, Tongxu Liu, Xiangzhong Li and John H. Xin, Multi-functional microcapsules produced by aerosol reaction，Journal of Aerosol Science，2008, 39 [12], 1089-1098.
7. Walid A. Daoud, John H. Xin, Yi-He Zhang and **Kaihong Qi**, Surface characterization of thin titania films prepared at low temperatures, Journal of Non-Crystalline Solids, 2005, 351 [16-17], 1486–1490.

Conference papers

1. **Kaihong Qi**, Walid A. Daoud, John H. Xin and C. L. Mak, Self-cleaning cotton fabrics, Proceedings, 2006 Materials Research Society Symposium 920 (Smart Nanotextiles). San Francisco, USA, pp.135-141, 17-21 Apr. 2006.
2. **Kaihong Qi**, John H. Xin, C. L. Mak, Yuyang Liu, Xianqiong Chen, Bin Fei and Walid A. Daoud, Fabrication of multi-functional textile surface**,** Proceedings, The 9th Asian Textile Conference. Taiwan, 28-30 Jun. 2007.

3. **Kaihong Qi**, Roger Ronghua Wang, Xiaowen Wang, John H. Xin, Nano TiO_2 based self-cleaning fabric technology, KSDF 20th Anniversary -The International Conference on Dyeing and Finishing, South Korea, 13 Mar. 2009.

4. Ronghua Wang, Xiaowen Wang, **Kaihong Qi**, John H. Xin, Advanced visible-light self-cleaning textiles, International Conference on Nanotechnology and Advanced Materials (ICNAM 2009), Hong Kong Science Park, Shatin, Hong Kong, 6-9 May 2009.

Acknowledgements

I would like express my sincerest gratitude to my chief supervisor, Prof. John. H. Xin, for providing the opportunity for this project to be taken. Without his expert advice, support and guidance, this project would not have been possible.

I would also like to thank Dr. C. L. Mak and Dr. Walid A. Daoud, my co-supervisors, for their enlightening suggestion, interesting discussion, critical comments and patience throughout the whole research period.

Sincere thanks to Mr Yeung of Materials Research Center of the Hong Kong Polytechnic University for his assistance in performing the XRD, Mr Lu of Applied Physics of PolyU in performing SEM and Dr. Pang of Applied Physics of PolyU for helping with the TEM experiments.

My thanks are also extended to the technical staffs in laboratories and workshops of Institute of Textiles and Clothing, PolyU for their assistance in experimental work. I would like to thank all of my fellow research personnel for their support and valuable discussion.

I gratefully acknowledge the Research Grants Council of the Hong Kong SAR Government (CERG Grant No.5289/03E).

Table of Contents

Chapter 4 Titania Nanoparticles and Their Application to Cotton Fabrics 47

Self-cleaning Properties on Cotton

List of Tables

List of Schemes

List of Figures

Abbreviations

FESEM = Field-emission scanning electron microscopy

XRD = X-ray diffraction

AFM = Atomic force microscopy.

XPS = X-ray photoelectron spectroscopy

HRTEM = High resolution transmission electron microscopy

SAED = Selected area electron diffraction

DSC = Differential scanning calorimetry

LTP = Low temperature plasma

DC = Direct current

RF = Frequency

MW = Microwave

UV = Ultraviolet

UPF = Ultraviolet protection factor

FWHM = Full width at half-maximum

CFU = Colony forming units

PBS = Phosphate buffer solution

S. aureus = *Staphylococcus aureus*

TTIP = Titanium tetraisopropoxide

MTMS = Methyl-trimethoxysilane

TiO_2 = Titanium dioxide

SiO_2 = Silicon dioxide

ZnO = Zinc oxide

Fe_2O_3 = Iron (Ⅲ) oxide

WO_3 = Tungsten (VI) Trioxide

ZrO_2 = Zirconium oxide

Fe^{3+} = Iron (Ⅲ) ion

Co^{2+} = Cobalt (II) ion

Ni^{2+} = Nickle (II) ion

Nb^{5+} = Niobium (V) ion

W^{6+} = Tungsten (VI) ion

Mo^{5+} = Molybdenum (V) ion

Au = Gold

OH = Hydroxyl

HO_2 = Perhydroxyl

OH* = Hydroxyl radical

O_2 = Oxygen

O_2^- = Superoxide radical

CO_2 = Carbon dioxide

H_2O = Water

NO_2 = Nitrogen dioxide

TiO_6^{2-} = Octahedron

NH_3 = Ammonia

NaOH = Sodium hydroxide

$TiCl_4$ = Titanium tetrachloride

Chapter 1: Introduction

1.1 Background

In the textile and apparel industry, fabrics and apparel products with functional surface finishing treatment can achieve better end use properties and high added value. Functional textiles can improve their applications, offer the textile and apparel industry new challenges and benefit for the future. And functional garments can meet consumer demands in terms of durability, comfort, easy care etc. and ensure stability against mechanical, thermal, chemical or photochemical destruction. Besides, functional textiles should maintain textile properties such as appearance, feel and durability to laundering as new functional finishing treatment is fabricated because these properties are important to the consumer. Therefore new, advanced and innovative technologies are required.

The development of self-cleaning textiles is an objective sought by the textile and apparel industry in the framework of new products classified as intelligent textiles (Mills & Lee, 2002). One benefit using these self-cleaning fabrics is the cost saving on cleaning. The other is to prolong the lifetime of the textile since the continuous self-cleaning takes place at the fabric surface under daylight irradiation, such as innovation comprises nanocrystallineTiO_2 thin films deposited on the textile surface. The sol-gel process has been widely employed to produce uniformly distributed nano-particles and functional films on substrates. It is advantageous in that it is capable of producing films of better homogeneity, high purity, involving lower processing temperatures and producing particles with characteristics that can be controlled (Aruna & Patil, 1996). Nanoscaled metal oxide photocatalytic films e.g. titanium dioxide films have drawn much research attention for a wide variety of applications such as environmental purification(Heller, 1995; Nosaka, Koenuma, Ushida, & Kira, 1996), anti-fouling (Paz, Luo, Rabenberg, & Heller, 1995), deodorizing (Sopyan, Watanabe, Murasawa, Hashimoto, & Fujishima, 1996), sterilization (Kikuchi, Sunada, Iyoda, Hashimoto, & Fujishima, 1997) and self-cleaning glass (Negishi, Iyoda, Hashimoto, & Fujishima, 1995). Although there are numerous types of sol-gel metal oxide films with photocatalytic activities in the literature, few research reports focused on the photocatalytic applications of sol-gel nanoscaled metal oxide films on textiles. Inorganic metal-oxide sol films by sol-gel hydrolysis of metal alkoxide precursors offer the challenging possibility of creating films on textiles with photocatalytic self-cleaning properties. This project aims to further study the photocatalytic activities of nanoscaled metal oxide films on textiles using a sol-gel process. Clearly, the functionalization of textiles by inorganic sol-gel metal oxide films can bring high added value to the textile and apparel industry.

1.2 Principle objectives

This project is concerned with a systematic study of photocatalytic activities of nanoscaled metal oxides on textiles based on sol-gel nanotechnology. The inorganic metal oxide sols of this investigation should be applicable to various textile materials by sol-gel process at a temperature around 60°C and normal pressure. The specific objectives can be defined as follows:

1. To synthesize and modify nanoscaled metal oxides by a sol-gel process with desired end-user properties, focusing on UV absorption and photocatalytic self-cleaning properties including anti-bacterial, colorant decomposition and stain removal.
2. To optimize the method of metal oxide nanosol application to the textile materials with the focus on cotton, polyester.
3. To investigate the doping and incorporation of various nanoparticles to sol-gel matrices for the enhancement of photocatalytic properties.
4. To study and characterize the nanostructures of sol-gel metal oxides using various characterization instruments.
5. To test the photocatalytic properties of the textiles treated by various sols used in this project.
6. To investigate the interfacial cohesion between treated layer and the textile substrates. The durability and mechanical properties tests will be conducted.

1.3 Research methodology

General research methodology is outlined as follows and the detailed information will be described in Chapter 3.

◇ The TiO_2 sols were prepared by the sol- gel process in aqueous solution at low temperatures using titanium tetra-isopropoxide as the precursor, only nitric acid, only acetic acids, and combined catalysts of nitric acid and acetic acid as catalyst, respectively. The mixture was heated and stirred at a temperature around 60°C for 18- 24 h or the mixture using only acetic acid as a catalyst was stirred at room temperature for 24 h then was stored without stirring at room temperature and atmospheric pressure for 1 week.

◇ The structure and morphology of TiO_2 films on fabrics were investigated using field-emission scanning electron microscopy. The crystal phases of solid powder extracted from the sols were studied by X-ray diffraction operating at 40 kV and 30 mA and transmission electron microscopy. The crystal phase of formed titania films on fabrics was studied by small angle X-ray diffraction at 3° of incident beam using Cu Ka radiation and detector scan mode operating at 40 kV and 30 mA. The morphology and particle size of TiO_2 was investigated using spin coated samples (spin coating at 1500 rpm for 50 seconds on glass and silicon substrates) by Atomic force microscopy. The change in the chemical composition on the polyester surface occurring in plasma pretreatment process and the relative amount of TiO_2 deposited on the polyester surface without and with plasma treatment are investigated using X-ray photoelectron spectroscopy by an X-ray photoelectron spectrometer.

◇ Photocatalytic activities of TiO_2 treated cotton and polyester fabrics were assessed by bactericidal activities, colorant decomposition activities and degradation of a red wine stain and a coffee stain.

◇ Low temperature plasma treatment was performed on polyester fibers with a Showa SPP-001 low temperature plasma generator. The oxygen gas was chosen for plasma treatment. The discharge power, pressure and gas flow rate were 100 W, 6 Pa and 15scc/min, respectively. The exposure time was 10 min.

◇ Changes in the mechanical properties of fabrics were analyzed by an Elmendorf Tearing Tester (Thwing-Albert Instrument Co.) and Instron 4411 Tester (England).

1.4 Project significance

The project involves the study of the new self-cleaning textiles. This functionalisation of textiles by inorganic sol-gel metal oxide nanostructure deposited can bring high added value to the textile and apparel industry. Although self-cleaning glass, ceramic tiles and building materials are commercially available, self-cleaning textiles are still in its infancy. Little research was done to investigate the application of anatase TiO_2 on textiles.

We explored and attempted to improve the effectiveness of the anatase TiO_2 system and the application of TiO_2 on textiles prepared at a low temperature for self-cleaning purposes. The known advantages of self-cleaning finishing in textile and apparel are:

- Applicable at temperatures from room temperature to 120 °C
- Suitable for various textile fibres, cotton, polyester etc
- Particles have the right arrangement of atoms - anatase form - This arrangement boosts the particles catalytic power
- High level UV-absorption
- High level of self-cleaning performance
- Low cost, energy saving and environmentally friendly
- Excellent wash fastness
- No skin irritation
- Able to utilize existing textile manufacturing equipments

The applications of TiO_2 films in textile industry are:

- Clothing: sportswear, leisurewear, footwear
- Interior textiles: wall fabrics, furniture fabric, carpets, curtains
- Automobile interior fabrics
- Medical fabrics
- Technical textiles, geotextiles, special

- Soft toys
- Leathers

1.5 Scope of thesis

This thesis comprises nine chapters. Chapter 1 introduced the background information stating the objectives, methodology and significance of the project.

Chapter 2 provides a comprehensive review for the recent developments in the chemical synthesis of nanoscaled metal oxides especially nanocrystalline TiO_2 at low temperatures and the photocatalytic activities of metal oxide photocatalyst.

Chapter 3 describes the research methodology including sample preparation, low temperature plasma treatment of polyester, preparation of TiO_2 sols, characterization of TiO_2, the evaluation of photocatalytic activities of TiO_2 treated textiles and fabric properties.

Chapter 4 studies the preparation of nanocrystalline anatase TiO_2 sols under ambient pressure and at temperatures close to or approaching to room temperature using hydrolysis of titanium tetraisopropoxide in an acidic aqueous solution, and evaluates the effect of catalysts and different temperatures on the formation of anatase TiO_2 and the self-cleaning performance of TiO_2 treated cotton fabrics under UV irradiation. The differences in crystalline phases are compared by XRD and TEM. The self-cleaning performance of TiO_2 treated cotton fabrics is evaluated by bactericidal activities, colorant decomposition activities and degradation of a red wine stain and a coffee stain.

Since polyester is the most widely applied synthetic fibre in textile and clothing, Chapter 5 studies the self-cleaning performance of TiO_2 treated polyester and the effect of the low temperature plasma treatment on polyester towards the self-cleaning effect and the adhesion between TiO_2 and polyester.The surface morphological changes of polyester fibers before and after plasma treatment, and of plasma-treated fibers before and after TiO_2 coating are characterized by SEM. The change in the chemical composition on the polyester surface occurring in plasma pretreatment process and the relative amount of TiO_2 deposited on the polyester surface without and with plasma treatment are investigated by XPS. The self-cleaning performance of plasma pretreated polyester treated by TiO_2 is evaluated by bactericidal activities, colorant decomposition activities and degradation of a red wine stain and a coffee stain under UV irradiation.

To improve the photocatalytic activity of TiO_2 films, Chapter 6 investigates the preparation of anatase TiO_2 /SiO_2 spherical nanocomposites at a low temperature and their improved photocatalytic activities. The spherical structural properties of TiO_2 /SiO_2 nanocomposites are characterized by SEM and XRD. The photocatalytic activities of TiO_2 /SiO_2 nanocomposites are evaluated by dye decomposition under UV irradiation.

To eliminate the need for high temperature operations and the use of corrosive chemicals such as nitric acid and hydrochloric acid for the synthesis of anatase TiO_2, Chapter 7 develops a new synthesis method for single-phase anatase TiO_2 at room temperature and ambient pressure using a sol-gel process in aqueous media followed by aging at room temperature. The self-cleaning performance of anatase TiO_2 treated cotton fabrics is studied by colorant decomposition activities and degradation of a red wine stain and a coffee stain under UV irradiation.

To extend the absorption of TiO_2 into visible region of the spectrum and to reduce electron-hole recombination so as to further improve photoactivity in UV-Visible region, Chapter 8 develops Fe^{3+} doped TiO_2 at a low temperature and studies the self-cleaning properties under visible light illumination. The crystal phases of Fe^{3+} doped TiO_2 are studied by XRD and TEM. The self-cleaning performance of Fe^{3+} doped TiO_2 treated cotton fabrics is studied by colorant decomposition activities under UV and visible light irradiation.

Chapter 9 summarizes the major results and findings of the present work and draws some conclusions. Recommendations for possible future research work are suggested.

Chapter 2: Literature Reviews

2.1 Introduction

This chapter aims to provide a comprehensive review of the past and current research on the chemical synthesis of nanoscaled metal oxides especially nanocrystalline TiO_2 at low temperatures and the photocatalytic activities of metal oxide photocatalyst. The chapter is divided into four main parts: Section 2.2 describes the mechanism of TiO_2 photocatalysis; Section 2.3 outlines metal oxide photocatalysts; Section 2.4 provides chemical synthesis of metal oxide nanoparticles and Section 2.5 presents self-cleaning titania films.

2.2 Heterogeneous photocatalysis

2.2.1 Introduction

The term photocatalysis consists of the combination of photochemistry and catalysis (Schiavello & Sclafani, 1989). It implies that light and a catalyst are necessary to bring about or to accelerate a chemical transformation. Heterogeneous photocatalysis is a reaction which uses light to activate a substance. The substance modifies the rate of a chemical reaction without being involved itself.

Photocatalytic oxidation of a wide range of organic contaminants taking place on metal oxide semiconductors has received great attention in many practical applications because it is capable of mineralizing completely organic contaminations, producing carbon dioxide, water and inorganic ions. Photocatalytic reactions proceed under moderate conditions at ambient temperature and atmospheric pressure. And light irradiation makes photocatalysis an efficient, clean and safe chemical process. This method has become very attractive because it can convert the organics into innocuous materials such as carbon dioxide and water. Furthermore, photocatalytic metal oxide semiconductor films are often stable to the photolysis conditions and nontoxic, and a large number of oxidative conversions per active site of the catalyst can be attained without significant degradation of the catalytic capacity of the semiconductor.

2.2.2 Mechanism of photocatalytic self-cleaning processes

Photocatalytic metal oxide semiconductors are usually selected as photocatalysts because of their characteristic of possessing a narrow band gap between their valence band and conduction band. Among various metal oxide photocatalysts, titanium dioxide (TiO_2) is one of the most promising photocatalytic materials due to its high oxidizing ability, nontoxicity, long term stability and low cost. The mechanisms of photocatalytic self-cleaning processes occurring on titania surfaces have been intensively studied in recent years (A. Fujishima, Hashimoto, & Watanabe, 1999; Hagfeldt & Gräetzel, 1995; Hoffmann, Martin, Choi, & Bahnemann, 1995; Mills & Le Hunte, 1997).Under normal conditions, when titanium dioxide absorbs incoming light

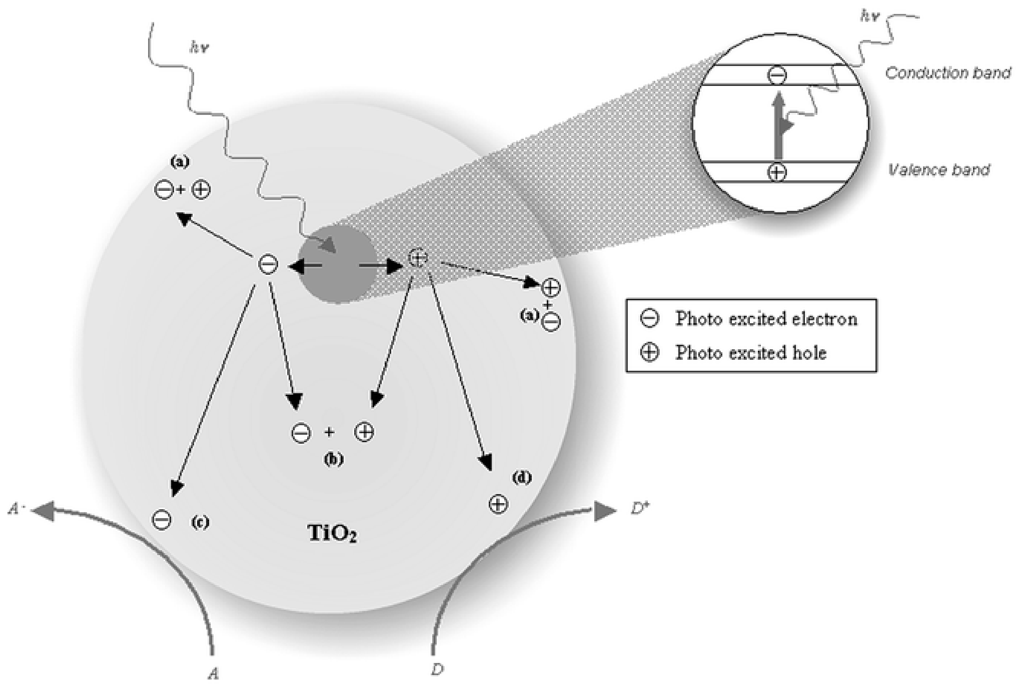

Fig. 2-1 Several events in the bulk inside and on the surface of a TiO_2 particle and subsequent events occurring on the surface towards photocatalytic oxidation TiO_2 undergoes photo-excitation under irradiation. The electron and the hole that result can follow one of several pathways: (a) electron–hole recombination on the TiO_2 surface; (b) electron–hole recombination in the bulk of TiO_2; (c) species *A* is reduced by photogenerated electrons; and (d) species *D* is oxidised by photogenerated holes (Parkin & Palgrave, 2005).

with energy equal to or greater than its band gap energy (Anatase and rutile have band gap energies of 3.2 and 3.0 eV respectively (Kesselman, Shreve, Hoffmann, & Lewis, 1994), an electron from the valence band is photo-excited into the conduction band leaving an electron hole in the valence band. Then the electron-hole pair can follow different pathways through its migration path to the surface. Through that migration process, the electron and hole undergo a series of charge trapping and releasing processes. The hole will be trapped within the subsurface of the titania while the electron quickly reaches the surface where it is trapped. If the migration path to the surface is too long, recombination of electron and hole becomes likely on either the surface or within the bulk as described in paths A and B of Fig. 2-1. This recombination is an undesired process as this represents a loss of just gained charge carriers and therefore a decrease in photon efficiency of titania. In the ideal case, electron

and hole migrate separately to the titania surface where they can transfer their charges to the adsorbed species on the titania surface. The holes combine with an adsorbed hydroxyl group forming an OH* radical and cause the oxidization of adsorbed organic molecules while the electrons eventually combine with atmospheric oxygen to give the superoxide radical anion O_2^-(ads), which quickly attacks nearby organic molecules. Reduction (electron acceptance) and oxidation (electron donation) of absorbed species are represented in paths C and D of Fig. 2-1, respectively. The result is the conversion of organics to carbon dioxide and water at ambient temperatures. This photocatalytic process is very effective and clean. Mills *et al*. (2003) reported that the total decomposition of stearic acid [$CH_3(CH_2)_{16}CO_2H$] in the presence of atmospheric oxygen to CO_2 and H_2O occurred with no detectable by-products on a TiO_2 surface. A wide range of solid-, liquid- and gas-phase organic pollutants can be decomposed in this way, including aromatics, polymers, dyes and surfactants (Mills & Le Hunte, 1997).

Scientists are still not exactly sure which one of the activated sites is the primary active site for the photocatalytic decomposition of various organic compounds (Linsebigler, Lu, & Yates, 1995). It is widely believed that the OH* radical is mostly responsible for the decomposition of organic compounds to CO_2 and H_2O (Cao, Huang, Spiess, & Suib, 1999; Mills G. & Hoffman, 1993; Soria et al., 1991). Complete degradation was reported throughout the attack of OH* radical on absorbed species where hydroxyl (OH) and perhydroxyl (HO_2) are considered as primary oxidants in the heterogeneous catalysis of organic molecules (Navio, Cerrillos, Marchena, Pablos, & Pradera, 1996). However, other researchers are still debating whether the superoxide radical (O_2^-) would contribute to the photodegradation reaction of organic molecules as well, besides serving as electron traps. Cermenati *et al*. (1997)concluded from aromatic pollutants degradation studies in water that not only OH* radical are involved in the oxidative steps in TiO_2 photocatalysis. By introducing OH* radical scavengers to the reaction system, they were able to show that species other than the OH* radical contributed to the substrate conversion. They inferred that also superoxide was chemically involved in the photocatalytic oxidative steps. However, the majority of the literature states that the OH* radical would be the primary species entering the oxidation system (Prairie, Evans, Stange, & Martinez, 1993; Sjogren & Sierka, 1994).

2.3 Metal oxide photocatalysts

2.3.1 Introduction

An appropriate catalyst for photocatalytic decomposition should have the following characteristics: it should be nontoxic, it needs to be stable and it should not be vulnerable to photo corrosion and chemical corrosion under constant band gap illumination. Most metal oxides possess these characteristics, however, they have very large bandgaps or they are even insulators. One exception is Fe_2O_3 with a band gap of 2.2 eV. It absorbs light in visible range below 560 nm, but the photocatalytic activity is too low compared to more effective semiconductors such as titanium dioxide or zinc oxide (Pelizzetti, Minero, & Vincenti, 1994). Of all the metal oxide semiconductors investigated with regards to photocatalysis, titanium dioxide has been found to be the material with the highest efficiency for photocatalytic destruction. Only zinc oxide (ZnO) demonstrated a similar activity to TiO_2. Several studies on metal oxide photocatalysts have been performed in order to find an ideal catalyst for photooxidation. Ibusuki and Takeuchi (1986) studied the photocatalytic activity of ZnO in a butane- NO_2- dry system and that of 16 other kinds of metal oxides for propylene- NO_2-dry system. They found that titanium dioxide revealed the highest photocatalytic activity compared to all other metal oxides.

From the coating point of view, there are two requirements for a good quality of photocatalytic metal oxide deposition. First, a good adhesion to the substrate especially textiles is needed; second, no degradation of the catalytic power with the presence of other coating substances. A suitable binder can play a significant role for assisting the attachment of the photocatalyst particles to the substrates. The binder agent must be transparent to UV irradiation and should not cause any negative effect on the activity of the photocatalyst.

2.3.2 Crystal structures and precipitation mechanism of titanium dioxide

Titanium dioxide is a metal oxide semiconductor with a band gap of 3.2 eV and absorbs light below 400 nm to create electron/hole pairs. With this characteristic, TiO_2 is photoactive at wavelengths produced by the sun or other artificial light sources. With the molecular oxygen from air, it is able to completely mineralize a wide range of organics. TiO_2 does not deactivate during photoreaction (Fernandez et al., 1995) and no or only traces of water are needed to maintain the catalyst active (Peral, Domenech, & Ollis, 1997). Moreover, there is no or little formation of intermediates or side products. These characteristics make TiO_2 the most promising candidate in photocatalytic processes of organic compounds.

There are three crystalline phases of TiO_2: anatase, rutile and brookite, among which rutile is the thermodynamically stable state, while the other two phases are metastable (Gopal, Chan, & De, 1997). Anatase and rutile are both tetragonal in structure while the brookite structure is orthorhombic. All of the

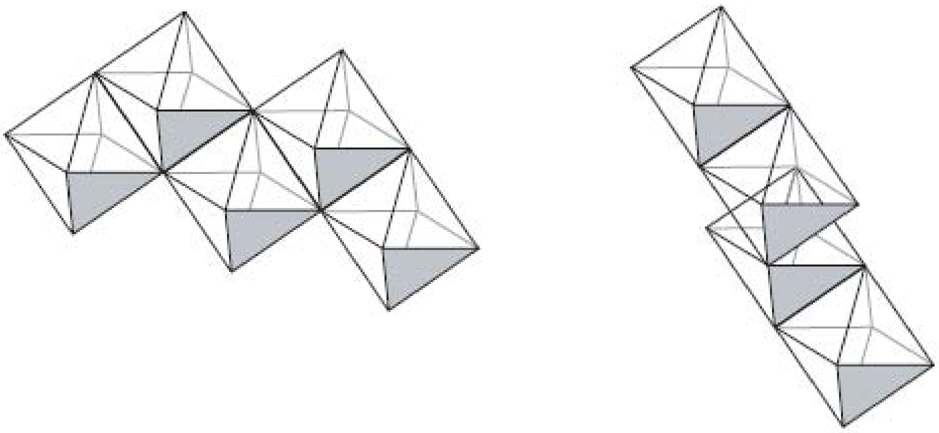

(a) Anatase

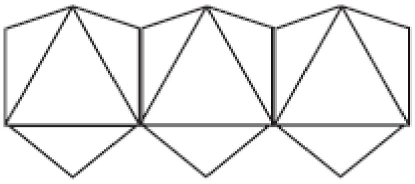

(b) Rutile

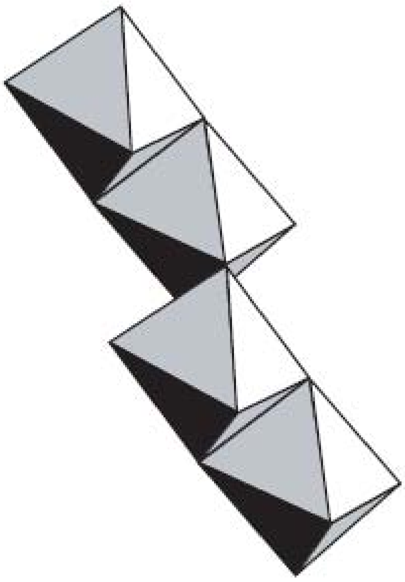

(c) Brookite

Fig. 2-2 The crystal structure of three TiO_2 forms.

three crystalline phases consist of TiO_6^{2-} octahedra, and the manner by which these octahedra (TiO_6^{2-}) bond to each other is different for rutile, anatase and brookite. The difference between anatase and rutile arises through the packing arrangements of the octahedra. The octahedra possess a body centred Ti^{4+} ion surrounded by a six fold coordination of O^{2-} ions. The Ti- Ti distances in anatase TiO_2 are greater while the Ti-O distances are shorter compared to that of rutile.

Anatase has four edges shared per octahedron and no corner oxygen sharing. The basic growth units possible for anatase are shown in Fig. 2-2 (a) (Zheng, Shi, Chen, Li, & Hu, 2001). This shows two edges are shared per octahedron forming a right-angled configuration and the third and fourth edges are shared into and out of adjacent layers. Effectively the arrangement of these octahedra gives the overall structure of anatase. In rutile, two (out of twelve) edges are shared forming a linear chain. If each titanium octahedron (TiO_6^{2-}) was represented by a building block, then the basic structural unit of rutile can be represented by Fig. 2-2 (b) (Gopal, Chan, & De, 1997). For rutile, the linear chains are then joined to each other by the sharing of corner oxygen atoms, producing the overall rutile structure. The octahedral linkages in brookite are that three edges are shared per octahedron (Jalava et al., 1998). The basic unit structure of brookite formed by TiO_6 octahedra is shown in Fig. 2-2 (c).

While the final crystal structures have 6-fold Ti-co-ordination, the titanium has 4-fold co-ordination in the initial alkoxide precursor $[Ti(OR)_4]$. However, when the alkoxide reacts with water, the metal ion increases its co-ordination by using its vacant d-orbitals to accept oxygen lone pairs from nucleophilic ligands (such as OH groups) by co-codination expansion (Livage, Henry, & Sanchez, 1988). Consequently, titanium ions in solution exist as 6-fold co-ordinated structures. The composition of this solution structure $Ti(O)_a(OH)_b(OH_2)_{6-a-b,}$ where a and b depend on the processing conditions. Since the reaction is performed in an acidic medium, only $-OH_2$ and -OH groups will be present, thus the composition reduces to $[Ti(OH)_x(OH_2)_{6-x]}{}^{(4-x)+}$ (Livage & Henry, 1988). These six-fold structural units undergo condensation and become the octahedra that are incorporated into the final precipitate structure. The octahedra agglomerate through corner and edge sharing during the condensation reactions. Face sharing does not occur in the titania system because of strong repulsion between the +4 charged metal ions. In a neutral solution, the aggregation is rapid and the precipitate appears amorphous by X-ray diffraction. However, work of others using small angle X-ray diffraction indicates that the precipitates have “short range order” similar to that in anatase (Bartlett & Woolfrey, 1992) or brookite (Q. J. Wang et al., 1991) The existence of this short range order is further substantiated by the observation that amorphous gels produced from alkoxides first convert to anatase instead of forming the more stable rutile structure (Edelson & Glaeser, 1988).

Photocatalytic activities of TiO_2 strongly depend on its phase structure, crystallite size, specific surface areas and pore structure (Anpo, Shima, Kodama, & Kubokawa, 1987; J. C. Yu, Yu, Ho, & Zhang, 2001). The photocatalytic study of brookite is quite limited, partly because brookite is rare in nature and brookite is sometimes observed as a by-product when the precipitation is carried out in an acidic medium at low temperature (Arnal, Corriu, Leclercq, Mutin, & Vioux, 1996; Bischoff & Anderson, 1995). Rutile phase possesses smaller band gap energy (3.0 eV) than the anatase phase (3.2 eV) (Kormann, Bahnemann, & Hoffmann, 1988; Sclafani & Herrman, 1996). It is commonly accepted that a larger band gap corresponds to more powerful redox ability. And it is believed that the crystal structure is the most primitive and essential property to predict the photocatalytic activities. For example, anatase crystallites have higher photocatalytic activities than rutile crystallites. And many studies have confirmed that the anatase phase of titania is a superior photocatalytic material attributable to the low recombination rate of its photogenerated electrons and holes (Akira Fujishima, Rao, & Tryk, 2000; Kato et al., 1994).

2.3.3 Enhancement of photocatalytic activities of metal oxide films

The major limitation of photocatalysis is the relatively low quantum efficiency of the oxidative substrate conversion. The catalyst efficiency is mainly limited due to the small range of the solar spectrum usable for excitation. Much research has aimed to find ways to improve the photocatalytic activities. Some strategies of improved films might involve the alteration of particle size, the increase of the surface area of the films, new or a combination of different metal oxide materials, the inclusion of dopants or the creation of films that are activated by lower energy light thus using a higher proportion of the solar spectrum.

One approach to enhance photocatalytic activities of the films through the increase of light sensitivity was focused on the shift of the band-edge positions by nanoscaled metal oxide particles (Linsebigler, Lu, & Yates, 1995). When the particle size of metal oxide crystallites is less than the De Broglie wavelength of the charge carriers in the metal oxide, the separated electron and the hole in the metal oxide nanoparticles are confined in a potential well of very small geometric dimensions where they do not experience the electronic delocalization present in the bulk metal oxide. As a result, the confinement produces a quantization of discrete electronic states. This leads to an increase of the effective band gap of metal oxide nanoparticles, enhancing the attainable potentials for oxidative or reductive reactions. The higher band-edge position can enhance the photo-induced electron transfer to adsorbed species on its surface. It is required that the relevant potential level of the acceptor species is below the conduction band potential of metal oxide. Likewise, the potential level of the donor needs to above the valence band position of metal oxide in order to donate an electron to the vacant hole.

An alternative would use metal oxides with a narrow band gap thus permitting catalyst excitation and photoresponsiveness within the visible range to utilize the solar spectrum more efficiently. Several metal oxides, including WO_3, ZrO_2, ZnO and Fe_2O_3 have been investigated over the years. However, among the metal oxide semiconductors suitable for photocatalytic processes, none have managed to surpass TiO_2 using light alone to activate the catalytic action (S. Kim, Park, & Choi, 2004; Mills & Le Hunte, 1997). TiO_2 has been the most widely used one in photocatalytic films. Its high photoactivity and the ease of deposition coupled with its established use in many existing products facilitate the release of commercial self-cleaning TiO_2 films. However, TiO_2 shows photocatalytic activities only under UV light which means that only 5% of solar spectrum is used. In addition, to deposit titania optically clear and robust in a smooth, nanocrystalline film, its photocatalytic activity is reduced compared to many other forms of the material. Besides, since such properties as optical clarity, hand feel, and durability to laundering of self-cleaning textiles are very important to consumers, a robust, easily deposited and a clear nanocrystalline film is required. In addition, the photocatalytic activities of nanocrystalline TiO_2 films need to be further improved. As a widely available and uniform commercial product, Pilkington Activ™ is one of the improved self-cleaning coatings (Mills et al., 2003).

To improve photocatalytic activities of TiO_2, doping of TiO_2 is an attractive method. It can easily be incorporated into a sol–gel process and has been studied in recent years (Karakitsou & Verykios, 1993). Titania photocatalysis can be remarkably affected by impurities even in low concentrations. Dopants can exist as a single phase mixed oxide or as a separate phase depending on the technique used to deposit the film. A particular dopant may behave differently depending upon which form it is in. Transition metal dopants have been widely investigated. When these dopants present as a single phase mixed oxide, they can be divided into low oxidation state and high oxidation state based on their effects (Karakitsou & Verykios, 1993; Park, Joo, & Kang, 2004). Lower valence metal cations than +4, such as Fe^{3+}, Co^{2+} and Ni^{2+}, inhibit photocatalytic activity, while higher valence metal cations, such as Mo^{5+}, Nb^{5+} and W^{6+}, increase photocatalytic activity. Park *et al*. (2004) reported that the high oxidation state dopants caused crystallization to occur around 20 ºC lower than low oxidation state dopants from differential scanning calorimetry (DSC) when present as a mixed oxide. An X-ray photoelectron spectroscopy (XPS) study indicated that the high valence metal doped films had a higher proportion of hydroxyl groups adsorbed onto the surface than undoped and low valence metal doped TiO_2. Since hydroxyl groups are important in photocatalysis, this could explain the increase in activity in the case of high oxidation dopants. Phase separated dopants such as a phase of pure TiO_2 containing a pure phase of a second material such as Au is another type. The incorporation of nanoparticles into a film has been focused on in the presence of a phase separated dopant (Subramanian, Wolf, & Kamat, 2004; Tada, Kokubu, Iwasaki, & Ito, 2004).

It is worth to note that the effect of dopants on the change in photocatalytic acitivties depends largely on the dopant concentration, the dopant dispersion and the type of reactants to be converted. Most studies confirmed that a maximum of dopant concentration above makes photoactivity decline again. However, the value of this maximum concentration itself depends more on the dopant and the reaction environment. The optimal dopant and dopant concentration have to be determined from experimental studies under the specific conditions of interest.

2.4 Chemical synthesis of metal oxide nanpparticles

Nanoscaled metal oxide, such as TiO_2 films can be synthesised by various wet chemistry methods such as the chloride ($TiCl_4$) method (Xia, Li, Zhang, & Xie, 1999), hydrothermal processing (Bacsa & Grätzel, 1996) and sol-gel method (Carl Anderson & Bard, 1995). To date, of all the above process, only sol-gel method can (Aruna & Patil, 1996)

- produce metal oxide nanoparticles at low temperatures,
- be scaled to large quantities (to be commercially viable) relatively cheaply,

- synthesize almost any metal oxide nanoparticles,
- co-synthesize two or more materials simultaneously,
- produce extremely homogeneous composites,
- synthesize ultra-high purity (99.9999%) materials,
- tailor the composition very accurately even in the early stages of the process, because the synthesis is actually performed on an atomic level,
- precisely control the microstructure of the final products, and precisely control the physical, mechanical, and chemical properties of the final products.

2.4.1 The sol-gel process

The basic steps involved in the sol- gel synthesis of metal oxide nanoparticles are based upon the hydrolysis and condensation of metal alkoxide $M(OR)_n$, where M is the metal, R is the organic group. Metal alkoxides are widely used precursors because of the presence of highly electronegative OR groups (hard-π donors) that stabilize M in its highest oxidation state and render M very susceptible to nucleophilic attack then they readily react with water (Brinker & Scherer, 1990; Livage, Henry, & Sanchez, 1988). Since the metal alkoxide and water are not soluble in each other, they must be dissolved in a common alcoholic solvent to carry out their reaction. The very high reactivity of water with the metal alkoxide is explained by the partial charge model (Shukla & Seal, 2003). According to the model, the alkoxide group, being highly electronegative, creates a positive charge on the central metal atom. On the other hand, in the water molecule, there is a partial negative charge on the oxygen atom. As a result, the water molecule attacks the metal atom from the alkoxide, resulting in the hydrolysis of the alkoxide. When no acid or base catalyst is present, hydrolysis and condensation both occur by nucleophilic substitution (S_N) mechanisms involving nucleophilic addition (A_N) of a water molecular followed by proton transfer from water to the alkoxy group which then leaves as alcohol or hydroxo-ligand within the transition state and removal of the protonated species as either alcohol (alcoxolation) or water (oxolation) (Brinker & Scherer, 1990; Wright & Sommerdijk, 2001). The hydrolysis and condensation occurs through reactions (1)–(3).

Hydrolysis:

$$\equiv M–OR + H_2O \rightarrow \equiv M–OH + ROH \qquad (1)$$

Oxolation condensation:

$$\equiv M–OH + HO–M\equiv \rightarrow M–O–M\equiv + H_2O \qquad (2)$$

or

Alcoxolation condensation:

$$\equiv M–OH + RO–M\equiv \rightarrow \equiv M–O–M\equiv + ROH \qquad (3)$$

The thermodynamics of these different processes are governed by the partial negative charge of the incoming nucleophile in hydrolysis, the partial positive charge of the electrophilic metal, and the partial charge and stability of the leaving group (with more positively charged groups leaving most readily).

2.4.2 Role of the catalyst

Acid and base catalysts can influence both the hydrolysis and condensation rates and the structure of the condensed product. Acid serves to protonate negatively charged alkoxide groups which enhance the reaction kinetics by producing good leaving groups. Hydrolysis completes when sufficient water is added. The relative ease of protonation of different alkoxide ligands can influence the condensation pathway as demonstrated by consideration of a typical partially hydrolyzed polymer (Livage, Henry, & Sanchez, 1988). The least positively charged species will react fastest, so chain end sites will be more reactive centre sites and long chains with little branching will be produced (Brinker & Scherer, 1990; Shukla & Seal, 2003). High acid concentrations ($H^+/Ti \rightarrow 1$) severely retard the condensation kinetics. The hydrolysis and condensation reactiosn by acid catalysed processes are shown in reactions (4-5).

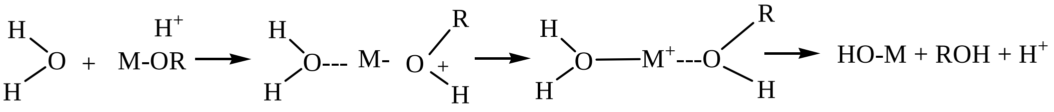

(4)

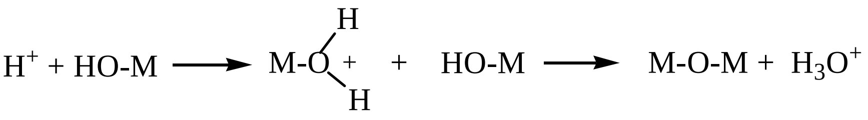

$$H^+ + HO\text{-}M \longrightarrow M\text{-}\overset{H}{\underset{H}{O}}{}^{+} + HO\text{-}M \longrightarrow M\text{-}O\text{-}M + H_3O^+$$

(5)

Alkaline conditions produce strong nucleophiles via deprotonation of hydroxo ligands. The hydrolysis and condensation reactions by base catalysed processes are shown in reactions (6-7).

$$\text{HO}^- + \text{M-OR} \longrightarrow \text{HO}^- \text{----M-OR} \longrightarrow \text{HO-M----OR}^- \longrightarrow \text{HO-M} + \text{OR}^- \qquad (6)$$

$$\overset{\curvearrowleft}{\text{M-OH} + \text{OH}^-} \longrightarrow \text{M-O}^- + \text{M-OH} + \text{H}_2\text{O} \longrightarrow \text{M-O-M} + \text{OH}^- \qquad (7)$$

The hydrolysis rate of $Ti(OBu)_4$ was less in basic conditions (NaOH) than in acidic or neutral conditions, perhaps because nucleophilic addition of OH- reduces charge distributions of Ti (Livage, Henry, & Sanchez, 1988). Condensation kinetics is systematically enhanced under basic conditions. For base catalysed reactions, the most positively charged species will react fastest. Therefore, base-catalyzed condensation (as well as hydrolysis) should be directed toward the middles rather than the ends of chains, leading to more compact, highly branched species (Brinker & Scherer, 1990).

2.5 Adhesion between metal oxides and textile surface

The durability and stability of metal oxide film on textiles to multiple home laundering is indicative of a good adhesion between the metal oxide film and the fabric surface. Hence good adhesion is essential for the practical application of sol–gel derived metal oxides in textiles. In addition, porous coatings on textiles may not have a high level of washfastness due to a peel-off effect.

ZnO@polystyrene core–shell nanohybrid coating was prepared on cotton fabrics. The cotton fabrics treated byZnO@polystyrene nanohybrid provided ultrahigh UV protection property and superior wash fastness, with UPF of >50 even after 50 home launderings. The ultrahigh UV-blocking property of the nanohybrid coating was attributed to a cooperative effect of the special electronic structure of semiconductor cores and the conjugated structure of phenyl groups in the polymer shells. And the superior adhesion of the nanohybrid coating is attributed to the crosslinking between nanohybrids and cotton fibers by in situ polymerization and esterification reactions. Therefore, this new nanohybrid material and its synthesis method are highly potential to various functional treatments of flexible surfaces.

Composite films were prepared from cellulose and nanocrystalline titania particles (J. Zhou, Liu, Qi, & Zhang, 2006).The TiO_2 particles in a cellulose matrix maintained the original nanocrystalline structure and properties and exhibited a certain miscibility with cellulose. The cellulose composite films containing nanocrystalline TiO_2 particles displayed distinct antibacterial abilities and excellent UV absorption. This study provides a potential way for preparing functional composite materials from cellulose and inorganic nanoparticles without the destruction of the structure and properties of the particles.

Poly(ethylene phthalate) (PET)/nano-TiO_2 composites prepared via *in situ* polymerization were spun into fiber by the melt-spinning process (K. Han & Yu, 2006). The rutile TiO_2 can be dispersed uniformly by the *in situ* polycondensation process. The mechanical properties of PET/TiO_2 fiber were decreased slightly by adding nano-TiO_2. The ultraviolet protection factor (UPF) of PET/nano-TiO_2 fabrics was greater than 50. The PET/TiO_2 nanocomposite fabrics exhibited excellent UV-blocking properties because of the high refractive index and absorption of UV light of rutile TiO_2.

It has been reported that a uniform film was formed on the cotton fiber surface treated by titania sol and titania-silica sol (Abidi, Hequet, Tarimala, & Dai, 2007; Daoud, Xin, Zhang, & Qi, 2005; Xin, Daoud, & Kong, 2004). This treatment imparted excellent UV protection to the cotton fabric before and after repeated home laundering especially in the region of the UVB (290-315 nm), which suggested good adhesion between titania and titania–silica and cotton. The excellent durability of the treatment to repeated home laundering could be attributed to the formation of covalent linkages between the many hydroxyl groups of cellulose and the hydroxyl groups of titania and titania–silica network.

It has also been reported that a uniform titania layer was formed on wool fibers (Daoud et al., 2008; Tung & Daoud, 2008). The homogeneous titanium dioxide layer without peel-off effect in SEM images suggested the possibility of chemical deposition, owing to the affinity between titanium dioxide and hydroxyl and carboxyl groups of wool fibers. Titania has high affinity toward hydroxyl and carboxyl groups, which are available in keratin fibers (Daoud et al., 2008; Tung & Daoud, 2008), resulting in effective binding and deposition uniformity. The stain removal ability of titania coated wool fibers was reproducible after repeated stability testing, simulated dry cleaning procedure in petroleum ether according to ISO 105-D01. And in the colorant decomposition of methylene blue, titania coated wool fibers possessed good reproducibility after the stability test by showing a very similar colorant decomposition rate to that before stability test. This indicated that titania coated protein fibers possess effective self-cleaning properties with good stability and that the titania layer has good adhesion to the fibers as evidenced by its ability to withstand the harsh conditions of the stability test.

In our study, adhesion between metal oxide film and textile surface will be evaluated by the photocatalytic activities of metal oxide films before and after repeated home laundering.

2.6 Self-cleaning TiO_2 films

Transparent films of TiO_2 have been studied for many years. Research studies have focused on their potential in self-cleaning applications due to their photocatalytic and superhydrophilic properties (Rong Wang et al., 1997; Rong Wang et al., 1998). Some TiO_2-based self-cleaning products such as tiles, glass and plastics have become commercially available (A. Fujishima, Hashimoto, & Watanabe, 1999; Mills & Lee, 2002). The TiO_2 coating of these products can decompose organic contaminants or kill bacteria adhering to the surface under

UV illumination. Moreover, superhydrophilic TiO_2 film favors the fast and complete spreading of water droplets on the surface, which also aids the decontamination process. However, with the thorough review of literature, few research works reported self-cleaning titania films on textiles.

Obviously, with self-cleaning textiles, the titania films must adhere strongly to the textile substrates because textiles are subject to frequent washing and hence good adhesion is essential for the practical application of sol-gel derived titania in textiles. The titania films must be optically clear so as not to affect the color of the textile substrates. Moreover, the titania films must usually be very thin to make hand feel of the textiles intact and composed of nanocrystalline particles to achieve good self-cleaning effect. The crystalline phase and crystallite size are important properties of the anatase films, controlling the efficient absorption of UV photons and the migration of photogenerated holes to the crystallite surface (Ohtani, Ogawa, & Nishimoto, 1997). The positions of the conduction and valence bands relative to key redox potentials cause pure anatase to be very photoactive (photocatalytic and super-hydrophilic) while pure rutile is less so (Mills & Le Hunte, 1997; Sun & Smirniotis, 2003). The absorption properties, surface properties and band gap of nanoscale titania particles vary with their size and shape(Hagfeldt & Gräetzel, 1995). However, the preparation of anatase thin films is usually achieved at relatively high temperature of 400°C and greater. The application of transparent anatase films is essentially infeasible to substrates with low thermal resistance such as textiles.

Recently, acid-catalysed reactions have been widely studied and have been employed to make films. Much work has reported the nucleation of anatase films on heat resistant surface using sol-gel process at relatively low temperatures, such as the formation of crystalline anatase films: (1) from sol-gel derived silica-titania films treated glass, silicon wafers and plastic substrates with hot-water treatment(Matsuda, Kotani, Kogure, Tatsumisago, & Minami, 2000; Atsunori Matsuda et al., 2003; Matsuda et al., 2005); (2) from sol-gel derived silica-titania films on silicon wafers exposed to water vapor at temperatures 60-180°C (Imai & Hirashima, 1999); (3) from titania films on glass and various kinds of organic substrates by immersing substrates into aqueous solutions of titanium tetrafluoride at 40-70°C for 0.5-260 h (Shimizu, Imai, Hirashima, & Tsukuma, 1999). However, in these cases, anatase films were obtained using some amount of alcohols under acidic conditions and some products are composed of a mixture of anatase and brookite, rather than pure anatase. It is evident that the formation of photocatalytic crystalline anatase in water medium at low temperatures is of great importance for the fabrication of transparent films on substrates, not only from the point of view of energy saving, but also for their application in low thermally resistant materials such as biomaterials and textiles. Furthermore, to make the whole chemical approach environmentally friendly, the use of aqueous solutions instead of organic solvents is desired. Therefore, it is very interesting and challenging to improve synthetic routes at low temperatures to broaden the applications of crystalline anatase films on substrates.

Nature has recently reported (Peblow, 2004) that Daoud and Xin (2004b) have successfully grown anatase nanocrystallites on cotton fabrics and these fabrics could be made into self-leaning clothes that tackle dirt, environmental pollutants and harmful microorganisms. The anatase phase could be obtained on the cotton textile surface by a boiling water treatment for 3h (Daoud & Xin, 2004b). Later on, self-cleaning wool-polyamide, polyester and cotton textiles treated with TiO_2 have been reported (A. Bozzi, Yuranova, Guasaquillo, Laub, & Kiwi, 2005; A. Bozzi, Yuranova, & Kiwi, 2005; Meilert, Laub, & Kiwi, 2005; Yuranova, Mosteo, Bandata, Laub, & Kiwi, 2006). In that work, the TiO_2 colloidal solution was prepared using titanium tetraisopropoxide as the precursor in 2-propanol acidified by nitric acid, then the TiO_2 solution was hydrothermally treated for 16h at 100°C. However, the rutile phase, not anatase phase, was attained on the TiO_2 treated textiles (A. Bozzi, Yuranova, & Kiwi, 2005). It is widely known that rutile is less photochemically active than anatase (Yuranova, Mosteo, Bandata, Laub, & Kiwi, 2006). This form of rutile TiO_2 on the wool-polyamide should, therefore, be less aggressive than the anatase form towards self-cleaning effect of the textile substrate upon light irradiation.

Moreover, the long term stability of these products is not known. More recently, Daoud *et al*. (2008) investigated self-cleaning keratins by the chemical modification and anatase coating processes.

2.7 Conclusions

In the past decade, commercial self-cleaning products have become available to the consumer, especially self-cleaning glass. One interesting feature of the titania-based films is their ability to destroy harmful bacteria and viruses by photocatalytic action using sunlight. The key factor that requires further development is the ability to extend the range of light that can be used for the photodestruction of dirt and bacteria. As the extising standard – ‘titania’ can only use sub-390 nm light, extending the absorption range by pushing this edge more into the visible region would significantly improve the efficacy of the film. The concept of self-cleaning when applied to garment would be attractive to both consumers and manufactures. However, the self-cleaning power, the effects to fabric substrates, and the durability are largely unknown.

Chapter 3: Research Methodology

3.1 Introduction

Based on the literature reviews in Chapter 2 above, it can be seen that the fabrication of TiO_2-based self-cleaning films on textiles at a low temperature is attractive and challenging. In order to obtain highly photoactive single-phase anatase on textile surfaces, systematic nanocrystalline titania preparation using a sol-gel process at a low temperature was carried out.

3.2 Sample preparation

Woven white cotton fabrics were scoured by nonionic detergent to remove the wax, grease, and other finishing chemicals from the fabrics before treatment. The scouring process was performed at 80°C for 30min.

White plain polyester fabrics were used in the present study. The polyester fabrics were first washed with 1% non-ionic detergent solution in 70 °C water for 15 min and then rinsed with ethanol by ultrasonic bath for 15 min and finally washed with plenty of water for another 15 min before low temperature plasma (LTP) treatment, in order to minimize the chance of contamination. The polyester fabrics were finally cut to the dimension of 20 cm×20 cm and were conditioned for 12 h under standard conditions before the next experiment.

3.3 Chemicals

Titanium tetraisopropoxide (97%), nitric acid (70%) and acetic acid (97%) was purchased from Aldrich. Ethanol (99.8%) was purchase from Riedel-de Haen. All of the chemicals were reagent grade. Neolan Blue 2G and Cibacron Blue F-R were supplied by Ciba. These two dyes were commercia1 products and were used as-received. Deionized water was used throughout the study.

3.4 Low temperature plasma treatment

A glow discharge generator (SPP-001, Showa Company of Japan) was employed for the plasma treatment of the polyester fibers. Oxygen was chosen as the LTP gas. The discharge power, pressure and gas flow rate were 100 W, 6 Pa and 15scc/min, respectively. The exposure time was 10 min. 100W discharge power and 10 min treatment time were considered enough for the surface structure modification. Longer treatment time only slightly increase the modified surface structure, and sometimes might result in surface melting on the polymer surface (Yip, 2003).

3.5 Preparation of TiO_2 sols and finishing process

The TiO_2 sols were prepared by the sol- gel process in aqueous solution at low temperatures using titanium tetra-isopropoxide as the precursor and nitric acid and combined catalysts of nitric acid and acetic acid as catalysts, respectively. The detailed procedure for preparing the TiO_2 sols was as follows. A 250 ml beaker was charged with 100 ml aqueous solution containing 1 ml nitric acid (70%) or the combined catalysts of 1ml nitric acid (70%) and 10 ml acetic acid (97%), then 5 ml or 10 ml titanium tetraisopropoxide was added dropwise into the acidic solution under vigorous stirring using a magnetic stirrer. The mixture was heated at 23, 40, 60 °C and maintained at that temperature while being stirred magnetically for 16-24 h respectively.

The as-prepared sols were used to prepare TiO_2 films on substrates by a dip-pad-neutralize (NH_3 gas)-dry-cure process. The cleaned substrates were dipped in TiO_2 sols for one minute, and pressed with an automatic padder (Rapid Labortex Co. LTD, Taipei, Taiwan) at the same nip pressure of 2.75 kg/cm^2 to keep the same amount of different TiO_2 sol on cotton substrates. After 5 min, the padded fabrics were put in ammonia gas for neutralization until a pH 7 of the fabric surface was achieved. The substrates were dried at 80°C for 5min in a preheated oven and finally cured at 120°C for 3min in a preheated curing oven (Mathis Labdryer Labor-Trockner Type LTE, Werner Mathis AG Co., Switzerland).

3.6 Characterization of TiO_2

The structure and morphology of TiO_2 films on cotton fabrics were investigated using field-emission scanning electron microscopy (FESEM, JSM-6335F at 3.0kV, JEOL, Tokyo, Japan). The surface morphological changes of polyester fibers before and after plasma treatment, and of plasma-treated fibers before and after TiO_2 coating are characterized by FESEM. The change in the chemical composition on the polyester surface occurring in plasma pretreatment process and the relative amount of TiO_2 deposited on the polyester surface without and with plasma treatment are investigated using X-ray photoelectron spectroscopy (XPS) by an X-ray photoelectron spectrometer (Physical Electronics PH1Quantum 2000 XPS/ESCA).

The crystal phases of solid powder of the titania sols were studied by X-ray diffraction spectroscopy (XRD, Bruker D8 Discover X-ray diffractometer) operating at 40 kV and 30 mA. The crystal phases of formed titania films on cotton and polyester fabrics were studied by small angle X-ray diffraction (XRD, Philips Xpert XRD system) at 3° of incident beam using Cu Ka radiation and detector scan mode operating at 40 kV and 30 mA. To prepare the transmission electron microscope (HRTEM, JEOL JSM-2010 microscope) samples, the titania films treated on silicon was glued on a copper grid followed by mechanical grinding and polishing until the thickness was reduced to 20 μm thick. Ion milling was performed on the substrate only by Ar^+ bombardment at 5 keV using a Gatan Precision Polishing System. Initially, the angle of ion milling was set at 10°; at the final stage, an angle of 7° was used and processing was performed at 3 keV. The morphology and particle size of

TiO_2 was investigated using spin coated samples (spin coating at 1500 rpm for 50 seconds on glass and silicon substrates) by Atomic force microscopy (AFM, Seiko SPI 3800). The formed coating films were first air-dried for 1 hour and then oven dried at 38 °C for 12 hours.

The UV-absorption of titania treated substrates was measured according to the Australian/New Zealand Standard AS/NZS 4399:1996 using Varian Cary 300 UV spectrophotometer.

3.7 Photocatalytic activities

3.7.1 Assessment of dynamic bactericidal activities

The dynamic antibacterial activity assessment was carried out according to a modified procedure of the shake flask method ASTM E2149-2001. Staphylococcus aureus, a gram-positive type of bacteria, was cultivated in a nutrient broth (containing 10 g/l beef extract, 10 g/l peptone, 5 g/l NaCl) by shaking for 18 h at 37 °C. All glassware and test samples were sterilized in an autoclave at 120 °C for 20 min or with UV irradiation before experiments. The formed inoculum was further diluted with nutrient broth and an appropriate volume was extracted into sterile phosphate buffer solution (PBS) (containing 0.9 ml of 0.5 M KH_2PO_4 in 900 ml ddH_2O) in order to obtain a final concentration of 1.5–3 × 10^5 cell forming colonies per ml. Two pieces of each test specimen (original cotton fabric and TiO_2 treated cotton fabrics,

TiO_2-treated polyester without plasma pretreatment and TiO_2-treated polyester with plasma pretreatment) with a fixed surface area of 42 cm^2 (cut into small pieces of about 0.5 cm^2) were transferred into 250 ml capped Erlenmeyer flasks. The flasks were autoclaved before the addition of 50 ml of sterile PBS. The flasks were capped, placed in a wrist-action shaker (Sheldon Manufacturing Inc SI4-2) and shaken at 250 rpm at 37 °C. At the predetermined time, 1 ml of solution from each flask was transferred to a test tube containing 4 ml of ddH_2O and plated out in agar plates (containing 10 g/l beef extract, 10 g/l peptone, 5 g/l NaCl and 15 g/l agar powder) in duplicate. A drop of 0.1 ml of the diluted sample was then spread onto solid growth agar plates. After incubation of the plates at 37 °C for 24 h, the number of viable cells (colonies) was counted manually and the results after multiplication with the dilution factor were expressed as mean colony forming units (CFU) per ml after averaging the duplicate counts. The UV irradiation was performed using a UV lamp (Philips TL05 8 W) with a maximum intensity wavelength (λ_m) at 365 nm.

3.7.2 Assessment of static bactericidal activities

The antibacterial assessment was carried out according to AATCC Test Method 100–1999. Four swatches of each test specimens (original cotton fabric and TiO_2 treated cotton fabrics, TiO_2-treated polyester without plasma pretreatment and TiO_2-treated polyester with plasma pretreatment) with a diameter of 5 cm were stacked up and in separate 150 ml wide-mouth jars. 1 ml of inoculum was added to each jar. The tops were immediately screwed tightly to prevent evaporation. For, “0” contact time sample, 100 ml of sterile phosphate buffer were added immediately after inoculation and the jars were shaken for one minute. 1 ml of the resulting solution was transferred from each jar to a test tube containing 4 ml of ddH_2O and plated out in duplicate as explained before. For “5 h” contact sample, the jars were incubated for 5 h in a 37 °C incubator before the plate count technique was performed. All the Petri dishes were incubated for 24 h in a 37 °C incubator. After incubation, the number of viable cells (colonies) was counted manually and the results after multiplication with the dilution factor were expressed as mean colony forming units (CFU) per ml after averaging the duplicate counts.

3.7.3 Assessment of decomposition activities of colorant stains

The decomposition activities of colorant stains were assessed by analyzing the decrease in absorbance of the colorants during exposure to UV irradiation (365 nm, Philips TLD 18W/08) or visible light illumination (Philips TLD 18W/54 Daylight). A 3g or 5g TiO_2–based treated white fabrics was cut into 1cm×1cm pieces. These pieces were placed in a 250ml beaker containing 75ml Neolan Blue 2G aqueous solution (0.2g/L), 100ml Cibacron Blue F-R (0.2g/L) and untreated fabric as well as a comparison. Then the beakers were exposed to UV irradiation provided by Philip UV lamps or Philip Daylight lamps while vigorously shaking was applied at the same time (IKA KS260 Basic Orbital Shaker). Prior to UV irradiation or visible light illumination, the colorant solution with fabric pieces was kept in dark condition for 4 h while shaking to establish the absorption-desorption equilibrium. UV-Vis absorption spectra of irradiated samples were recorded on a UV-Vis spectrometer (Perkin Elmer UV-Vis spectrometer Lambda 18). The colorant solution was centrifuged to precipitate fibers at the bottom of the tube and the upper clear colorant solution was used for measurement. The changes in absorbance of colorants were estimated by the absorbance at the absorption peak around 630nm for Neolan Blue 2G and 610nm for Cibacron Blue F-R.

3.7.4 Assessment of degradation activities of red wine and coffee stains

The degradation activities of a red wine stain (Carlo Rossi California Red, 11.5% alc/vol) and a coffee stain (Nestle, 1.8g 100% pure soluble coffee power/150ml hot water) were evaluated. Untreated and titania treated white fabrics were cut into 4.5cm x 6.5cm respectively. One drop of red wine and coffee were applied onto the treated fabrics and untreated fabrics using 10 ml medical syringe with pinhead close to the fabric surface when dropping. The irradiation of all samples were carried out in Xenotest Alpha LM light exposure and weathering test instrument (air cooled xenon arc lamp, irradiance 4.5 mW/cm^2 at 300-400 nm Wavelength, Xenotest Alpha LM, Heraeus Industrietechnik, Hanau, Germany). The red wine and coffee stained fabrics were irradiated with predefined durations.

3.8 Mechanical properties of fabrics

The tearing strengths of untreated and titania treated fabrics before and after 20 hours of light irradiation were measured by an Elmendorf Tearing Tester (Thwing-Albert Instrument Co.) in accordance with ASTM D 1424-96. The tensile strengths of untreated and titania treated fabrics before and after 20 hours of light irradiation was performed according to ASTM-D5035-2001 using Instron 4411 Tester (England) on specimens.

Three samples were prepared in the warp direction and the average value of strength was obtained. The irradiation of all samples was carried out in light exposure and weathering test instrument (air cooled xenon arc lamp, irradiance 4.5 mW/cm^2 at 300-400 nm Wavelength, Xenotest Alpha LM, Heraeus Industrietechnik, Hanau, Germany)..

3.9 Durability of TiO_2 films

The durability of TiO_2 layers on cotton and polyester was evaluated by comparing UV-absorption or dye decomposition of treated cotton fabrics before and after repeated washing following the AATCC Test Method 61-2003 Test No. 2A using AATCC Standard Instrument Atlas Launder-Ometer LEF.

3.10 Determination of the surface acidity of pure TiO_2 powder and TiO_2/SiO_2 nanocomposite powder

The surface acidity of pure TiO_2 powder and TiO_2/SiO_2 nanocomposite powder was determined by titration with n-butylamine following a procedure as follows. 0.5g photocatalyst powder was dispersed ultrasonically in 50 ml of benzene. Five drops of a 1.0 g l^{-1} methyl red (pKa = +4.8, $H_0 \leq +4.8$) indicator solution in benzene were added to the flask. N-Butylamine (0.01 mol l^{-1}) was titrated against the powder, and the amount of titrant necessary to cause the color change on the indicator solution was recorded. Precautions were taken to handle the samples in a consistent manner to ensure that the results were reproducible and could be confidently compared on a relative basis. The titration was repeated three times and the average of which is quoted in this study.

Chapter 4: Titania Nanoparticles and Their Application to Cotton Fabrics

4.1 Introduction

Among different crystalline phases of TiO_2, anatase is reported to have the highest photoactivity. It is also widely regarded that anatase titania with both a high surface area and a high degree of crystallinity is desirable to enhance the photocatalytic activity, since such a structure will have relatively few disruptions in its electronic band structure (Legrini, Oliveros, & Braun, 1993; Linsebigler, Lu, & Yates, 1995). However, the preparation of anatase thin films is usually achieved at relatively high temperature, usually around 450 °C. The applications of anatase films are essentially infeasible to textiles due to their low thermal resistance. Therefore, a systematic study is required in order to investigate the effect of the acid catalyst and the preparation temperature on the phase and size of colloidal titania crystallites by a sol-gel process at low temperatures in an acidic aqueous medium. In this chapter, comprehensive studies are reported on the surface morphology, crystal phase and particle size of nanocrystalline TiO_2 films deposited on cotton fabrics using SEM, XRD, and TEM. The photocatalytic activities of different titania treated cotton fabrics have been also studied. The mechanical properties and durability of titania film on cotton fabrics have been investigated.

4.2 Preparation of TiO_2 sols, TiO_2 powder and TiO_2 films on cotton fabrics

Titania sols were prepared from two routes given below:

(1) TiO_2 sols were prepared at room temperature (23°C) and 60°C by hydrolysis and condensation of 10 ml titanium tetraisopropoxide (TTIP, Aldrich, 97%) in 100 ml deionized water containing 1 ml nitric acid (Aldrich, 70%). The two samples are referred to as sample N23 and N60 respectively. N23 was stirred at room temperature for 24 hours after the addition of the TTIP to the acidic water, while N60 was heated to 60 °C and kept at that temperature for 24 hours while being stirred.

(2) TiO_2 sols were prepared at low temperatures, being room temperature (23°C), 40°C and 60°C, by hydrolysis and condensation of 10 ml titanium tetraisopropoxide in 100 ml deionized water containing 10 ml ethanol (Riedel-de Haen, 99.8%), 1 ml nitric acid and 10 ml acetic acid (Aldrich, 97%). The TiO_2 samples are referred to as sample S23, S40 and S60 respectively. S23 was stirred at room temperature for 24 hours. S40 and S60 was heated to 40 °C and 60 °C and kept at that temperature while being stirred for 24 hours respectively.

Solid TiO_2 powders were obtained from the corresponding sols by adding adequate amounts of 0.3% sodium carbonate until precipitation occurred. The formed suspensions were centrifuged at 4000 rpm for 5 minutes, followed by removal of the liquid phase. The precipitates were then washed three times with water and finally with acetone twice before being dried at room temperature overnight.

The as-prepared TiO_2 sols were used to treat cotton fabrics. Dipping-padding-neutralizing-drying-curing process of cotton fabrics was used to fabricate TiO_2 layers on cotton. The as-prepared cotton fabrics were used for the characterization by SEM and XRD pattern, the measurement of UV absorption, self-cleaning performance and tearing strength of the fabrics.

4.3 Characterization of TiO_2 nanoparticles

4.3.1. XRD spectroscopy

The crystal phases of titania particles were studied by XRD. Results of gel properties and XRD measurements are summarized in Table 4-1. It is apparent that the peptizing conditions greatly affect the crystal structure of the resulting particles. From the XRD patterns of titania powders obtained from freshly prepared N23 and N60 solution respectively in Fig.4-1, it can be seen that N23 is amorphous TiO_2 since almost no peak can be observed in Fig.4-1 (a). However, N60 is predominantly anatase with a small amount of brookite as sharper anatase peaks with greater intensities at 25.4°, 38.0°, 48.0° and brookite peaks at 27.7°, 31.1°, 37.6°, 42.6° and 48.3° are observed respectively in Fig.4-1 (b). This indicates that amorphous titania which is formed by hydrolyzing TTIP in an acidic aqueous solution containing only nitric acid can be transformed to anatase with a small amount of brookite as a low temperature of 60° similar to a previous report (Hu & Yuan, 2005). Luo *et al*. (2003) reported that tri-crystalline titania (anatase, rutile and brookite) was obtained by hydrolysis of $TiCl_4$ at 40°C in a mixed solvent of ethanol and water and they thought the formation of brookite might be ascribed to the strong acidic conditions (Luo, Wang, & Yan, 2003). Pottier *el at*. (2001) also reported that hydrothermal treatment in a strongly acidic aqueous media benefited the formation of brookite. It was also reported that the photocatalytic activity of the mixture of anatase and brookite would be lower than that of single-phase anatase(Li, Lee, Song, Lee, & Kim, 2005)

In an attempt to obtain highly photoactive pure phase, titania solutions were prepared by adding more organic acetic acid in aqueous solutions containing the same amount of nitric acid as N23 and N60. Fig.4-2 displays the XRD patterns of titania powders obtained from S23, S40 and S60 solution respectively. As shown in Fig.4-2 (a), S23 is predominantly amorphous TiO_2 with a very small amount of anatase crystallites with small crystal size as broad weak anatase-associated peaks were observed at 25.4°. On the other hand, sharper anatase peaks of solid titania particles with greater intensities at

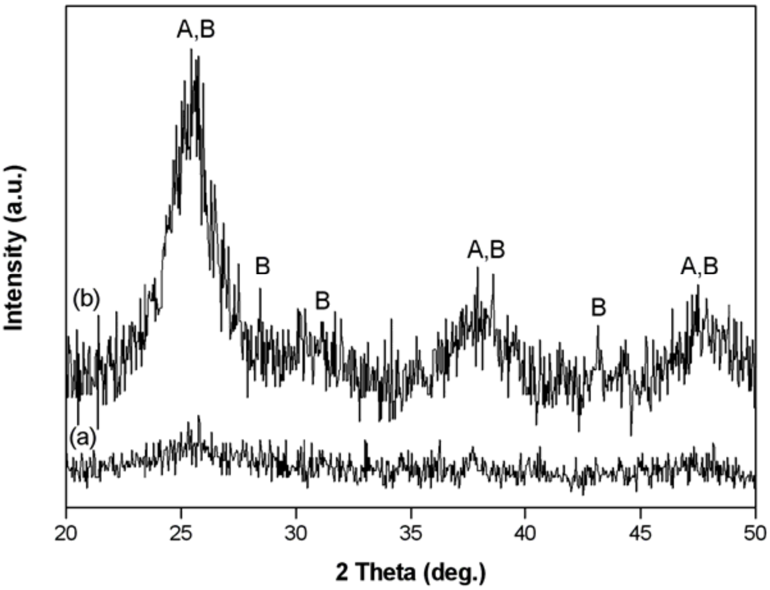

Fig.4-1 XRD patterns of solid powder extracted from (a) N23 and (b) N60 (A: anatase, B: brookite).

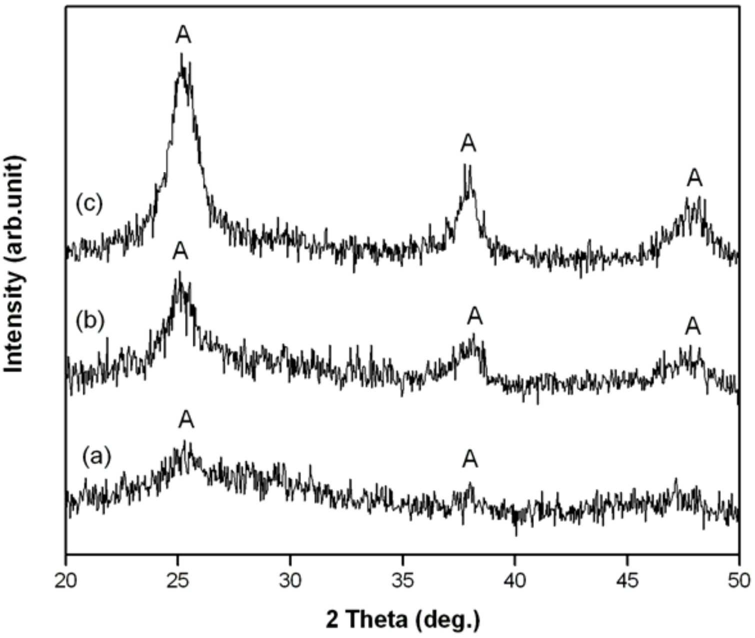

Fig. 4-2 XRD patterns of solid powder extracted from (a) S23, (b) S40 and (c) S60 (A: anatase).

Table 4-1 Conditions of sample preparation and their resultant products

Sample	**Catalysts**	**Temperature (°C)**	**Appearance of gels**	**Crystal structure**	**Stability**
N23	nitric acid	23	transparent	amorphous	precipitation in 3 months
N60	nitric acid	60	transparent with slight blue tint	anatase and brookite	stable for one year
S23	nitric acid and acetic acid	23	transparent	predominantly amorphous with anatase	precipitation in 6 months
S40	nitric acid and acetic acid	40	transparent	anatase	stable for one year
S60	nitric acid and acetic acid	60	transparent with slight blue tint	anatase	stable for one year

25.4°, 38.0°, 48.0° were observed evidently in Fig.4-2 (b) and (c), confirming that crystalline TiO_2 could be obtained in an acidic aqueous solution at low temperatures. The amount of brookite can be revealed by XRD at 27.7°, 31.1° etc. (Hengzhong Zhang & Banfield, 2000) while the amount of rutile can be revealed by XRD at 27.5°, 36.0° etc. (W. Wang, Gu, Liang, Hamilton, & Wesolowski, 2004). Careful investigation of the XRD spectra showed no traces of brookite or rutile in either S40 or S60, indicating that S40 and S60 are single-phase anatase. This result is in good agreement with a previous study (Daoud & Xin, 2005). Compared with Fig.4-1 (b), it can be seen that the addition of organic acetic acid in a HNO_3-contained aqueous solution may benefit the formation of pure anatase phase at low temperatures. The effect of ethanol to the formation of anatase TiO_2 and its crystal size is not significant based on XRD examinations, which did not show any difference with or without the use of ethanol in our study. Hence, only XRD patterns of S23, S40 and S60 with ethanol are given.

Fig.4-2 also reveals that the peak intensities increase and become sharpened with increasing reaction temperature from room temperature to 60°C, indicating that the crystallization of as-synthesized anatase does become better. In general, the full width at half-maximum (FWHM) of XRD peak corresponds to the crystal size of porous materials. When FWHM is broader, the crystallites exhibit smaller size. It can be seen from Fig. 4-2 that the average size of as-synthesized anatase crystallites increases when the reaction temperatures increase from room temperature to 60°C. This is in agreement with previous study which showed that the size of crystallites obtained at a lower temperature (38°C) is smaller than that obtained at a relatively higher temperature (58°C) (Daoud & Xin, 2005). The results above show that the temperature has a significant effect on the crystallization and crystal size of TiO_2 particles prepared by a sol-gel method. This is also evident from Fig. 4-1 that the average size of the crystallites increases from room temperature to 60°C while the crystallinity of the obtained anatase and brookite particles increases. S23 was transparent and would precipitate in six months. However, S40 and S60 were transparent with a slight blue tint and very stable without sedimentation and delamination for one year. This indicates that anatase phase is more stable than the amorphous phase in acidic condition (Terabe et al., 1994).

4.3.2. TEM observations

The microstructure and size of the grains in the titania film grown on silicon was studied by a plan view TEM. High resolution transmission electron micrographs of S40, S60 and S23 in Fig. 4-3 confirmed earlier observations of phase and size of crystallites. Figs. 4-3 (a, c, e) are bright field low resolution micrographs of S40, S60 and S23, respectively. The insets, located on the top left corner of the images, show the corresponding selected area electron diffraction (SAED). The strongest halo rings and the weakest Debye–Scherrer rings in Fig. 4-3 e (S23) are associated with the amorphous region between the

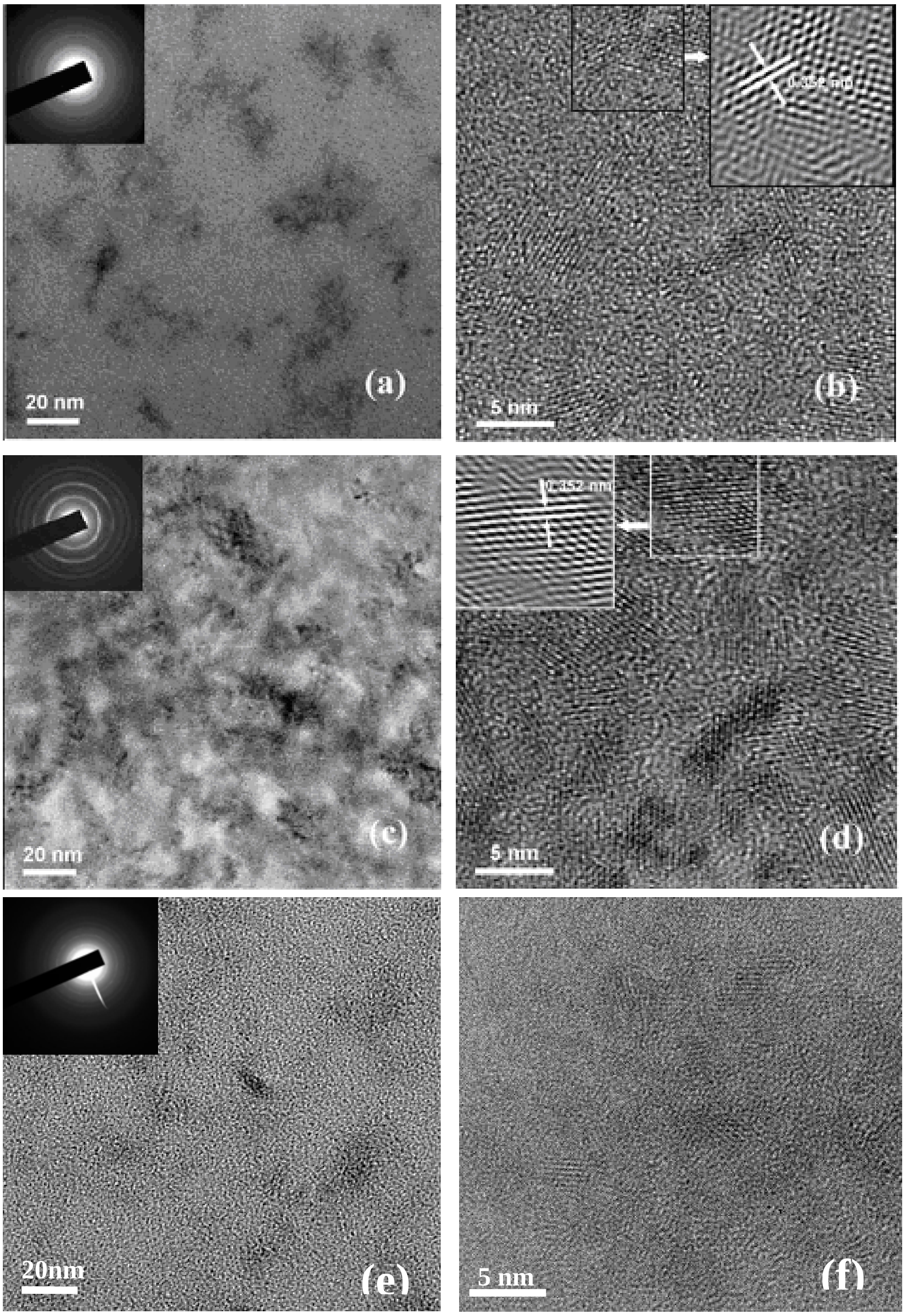

Fig.4-3 Plan view TEM micrographs of (a) S40 at low resolution; inset located on the top left corner is the corresponding selected area electron diffraction (SAED), (b) S40 at high resolution, (c) S60 at low resolution; inset located on the top left corner is the corresponding SAED, (d) S60 at high resolution, (e) S23 at low resolution; inset located on the top left corner is the corresponding SAED and (f) S23 at high resolution.

nanocrystallites. The strong diffuse scattering indicates poor crystallinity. Sharper and more intense Debye–Scherrer rings were observed in Fig. 4-3 c (S60) than those in Fig.4-3 a (S40). This may be attributed to the difference in the size of crystallites as larger crystallites cause the formation of more intense electron diffraction spots. Fig. 4-3 b (S40) and Fig.4- 3 d (S60) show lattice fringes with d-spacing of 0.352 nm and interplanar angle of 82.3°, which are characteristic values of the anatase phase. Intergranular amorphous phase can be seen clearly in Fig. 4-3 f (S23). Extra effort was devoted to find any traces of the brookite phase; however nothing could be found, indicating that S40 and S60 were pure anatase phase.

4.3.3 AFM analysis

Atomic force microscopy of thin films deposited from S23 (Fig. 4-4 a), S40 (Fig. 4-4 b) and S60 (Fig. 4-4 c) by spin film on silicon wafer revealed a low porosity structure and a spherical morphology of the crystallites. The size of grains in the S23 film was the smallest (2–3 nm), followed by that in the S40 film (4-5 nm). The size of grains in the S60 film was the largest (5-7 nm). Aggregation of grains was clearly observed in S23, suggesting that high tendency of clustering is a characteristic property of very small grains. These observations are consistent with the calculated half width of the 101 peaks of S23, S40 and S60 (Fig. 4-2), confirming that the sizes of crystallites are in an ascending order of S23, S40, and S60. Although such a difference in preparation temperature did not affect the phase of formed crystallites, it did have an effect on their size, suggesting that particle size can be tailored by temperature.

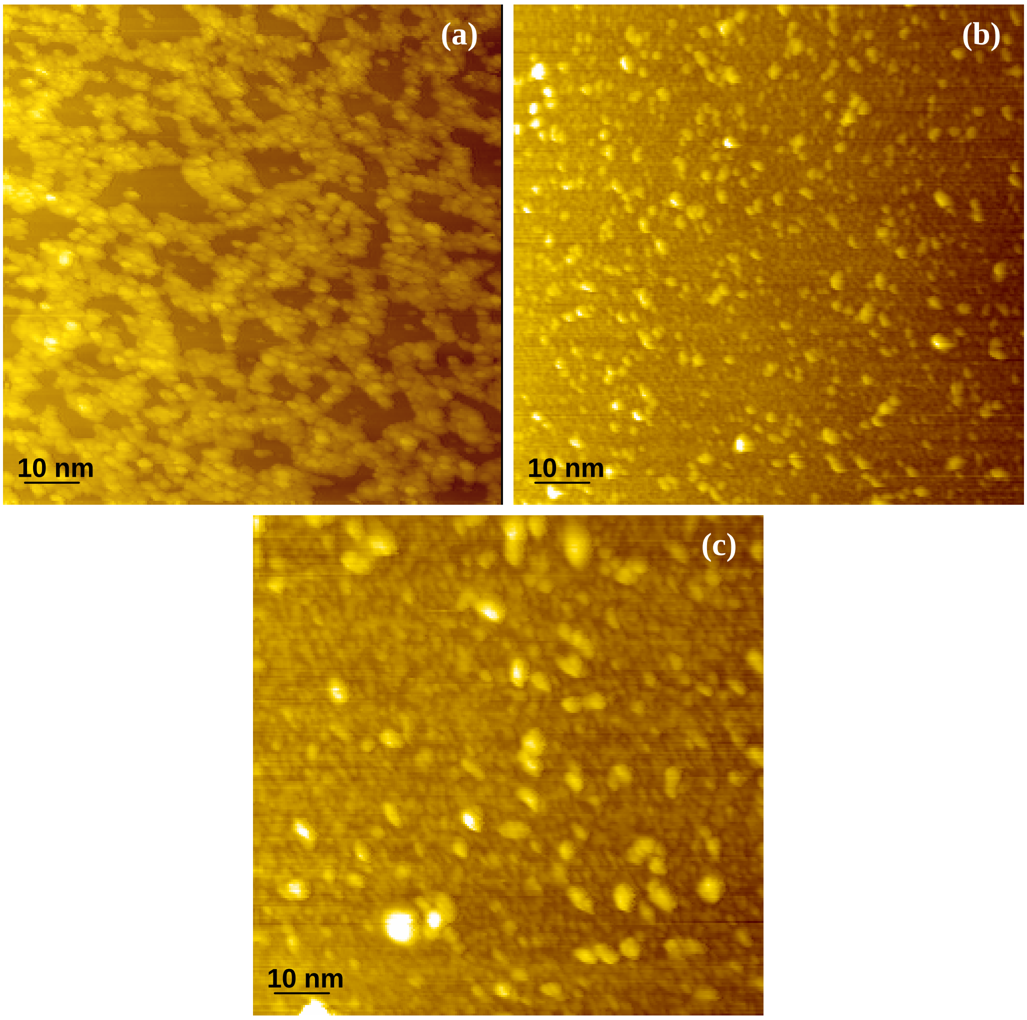

Fig. 4-4 Tapping AFM micrographs of thin films of (a) S23, (b) S40 and (c) S60 coated on silicon wafer.

4.4 Titania treated cotton fabrics

4.4.1 SEM observations

SEM analysis of S23, S40 and S60 films on cotton fibres in Fig. 4-5 shows that

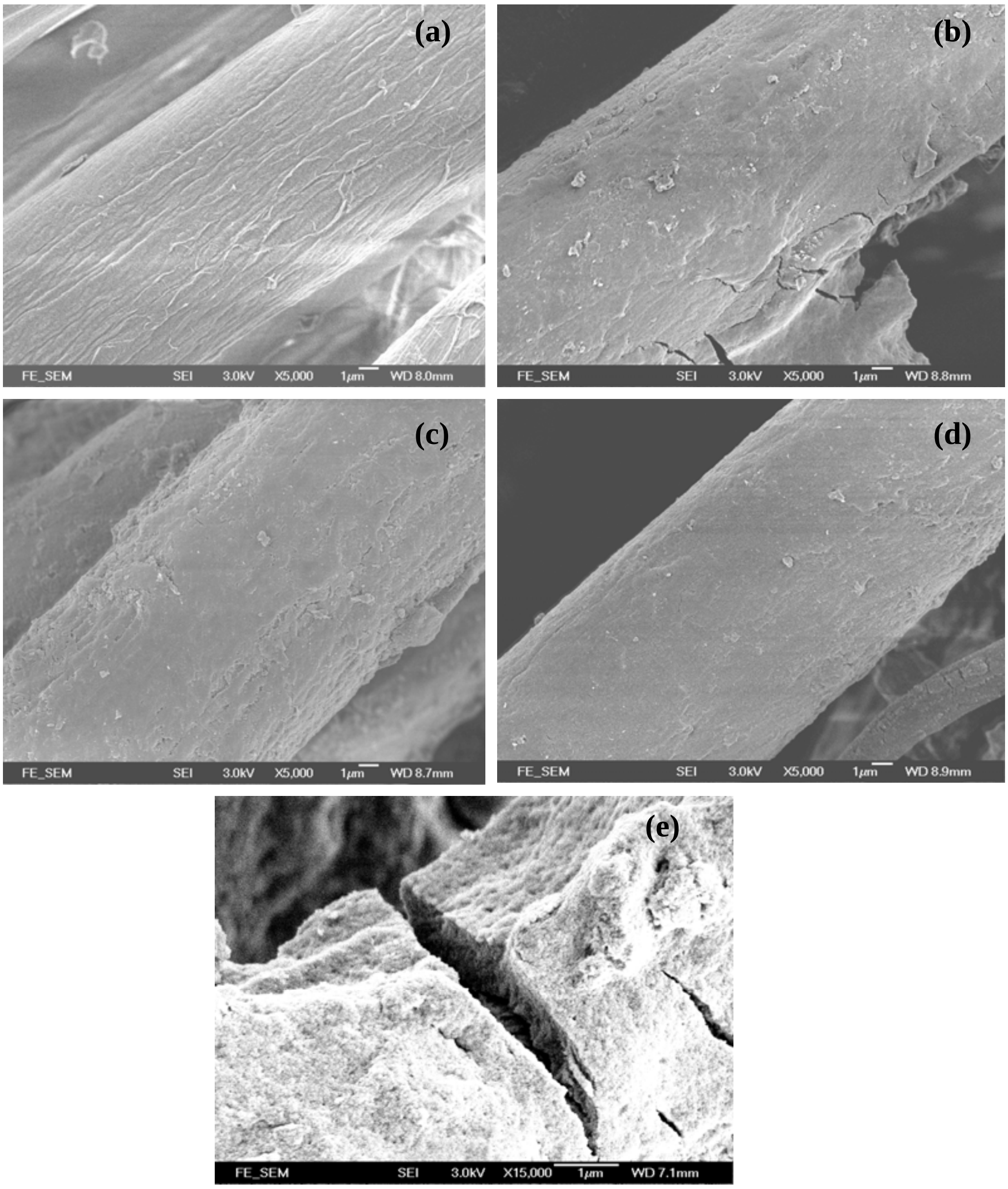

Fig.4-5 SEM images of (a) original cotton fiber, (b) S23 treated cotton fiber, (c) S40 treated cotton fiber, (d) S60 treated cotton fiber and (e) expansion of the cracks region showing inter-fiber sticking between TiO_2 films and cotton and the thickness of the films to be about 200 nm.

the surface structures of the three titania-treated cotton fibres look similar. In contrast to the fibrillous texture of the cotton fibre (Fig.4-5a), the surface structure of these titania treated cotton fibres shows that titania layers have been formed (Fig.4-5 b-d). A high magnification SEM image in Fig. 4-5 e shows that inter-fiber sticking between TiO_2 and cotton was observed and the depth of the crack in the thickness of the titania films on cotton was about 200 nm.

4.4.2 XRD of titania treated cotton fabrics

The crystal phases of titania films on cotton fabrics were studied by XRD. The bulk of the X-ray signal originated from cotton as cotton is the underlying substrate. With the same amount of S23, S40 and S60 TiO_2 films on cotton fabrics, S23 films on cotton do not show a crystalline phase in Fig. 4-6 d. It might be due to the small content of anatase crystallites of small crystalline size. So the peak is very broad and hence intensity is small. On the other hand, sharper anatase peaks with greater intensities at 25.4°, 38.0°, 48.0° of titania treated cotton (Fig.4-6 b, c) are observed evidently in the spectra of S40 and S60 respectively, confirming that higher crystallinity was formed in S40 and S60. From Fig. 4-6, it can be seen that the intensities of the peaks of cotton coated with titania became weaker compared to those of pristine cotton. This may be attributed to titania coatings on cotton which shield the X-ray beam, therefore the intensities of the peaks of cotton coated with titania became weaker.

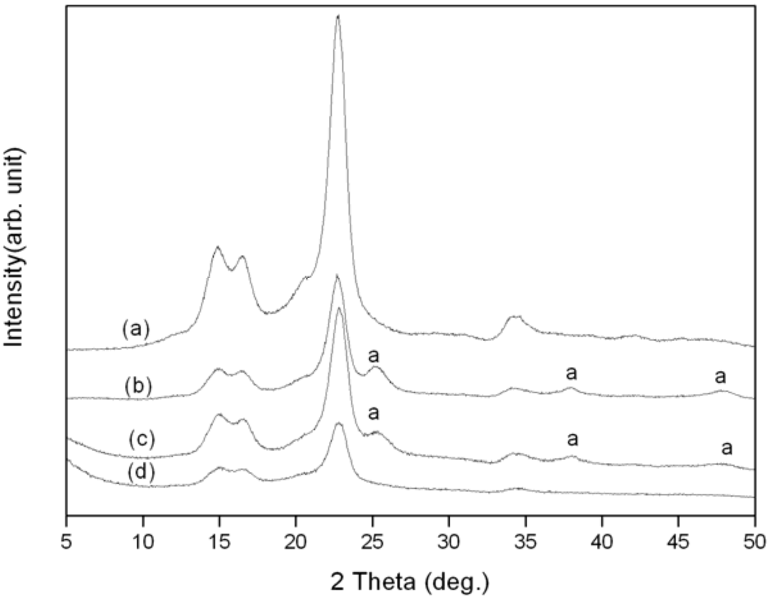

Fig.4-6 XRD patterns of (a) original cotton, (b) S60 treated cotton, (c) S40 treated cotton, (d) S23 treated cotton (a, anatase).

4.4.3 UV-absorption and durability of TiO_2 films on cotton

The UV-absorption property is a natural attribute of TiO_2. Due to the electronic structure of TiO_2, photons with energy of *hv* that matches the band gap energy of TiO_2 can be absorbed (Y. Zhang, Xiong, Yao, Yang, & Fu, 2001). The band gap energy of titania lies in the UV region of the solar spectrum. UPF (Ultraviolet Protection Factor) can directly evaluate the UV-absorption property of the as-prepared products. It is interesting to note that there is a corresponding relation between the absorption intensity of UV radiation and the activity of the photocatalyst (Y. Zhang, Xiong, Yao, Yang, & Fu, 2001). The stronger the UV-absorption intensity, the higher the activity, where the strong absorption intensity implied that more electrons could be promoted from the valence band into the conduction band and more separate electron or holes could be produced, which would help to enhance the photocatalytic activity. Strengthened absorption of UV by nano-TiO_2 results from certain unique effects of nanomaterials, such as quantum-size effect, nanoscale effect and quantum field emission effect (L. Zhang & Mou, 2001), which is beneficial for UV blocking (Yang, Zhu, & Pan, 2004).

The UV absorption study of S23, S40 and S60 treated white woven cotton fabrics revealed a high UPF value of 636.5 (Fig. 4-7 c), 789.5 (Fig. 4-7 d) and 882.5 (Fig. 4-7 e) respectively according to the Australian/New Zealand Standard in contrast to a low UPF value of 6.1 for untreated white cotton fabric (Fig. 4-7 a). These high UPF values of titania treated cotton fabrics belong to an excellent protection classification compared to a low and non-ratable UPF rating of 5 for original white cotton fabric. Of the three treated cotton fabrics, S60 treated fabric showed the highest UPF value, followed by S40 and S23 treated fabrics.

Fig.4-7 also shows that UV transmissions of the S23, S40 and S60 treated cotton fabrics were completely cut off in the UV-B region (280-315 nm). In the spectral UV-A region (315-400 nm), UV transmissions of the three treated cotton fabrics were relatively higher, but they remained much lower than that

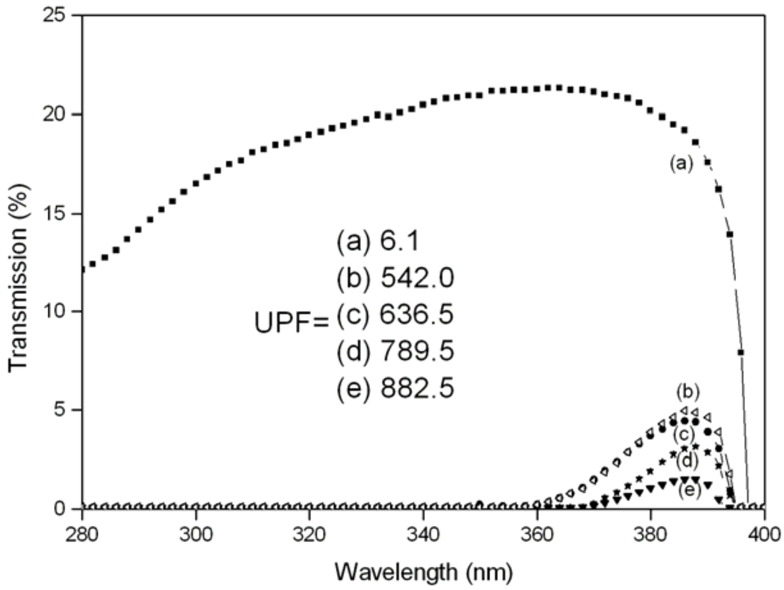

Fig.4-7 UV-absorption of (a) original cotton, (b) S60 treated cotton after 20 washings, (c) S23 treated cotton, (d) S40 treated cotton and (e) S60 treated cotton before washing.

of the original cotton fabric. Of the three treated fabrics, S60 treated fabric showed the lowest UV transmission, followed by S40 and S23 treated fabrics, which means that S60 shows the strongest absorption power, S40 the second strongest, followed by S23. The stronger the UV-absorption, the higher the activity. This is in accord with the XRD study above, which showed that S60 had the highest crystallinity of anatase, therefore it should have the highest photocatalytic activity following the views of previous literature(Y. Zhang, Xiong, Yao, Yang, & Fu, 2001).

The durability of the titania film on cotton was studied by comparing

UV-absorption of S60 treated cotton fabrics before and after 20 washings according AATCC Test Method Test No. 2A at 49±2 °C. For S60 treated cotton fabrics, a high UPF value of 542.0 after 20 home launderings (Fig. 4-7 b) were reproducible which still belongs to an excellent protection classification, although it was lower than the UPF value of 882.5 before washing (Fig. 4-7 e). It can be seen that the transmission of S60 treated cotton fabrics after 20 washings was also completely cut off in the UVB region (280–315 nm) and up to 360 nm in the UVA region due to the UV absorption of TiO_2. Although the transmission of S60 treated cotton fabrics after 20 washings was slightly higher in UVA (315-400 nm) region, it remained much lower than that of original cellulose fibers. These results suggest a high level of adhesion between the titania film and cotton, which may be attributed to the formation of covalent bonding resulting from dehydration reaction between the hydroxyl groups of cotton and the hydroxyl groups of the titania (Daoud & Xin, 2004a; Daoud, Xin, & Zhang, 2005).

4.4.4 Self-cleaning performance

4.4.4.1 Bactericidal activities

Bactericidal activities of original white cotton and S23, S40 and S60 treated white cotton fabrics were quantitatively assessed against a gram positive bacterium, *Staphylococcus aureus* according to a modified procedure of the shaking method (ASTM E2149-01). The UV intensity of the UV lamp used

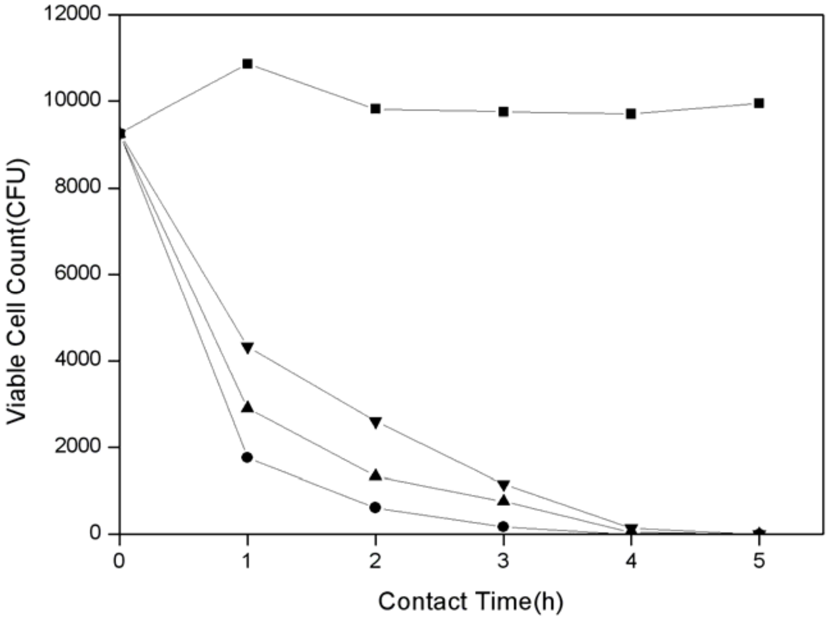

Fig. 4-8 Viable *S. aureus* bacterial count as a function of shaking time while in contact with different substrates: original cotton fabric (■), S60 treated cotton fabric (▼), S40 treated cotton fabric (▲), S23 treated cotton fabric (●).

during the contact period between fabrics and bacteria was 35μW/cm^2.

From Fig.4-8, there are 98-100% viable cell reduction of S60, S40 and S23 treated cotton fabrics irradiated with UV for 4 h, and 100% viable cell reduction for the three specimens after 5 h, which means that the three specimens showed excellent anti-bacterial activities. Furthermore, it can be seen that S23 treated cotton fabrics showed the highest bactericidal activity, followed by S40 and S60 treated cotton fabrics. This may be due to the largest specific surface area of the S25 film as a result of their smallest particle size, surface area of S40 film being the second largest, followed by that of the S60 film, which was showed in Fig. 4-2 XRD pattern, Fig. 4-3 TEM and Fig. 4-4 AFM. The increase of viable bacterial counts in original cotton fabrics in Fig. 4-8 is in line with the fact that cellulosic materials are good media for the growth of bacteria (Neely & Maley, 2000). Under the same experimental conditions, the larger surface area of titania films on substrates might enhance the contact area between the titania film and bacterial cells which may result in a higher bactericidal activity. Previous studies reported that substrates coated with smaller size titania had greater bactericidal activity than those coated with larger size titania, which was also considered to be attributable to a larger specific surface area of the titania films (Daoud & Xin, 2005). Bactericidal activity of titania in the dark to some bacteria and oral microorganisms was also found (Daoud, Xin, & Zhang, 2005; Nagame, Oku, Kambara, & Konishi, 1989). These results suggest that TiO_2 films may not only perform as a bactericidal agent but also as a protective shield to prevent the formation of biofilms of adsorbed bacteria in the dark and light conditions (Daoud, Xin, & Zhang, 2005).

The mechanism of photocatalytic process of TiO_2 involves several steps (Linsebigler, Lu, & Yates, 1995). When TiO_2 is exposed to ultraviolet light (λ<385 nm), the photocatalyst initially generates excited holes (h^+) and excited electrons (e^-) that will migrate to the surface. The hole in the valence band will subsequently react with H_2O or hydroxide ions adsorbed on the surface to produce hydroxyl radicals (OH•), and the electron in the conduction band will reduce O_2 to mainly produce superoxide ions ($O_2^{-}\bullet$), as indicated in Eqs. (1)-(3).

$TiO_2 + h\nu \rightarrow e_{cb}^{-} + h_{vb}^{+}$ (1)

$O_2 + e_{cb}^{-} \rightarrow O_2-\bullet$ (2)

$H_2O + h_{vb}^{+} \rightarrow OH\bullet + H^{+}$ (3)

All of the above reactive oxygen species (ROS) will oxidize the bacteria adsorbed on the TiO_2 surface. Different mechanisms involved in the bactericidal action of TiO_2 photocatalysis have been proposed (Huang et al., 2000; Jacoby, Maness, Wolfrum, Blake, & Fennell, 1998; Lu et al., 2003; Maness et al., 1999; Matsunaga, Tomoda, Nakajima, Nakamura, & Komine, 1988; Matsunaga, Tomoda, Nakajima, & Wake, 1985; Saito, Iwase, & Morioka, 1992; Sunada, Kikuchi, Hashimoto, & Fujishima, 1998; Sunada, Watanabe, & Hashimoto, 2003). Results from the above studies suggest that the initial oxidative damage took place on the cell wall, where the TiO_2 film surface made first contact with intact cells. Cells with damaged cell wall were still viable. After eliminating the protection of the cell wall, the oxidative damage took place on the underlying cell membrane. Photocatalytic action progressively increases the cell permeability, and subsequently allows the free efflux of intracellular contents that eventually leads to cell death. Free TiO_2 particles may also gain access into membrane-damaged cells, and the subsequent direct attack on the intracellular components can accelerate cell death. Since photodegradation of the bacterial cells occurs only when the cells are in contact with the TiO_2 film, a single cell in contact with TiO_2 surface with larger surface area would be killed in a shorter time, as the chance of the cell being damaged by the oxidizing species would be higher. Moreover, the smaller TiO_2 particles may also gain entry into cells faster and thereby promote direct photooxidation of critical cell components (Huang et al., 2000).Therefore, S23 with the largest surface area of TiO_2 film showed the highest bactericidal activity, followed by S40 and S60 treated cotton fabrics.

4.4.4.2 Colorant decomposition activities

Self-cleaning effect of TiO_2 treated white cotton fabrics can also be evaluated by the decomposition of colorants in aqueous solution under UV light irradiation (UV intensity is 1.2-1.3 mW/cm^2). The weight of each fabric sample used was 3g. Neolan Blue 2G was used throughout this study to determine the photocatalytic effect of TiO_2 or modified TiO_2 systems. To confirm the decomposition of colorant by TiO_2 systems, another dye Cibacron Blue F-R was also used in this chapter.

4.4.4.2.1 Neolan Blue 2G

The structure formula of Neolan Blue 2G is shown in Scheme 4-1.

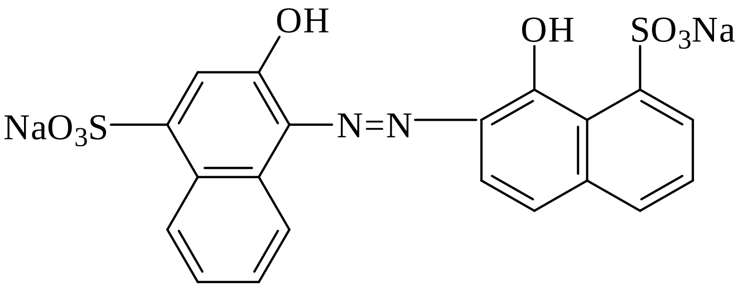

Scheme 4-1 Structure of Neolan Blue 2G

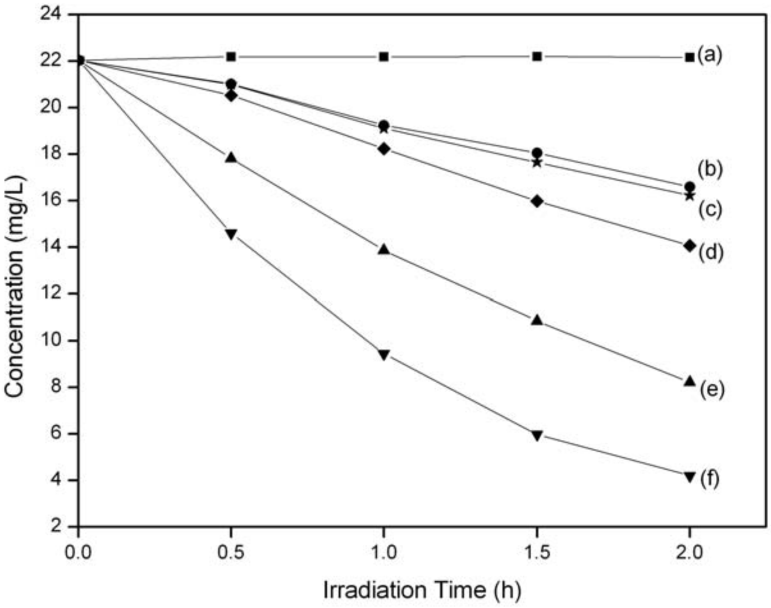

Fig.4-9 Variations in concentration of Neolan Blue 2G in an aqueous solution as a function of UV irradiation time for different substrates: (a) original cotton fabric, (b) S23 treated cotton fabric, (c) S60 treated cotton fabric after 20 washings, (d) S60 treated cotton fabric after 10 washings, (e) S40 treated cotton fabric, and (f) S60 treated cotton fabric before washing.

The decrease in the concentration of the blue colorant Neolan Blue 2G was observed in the following descending order, in aqueous solution containing S60 treated substrates (Fig.4-9f), S40 treated substrates (Fig.4-9e), and S23 treated substrates (Fig.4-9b). Meanwhile the concentration in contact with untreated substrate (Fig.4-9a), remained almost at the same level during UV irradiation. This indicates that S60 treated cotton fabric possesses the strongest decomposition ability for the blue colorant during UV irradiation followed by S40 and S23 treated cotton fabrics, whereas untreated cotton fabric has no colorant decomposition ability. The mechanisms of photocatalytic reaction occurring on titania surface under UV irradiation have been intensively studied in recent years (A. Fujishima, Hashimoto, & Watanabe, 1999; Hagfeldt & Gräetzel, 1995; Hoffmann, Martin, Choi, & Bahnemann, 1995; Mills & Le Hunte, 1997). When TiO_2 is subject to irradiation with UV light, the photon energy generates electron-hole pairs on the TiO_2 surface. The generated electron-hole pairs can induce the formation of reactive oxygen species, such as OH• and O_2^-•. With holes (h^+) and hydroxyl radicals (OH•) generated in the valence band, and electrons and superoxide ions (O_2^-•) generated in the conduction band, TiO_2 can decompose and mineralize organic compound (colorant) by participating in a series of oxidation reactions resulting in carbon dioxide. The molecule of Neolan Blue 2G contains one azo bond (-N=N-), which is more reactive and can be oxided by positive hole, hydroxyl radical, and reduced by electron, superoxide ion (Ganesh, Boardman, & Michelsen, 1994). The discoloration of Neolan Blue 2G indicates that the chromophoric azo bond attached to the naphthalene ring was destroyed. The degradation of aromatic part of the colorant molecule produced a number of intermediate compounds and the total decomposition of these intermediates took longer time.

The photocatalytic activity of titania coatings is related to the crystalline phases of titania, crystallinity, surface area and surface –OH group density and so on. It is believed by most researchers that the titania crystalline phase is the most foundamental and essential property to predict the photocatalytic activity (Ohtani, Ogawa, & Nishimoto, 1997). Anatase with higher crystallinity is beneficial for enhancing the photocatalytic activity since it has relatively little disruption in its electronic band structure and dimishes e^--h^+ recombination (Yanagisawa & Ovenstone, 1999). Therefore, the highest photocatalytic activity of S60 which is considered to be attributed to the highest anatase crystallinity as demonstrated by its sharpest anatase peaks with greatest intensities from the XRD studies in Fig. 4-2 and Fig. 4-6.

The durability of the titania film on cotton was also investigated by comparing the colorant decomposition activities of S60 treated cotton fabrics before and after 10 and 20 washings according AATCC Test Method Test No. 2A at 49±2 °C. Although the rates of the colorant decomposition of S60 treated samples were decreased after 10 washings (Fig.4-9d) and after 20 washings (Fig.4-9c) comparing to that before washing (Fig.4-9f), they remained much higher than that of untreated cotton substrates (Fig.4-9a). Moreover, the colorant concentration of S60 treated cotton substrates after 20 washings was reduced a bit more than that after 10 washings. These results suggest good adhesion between TiO_2 and cotton. This might be attributable to the formation of covalent bonding at their interface as a result of dehydration reactions between the cellulosic hydroxyl groups and the hydroxyl groups of titania (Daoud & Xin, 2004a; Daoud, Xin, & Zhang, 2005). It can also be found that under the same UV irradiation, the colorant concentration in contact with only the cotton substrates without TiO_2 films remained almost at the same level during UV irradiation (Fig. 4-9a), which means that this type of cotton substrates has no colorant decomposition ability and the dye itself would not be decomposed by UV radiation.

Fig.4-10 displays the color changes of Neolan Blue 2G solutions in presence of original white cotton and S60 treated white cotton fabrics before and after UV irradiation. The color of the blue colorant solution was turned into a paler one by S60 treated white cotton fabrics after 2 h of UV irradiation (Fig.4-10 d), compared to that before UV irradiation (Fig.4-10 c) and became colorless after 8 h of irradiation (Fig.7e), whereas the color of the blue colorant solution in contact with original cotton fabrics after 8 h of UV irradiation (Fig. 4-10 b) remained the same as that before UV irradiation (Fig.4-10 a). This means that the blue colorant can be completely discoloured by the titania layers on cotton.

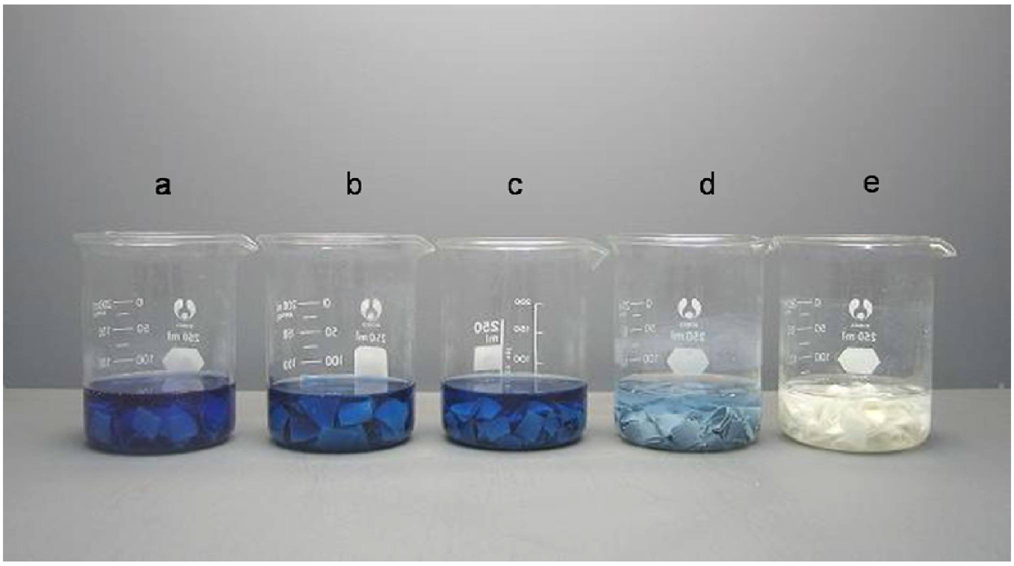

Fig.4-10 Decomposition of Neolan Blue 2G in aqueous solution by white woven cotton fabrics: (a) original cotton before UV irradiation, (b) original cotton after UV irradiation for 8 h, (c) S60 treated before UV irradiation, (d) S60 treated after UV irradiation for 2 h and (e) S60 treated after UV irradiation for 8 h.

4.4.4.2.2 Cibacron Blue F-R

The structure formula of Cibacron Blue F-R is shown in Scheme 4-2.

Fig.4-11 shows the concentration change of the colorant for original cotton and S23, S40 and S60 treated white woven cotton fabrics during UV irradiation. The concentration of the colorant solution containing treated white cotton fabrics decreased in the same descending order as that of Neolan Blue 2G, i.e.

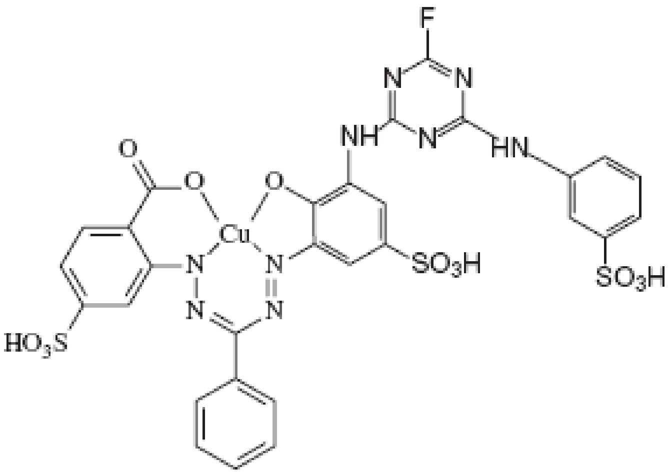

Scheme 4- 2 Structure of Cibacron Blue F-R

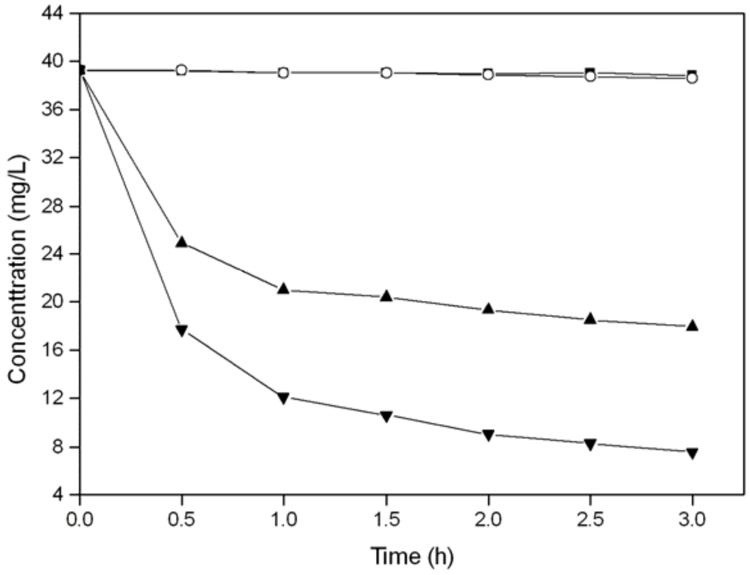

Fig.4-11 Variations in concentration of Cibacron Blue F-R in aqueous solution as a function of UV irradiation time for original cotton fabric (■), S23 treated cotton fabric (○), S40 treated cotton fabric (▲) and S60 treated cotton fabric (▼).

S60 treated cotton fabrics demonstrated the largest decomposition rate of Cibacron Blue F-R followed by S40 and S23. It can be seen that S23 layers oncotton was unable to discolour the dye after the 3 h irradiation. This may be due to predominantly amorphous nature of TiO_2 of S23 which is less photocatalytic active compared to that of the anatase TiO_2. The concentration of the colorant for original cotton fabrics remained at the same level in the entire UV irradiation duration. This further confirmed that cotton fabric alone has no ability to decompose Cibacron Blue F-R, while S60 treated cotton fabric has the strongest ability to decompose the colorant under UV irradiation.

The mechanism of degradation of Cibacron Blue F-R is similar to that of Neolan Blue 2G. The copper formazan chromophore in the colorant is oxidized by positive hole, hydroxyl radical, and reduced by electron, superoxide ion. The degradation of Cibacron Blue F-R suggested that the copper formazan chromophore was destroyed. Similar to the decomposition of Neolan Blue 2G, S60, possessing the highest anatase crystallinity, has the highest photocatalytic activity. Due to the similar results of photo-decomposition compared to Neolan Blue 2G, in later chapters, Cibacron Blue F-R was no longer used.

4.4.4.3 Degradation of red wine stain and coffee stains

Considering that S60 treated cotton fabric showed the best discoloration ability to the dyes, the following stain decomposition test was carried out using S60 treated white cotton fabrics only. Fig. 4-12 and Fig.4-13 present respectively the degradation of a red wine stain and a coffee stain on original white woven cotton and S60 treated white woven cotton fabrics before and after 8 h and 20 h of light irradiation in light exposure and weathering test instrument. The color, area and shape of stains are different on original cotton and titania treated cotton. Titania surface (freshly prepared) on cotton is hydrophobic (Rong Wang et al., 1997; Rong Wang et al., 1998; R. Wang, Sakai, Fujishima, Watanabe, & Hashimoto, 1999) so stains on titania surface spreaded in a smaller area and the color of stains was more intense, while original cotton surface is hydrophilic and the area of stains was larger and the color is lighter.

A significant discoloration of both a red wine stain and a coffee stain on treated cotton fabrics can be observed after 8 h of light irradiation compared to those of the samples before light irradiation and a complete discoloration was observed after 20 h of light irradiation. However, almost no discoloration of a red wine stain or a coffee stain on original white cotton was observed after 8 h even after 20 h of light irradiation. It means that TiO_2 films on cotton fabrics can completely degrade a red wine stain and a coffee stain while original cotton fabrics have no degradation activities for a red wine stain or a coffee stain. Furthermore, the discoloration of a red wine stain and a coffee stain was almost complete on the exposed side of titania treated cotton fabrics after 8 h of light irradiation, however, the color of the wine stain or the coffee stain on

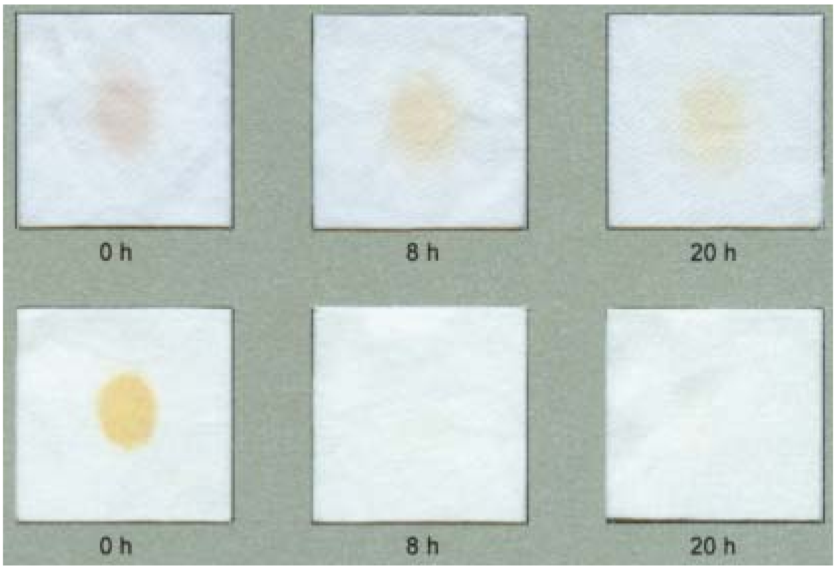

Fig. 4-12 Stain removal test using a red wine. The images shown are the exposed side of original cotton (the upper row) and S60 treated white cotton fabrics (the bottom row) after 0 h, 8 h and 20 h of light irradiation in Xenotest Alpha LM light exposure and weathering test instrument.

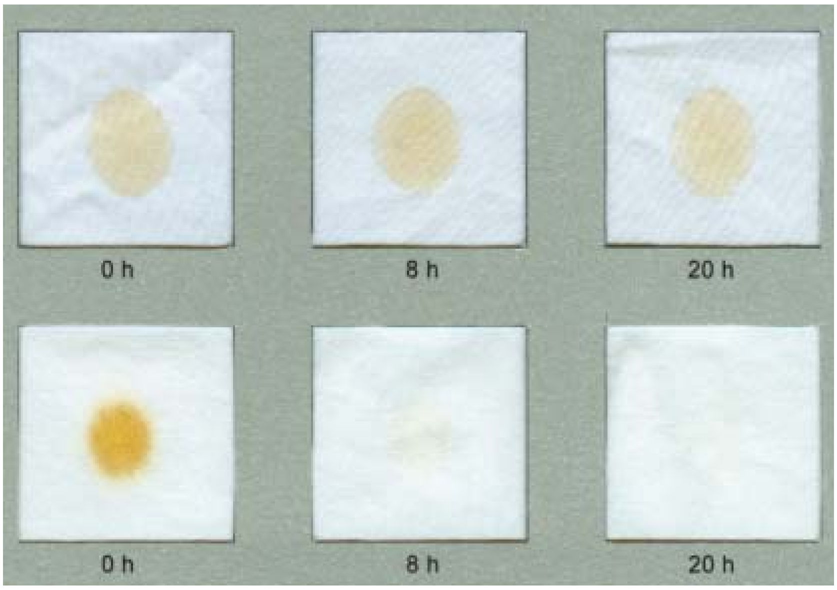

Fig.4-13 Stain removal test using a coffee stain. The images shown are the exposed side of original cotton (the upper row) and S60 treated white cotton fabrics (the bottom row) after 0 h, 8 h and 20 h of light irradiation in Xenotest Alpha LM light exposure and weathering test instrument.

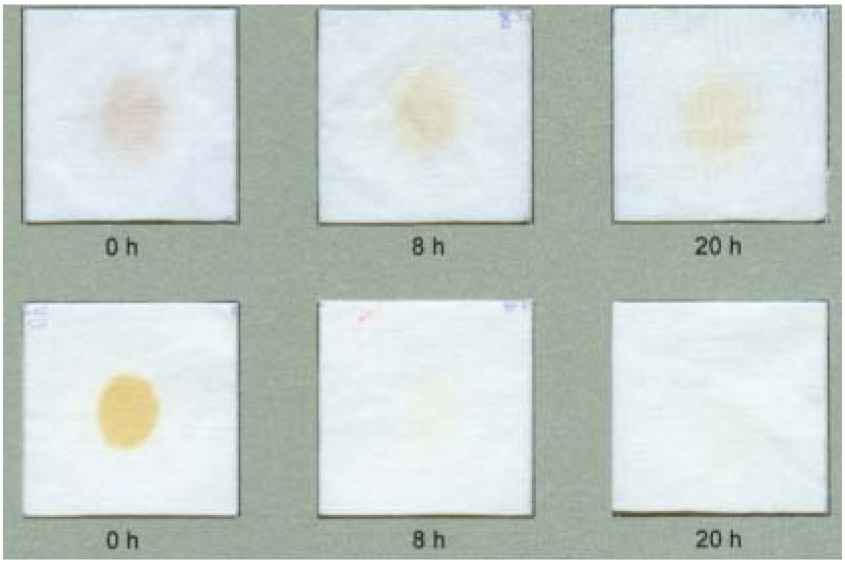

Fig. 4-14 Stain removal test using a red wine. The images shown are the unexposed side of original cotton (the upper row) and S60 treated cotton fabrics(the bottom row) after 0 h, 8 h and 20 h of light irradiation in Xenotest Alpha LM light exposure and weathering test instrument.

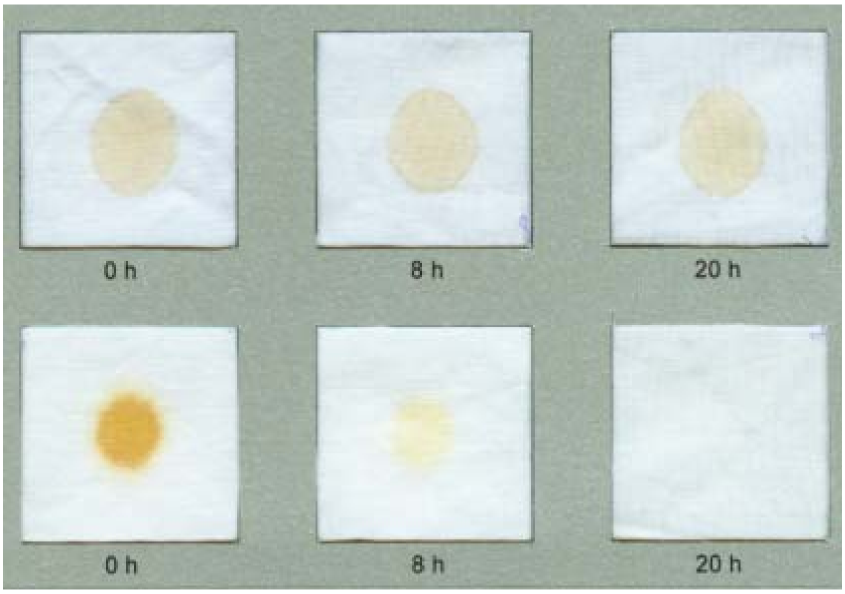

Fig. 4-15 Stain removal test using a coffee stain. The images shown are the unexposed side of original cotton (the upper row) and S60 treated cotton fabrics (the bottom row) after 0 h, 8 h and 20 h of light irradiation in Xenotest Alpha LM light exposure and weathering test instrument.

the unexposed side of titania treated cotton fabrics could still be observed. It can been seen that the wine stain and the coffee stain became colorless on the unexposed titania treated cotton fabrics after 20 h of light irradiation (Fig.4-14 and Fig.4-15).

The mechanism of photodegradation of red wine and coffee stains on TiO_2 treated cotton surface was proposed (A. Bozzi, Yuranova, Guasaquillo, Laub, & Kiwi, 2005; A. Bozzi, Yuranova, & Kiwi, 2005; Yuranova, Mosteo, Bandata, Laub, & Kiwi, 2006). The reactive oxygen species generated on the irradiated S60 TiO_2 surface decomposed red wine and coffee stains adsorbed on TiO_2. Visible light induces an excited state in the wine and coffee pigment (Reaction (1)). Then, this excited state produces an unstable stain cation (Reaction (2)) that further decomposes to CO_2 (Reaction (4)), and concomitantly injects an electron into the conduction band of TiO_2 (Reaction (3)). This leads to the formation of O_2^{-}•. Due to the conduction band electron, the reaction with O_2 leads to the highly oxidative radicals HO_2^{-}•, OH•, RO• and RO_2•, which are able to decompose the stains.

$R + h\nu \rightarrow R^*$ (light absorption) (1)

$R^* \rightarrow R^+ + e_{cb}^-$ (stain cation decomposition) (2)

$e_{cb}^- + O_2(ads) \rightarrow O_2^-$ (oxygen reduction) (3)

$R^+ + O_2 \rightarrow$ degradation products (4)

The direct reaction of the excited pigment of the organic compound (R*) with photo-induced holes (h^+) at later stages of the degradation(Reaction (5)) is possible due to the transparent intermediates produced consisting of carboxylic acid and other colorless organic compound. At this stage, the TiO_2 adsorbs the incoming UV light generating h_{vb}^+.

$R* + h_{vb}^+ \rightarrow R^+\bullet \rightarrow$ degradation products (5)

In reaction (5) the generated holes can react directly with carboxylic acids generating CO_2 through a photo-Kolbe type reaction as shown in Reaction (6) (Kraeutler & Bard, 1978).

$RCOO^- + h_{vb}^+ \rightarrow R\bullet + CO_2$ (6)

4.4.5 Tearing strength property

Table 4-2 shows the tearing strength of original cotton and S60 treated cotton before and after 20 h of light irradiation in Xenotest Alpha LM light exposure and weathering test instrument.

The tearing strength of S60 treated cotton fabrics was reduced by 56.6% in warp direction before irradiation compared to that of original cotton fabrics. This may be attributed to the acidic sol used for the cotton treatment and stiffness of TiO_2 treated cotton fabrics with high add-on of TiO_2. After 20 h of solar simulated irradiation, the tearing strength of both original cotton fabrics and S60 treated cotton fabrics were reduced by 5.7%, and 4.06% respectively. In comparison with the tearing strength of original cotton after light irradiation, the decrease in S60 treated cotton is less severe. This suggests that there was no sign of photocatalytic decomposition of the cellulosic chains of cotton caused by the titania film. On the contrary the titania film can prevent to a small degree drop of tearing strength due to its ability to absorb UV irradiation.

Table 4-2 Tearing strength study in warp direction

Samples	**Tearing Strength (N)**		**Reduction (%)**
	Before light irradiation	**After 20 h light irradiation**	
Original cotton	17.6	16.6	5.7
Titania treated cotton	7.63	7.32	4.06

4.5 Conclusions

Nanocrystalline anatase films were prepared on cotton fabrics by a near room temperature sol–gel process. The anatase nanocrystallite coated fabrics showed significant self-cleaning performance as demonstrated by their bactericidal activities, colorant decomposition and degradation of red wine and coffee stains under UV irradiation. The UV absorption by the titania film was quite substantial, providing excellent UV protection to the treated cotton. No photodegradation of the cellulosic chains of cotton by the titania film could be observed as demonstrated by a comparison study of the tearing strength of treated cotton fabrics before and after prolonged solar-simulated light irradiation.

Chapter 5: The Application of Titania Nanoparticles to Polyester Fabrics

5.1 Introduction

Polyester textile fabrics have found widespread applications in apparel, home furnishings and so on. Improving their properties, especially functional properties, is important for their added values. When applying TiO_2 to polyester textile products which may likely be subject to frequent washing, it is necessary to improve the adhesion between the TiO_2 and polyester as it is known that the adhesion between TiO_2 and polyester is not good because of the lacking of chemical bonding. To improve the adhesion, surface treatments for altering the chemical and physical properties of the polyester surface may be needed. Low temperature plasma (LTP) pretreatment of polyester surface is one of the techniques to improve the bondability of TiO_2 on polyester fibers. The surface pretreatment only modifies the outmost surface layers of polymers without affecting the bulk properties (Kinloch, 1987) and the modifications are dependent on the composition of gaseous medium and the processing parameters. These two factors are important with regard to the increase of the adhesion to the titania. The use of direct current (DC) glow discharge plasma was the most successful approach for an improvement in polymer surface reactivity(Friedrich et al., 1993) compared to radio frequency (RF) plasma and microwave (MW) plasma. Oxygen gas is the most widely used gas in plasma treatment (Carlotti & Mas, 1998; Chen, Wang, & Tomiji, 1999; Norihiro

Inagaki, Narushim, Tuchida, & Miyazaki, 2004; Petasch, Rauchle, Walker, & Elsne, 1995) leading to the introduction of negative groups COO^{-} ,$-O-O^{-}$ onto polyester surface and it was reported that (Carlotti & Mas, 1998; Chen, Wang, & Tomiji, 1999; Norihiro Inagaki, Narushim, Tuchida, & Miyazaki, 2004; Petasch, Rauchle, Walker, & Elsne, 1995) oxygen plasma gives the most oxygenated polyester surface, which results in better adhesion. The TiO_2 can be attached to the modified polyester surface through ionic attraction with the positively treated Ti^{4+} of TiO_2.

Considering the aforementioned views, oxygen gas was used in low temperature plasma pretreatment of polyester surface to improve the wettability of polyester to the titania sol and the adhesion of titania layers to polyester textiles in this part of the work. Only S60 anatase sol in Chapter 4 was applied to polyester fabrics owing to its highest photocatalytic activity. S60 was prepared by a sol-gel process in an acidic aqueous medium at a low temperature of 60 °C, and then TiO_2 thin layers were coated on LTP-pretreated polyester fibers by a dip-pad-dry-cure process. The self-cleaning performance of the functionalized polyester, including their bactericidal activity, ability to decompose organic materials and stains, such as red wine and coffee stains was carefully investigated.

5.2 Preparation of TiO_2 sol

10 ml titanium tetraisopropoxide (Aldrich, 97%) was added dropwise into 100 ml deionized water containing 1 ml nitric acid (Aldrich, 70%) and 10 ml acetic acid (Aldrich, 97%) under vigorous stirring. The mixtures were heated to 60 °C and kept at that temperature for 16 hours while being stirred.

5.3 Characterization of TiO_2 nanoparticles

5.3.1 SEM analysis

Fig. 5-1 shows the representative SEM micrographs of polyester fiber surfaces before and after oxygen plasma treatment, and the plasma-treated surface before and after TiO_2 coating. It can be seen that the surface etching process occurs on the surface of oxygen plasma pretreated fiber. Granules, micro-craters and ripple-like structures of sub-micrometer size are observed on the oxygen plasma pretreated surface (Fig.5-1 b) (Carlotti & Mas, 1998; Norihiro Inagaki, Narushim, Tuchida, & Miyazaki, 2004). The removal of the surface layers leads to an increase in the roughness and the roughness of this surface is far more accentuated than that of the original fiber surface (Fig.5-1 a). In contrast to the original polyester filament, the surface structure of the TiO_2-coated polyester filament pretreated with oxygen plasma indicates the formation of TiO_2 layers (Fig.5-1 c, d). It is noted that the surface structure of the TiO_2-coated polyester filament without oxygen plasma pretreatment is similar to that of TiO_2-coated polyester filament pretreated with oxygen plasma

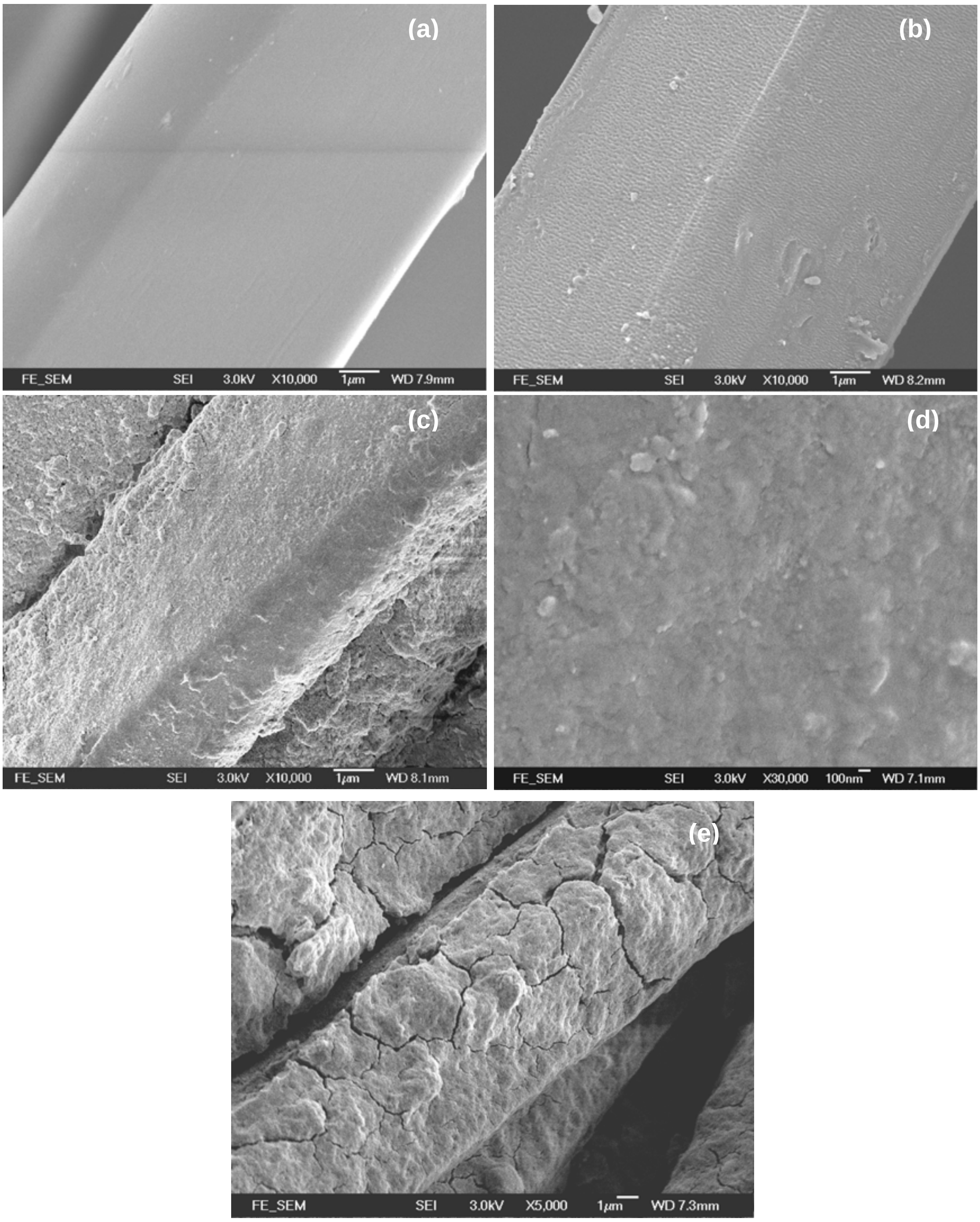

Fig.5-1 SEM images of (a) original polyester filament, (b) oxygen plasma pretreated polyester filament, (c) TiO_2 coated polyester filament pretreated with oxygen plasma, (d) TiO_2 coated polyester filament pretreated with oxygen plasma at high resolution and (e) the cracks showing inter-fiber sticking between TiO_2 and polyester and the thickness of the films to be about 150 nm.

and hence it is not shown in Fig. 5-1. A high magnification SEM image in Fig. 5-1 e shows that inter-fiber sticking between TiO_2 and polyester filament was observed and the depth of the crack in the thickness of the titania films on cotton was about 150 nm.

5.3.2 XPS analysis

The change in the chemical composition on the polyester surfaces occurring in the oxygen plasma pretreatment process and the relative amount of TiO_2 deposited on polyester surface without and with oxygen plasma pretreatment were investigated by XPS. Table 5-1 shows the atom composition of polyester surface before and after oxygen plasma pretreatment, and the atom composition of TiO_2 coated polyester surface without and with oxygen plasma pretreatment. From a semi-quantitative comparison of relative atomic percentages of oxygen and carbon on the polyester filament surface before and after the oxygen plasma pretreatment, it was found that oxygen plasma pretreatment led to an increase in oxygen concentration and a decrease in carbon concentration due to the plasma oxidation of polyester substrates, thus indicating the creation of oxygenic functional groups (-CO-, COO-) on the polyester filament surface (Chen, Wang, & Tomiji, 1999; N. Inagaki, Tasaka, & Shimada, 2000). From the relative element content in the TiO_2 coated polyester surface without and with oxygen plasma pretreatment shown in Table 5-1, it can be seen that Ti percentage in TiO_2 coated polyester surface with oxygen

Table 5-1 Atom composition of original polyester surface, oxygen plasma pretreated polyester surface, TiO_2 coated polyester surface without oxygen plasma pretreatment and TiO_2 coated polyester surface pretreated with oxygen plasma

Samples	**Surface composition (at. %)**		
	C	O	Ti
Original polyester	73.2	26.8	-
O_2 plasma pretreated polyester	70.0	30.0	-
TiO_2 coated polyester without oxygen plasma pretreatment	33.6	49.8	16.6
TiO_2 coated polyester with oxygen plasma pretreatment	25.7	56.0	18.3

plasma pretreatment was 18.3%, which was higher than that in TiO_2 coated polyester surface without oxygen plasma pretreatment (16.6%). This means that oxygen plasma pretreated polyester surface is beneficial to the formation of TiO_2 coating and the quantity of TiO_2 on polyester filament pretreated by oxygen plasma is increased. This is considered to be attributable to the increase in the roughness of polyester filament surface (Carlotti & Mas, 1998) shown in SEM micrographs above and the introduction of negative groups COO^-, $-O-O^-$ at polyester surface (Chen, Wang, & Tomiji, 1999) to which TiO_2 can attach through ionic attraction with the positively charged Ti^{4+} of TiO_2 (A. Bozzi, Yuranova, & Kiwi, 2005).

5.3.3 XRD patterns

In Chapter 4, single-phase anatase TiO_2 sol was prepared by a sol-gel process at 60°C and single-phase anatase layers were obtained on cotton substrates. In the present work, we confirmed that the single-phase anatase TiO_2 layers were formed on polyester substrates. The crystal phase of the TiO_2 layers on polyester substrates was identified by XRD. In the profiles, the broad features as well as the strong diffraction peaks at 17.8°, 22.8° and 25.4° are originated from original polyester substrates. Weak peaks at 38.0° and 48.0° are observed

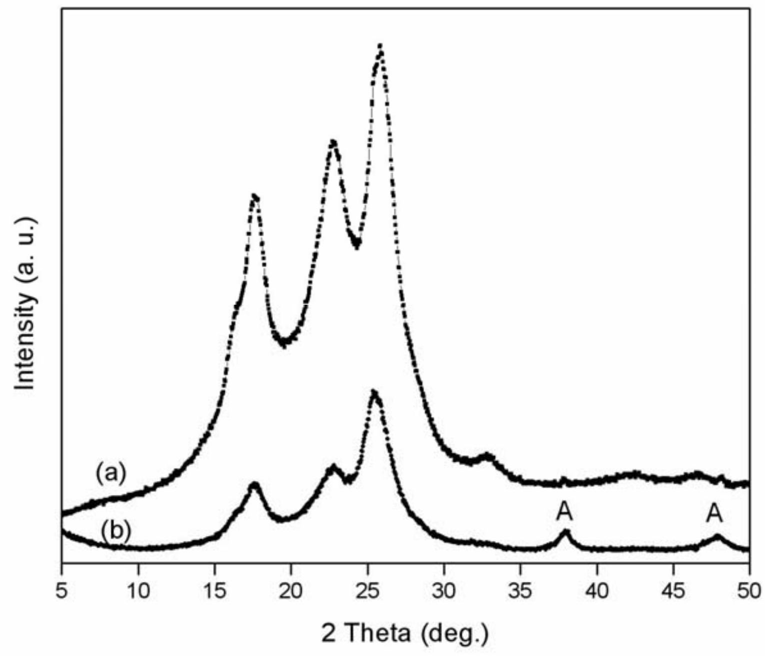

Fig. 5-2 XRD patterns of (a) original polyester and (b) TiO_2 coated polyester pretreated with oxygen plasma (A: anatase).

in the TiO_2 coated polyester pretreated with oxygen plasma (Fig.5-2 b). The peak of anatase phase at 25.4° was not observed in Fig. 5-2b which may be attributed to the peak overlapped with the strong diffraction peak of polyester at 25.6°. These peaks at 38.0° and 48.0° match well with these observed in the anatase phase TiO_2, indicating that nanocrystalline TiO_2 of anatase phase has been formed on polyester substrates. It is well accepted that anatase has the highest photoactive among the crystalline phases of TiO_2 (Kato et al., 1994). Therefore, the single-phase anatase layers on polyester should have high photocatalytic activity. As the XRD pattern of the TiO_2-coated polyester filament without oxygen plasma pretreatment is almost the same as that of TiO_2-coated polyester filament pretreated with oxygen plasma, it is not shown in Fig.5-2.

5.3.4 Raman spectroscopy

The crystal phase of the TiO_2 layers on polyester substrates was confirmed by Raman spectroscopy. It is well known that XRD usually reveals the long-range order of materials and gives average structural information within several unit cells. Raman scattering as a local probe is very sensitive to crystallinity and microstructures of materials. Fig. 5-3 shows the Raman spectra of original polyester and TiO_2 coated polyester pretreated with oxygen plasma. The Raman peaks at 128, 143, 280, 633, and 704 cm^{-1} are originated from original polyester substrates. The Raman peaks in Fig. 5-3 (b) at 398 and 520 cm^{-1} are

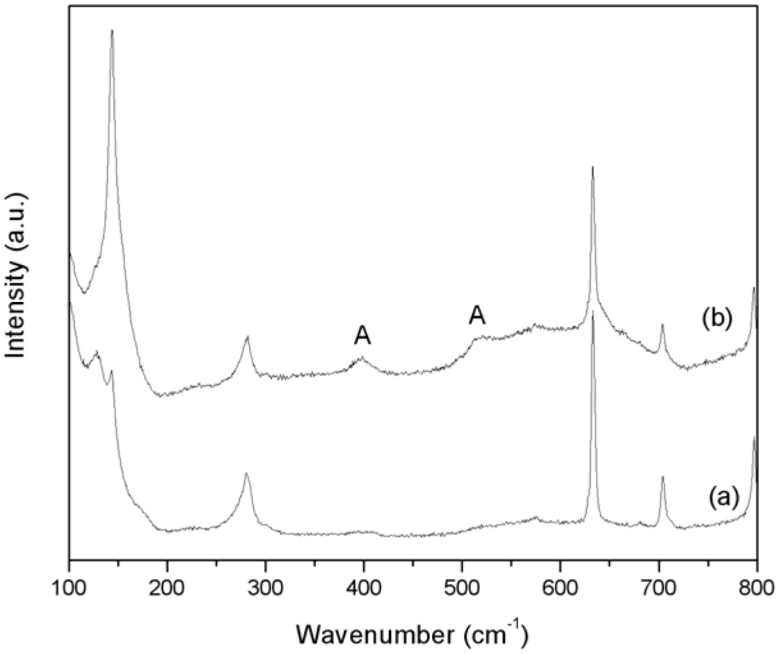

Fig. 5-3 Raman spectra of (a) original polyester and (b) TiO_2 coated polyester pretreated with oxygen plasma (A: anatase).

observed in the TiO_2 coated polyester pretreated with oxygen plasma, which can be assigned as the anatase phase. The Raman peaks at 154 and 636 cm^{-1} of TiO_2 coated polyester in Fig. 5-3 (b) overlapped with the Raman peaks of original polyester substrates at 143 and 633 cm^{-1}. This indicates that TiO_2 nanocrystals of anatase phase have been formed on polyester substrates. Such an observation is consistent with the XRD result shown in Fig. 5-2. The Raman spectrum of the TiO_2-coated polyester filament without oxygen plasma pretreatment is almost the same as that of TiO_2-coated polyester filament pretreated with oxygen plasma and hence it is not shown in Fig.5-3.

5.4 UV absorption

Fig. 5-4 presents the UV absorption of the oxygen plasma pretreated polyester substrate, TiO_2 coated polyester substrate without oxygen plasma pretreatment and TiO_2 coated polyester substrate pretreated with oxygen plasma according to the Australian/New Zealand Standard. Oxygen plasma pretreated polyester substrate (Fig.5-4a) had a low UPF value of 107.9 and the transmission in UV-A range (315-400 nm) was about 19%. TiO_2 coated polyester substrate without oxygen plasma pretreatment (Fig.5-4b) revealed a UPF value of 259.7 which was higher than that of oxygen plasma pretreated polyester one, and the transmission in the UV-A range was about 14% which was lower than that of

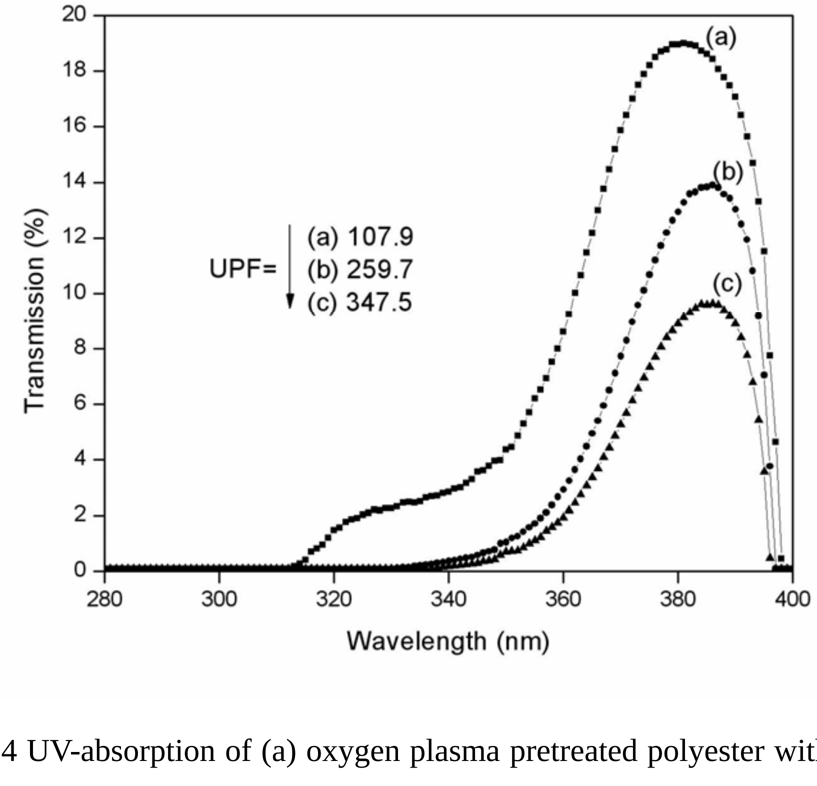

Fig.5-4 UV-absorption of (a) oxygen plasma pretreated polyester without TiO_2 coating, (b) TiO_2 coated polyester without oxygen plasma pretreatment and (c) TiO_2 coated polyester pretreated with oxygen plasma.

the oxygen plasma pretreated polyester. On the other hand, TiO_2 coated polyester substrate pretreated with oxygen plasma (Fig. 5-4c) demonstrated the highest UPF value of 347.5 among the three substrates and the transmission of the substrate in the UV-A range was less than 10% which was the lowest. This may be attributed to greater deposition of TiO_2 particles on polyester surface resulting from the increase in the roughness (Carlotti & Mas, 1998) demonstrated in SEM above and the introduction of negative groups COO^-, $-O-O^-$ onto polyester surface (Chen, Wang, & Tomiji, 1999) shown in XPS above after oxygen plasma pretreatment. These results indicate that TiO_2 coated polyester substrate can provide excellent protection classification, and a higher UPF and stronger UV absorption power are achieved after oxygen plasma pretreatment. The stronger UV-absorption implies the higher photoactivity as shown in the previous chapter. Therefore, TiO_2 coated polyester substrate pretreated with oxygen plasma would have higher photocatalytic activity than TiO_2 coated polyester substrate without oxygen plasma pretreatment.

5.5 Self-cleaning performance

5.5.1 Bactericidal activities

Fig.5-5 displays the bactericidal activities under UV irradiation (UV intensity was about 35 $\mu W\ cm^{-2}$) of oxygen plasma pretreated polyester without TiO_2 coating, TiO_2 coated polyester without oxygen plasma pretreatment and TiO_2

coated polyester with oxygen plasma pretreatment according to a modified procedure of the shaking method (ASTM E2149-01) (Daoud, Xin, & Zhang, 2005), in which a gram positive bacterium, *Staphylococcus aureus (S. aureus)* was used to assess the activities. It is readily seen from Fig.5-5 that the oxygen plasma pretreated polyester substrate without TiO_2 coating showed almost no bacteria reduction within 5 h under UV irradiation, which indicates that polyester substrates possess no bactericidal activity and *S. aureus* itself would not be killed by the UV radiation. On the other hand, *S. aureus* was completely killed on TiO_2 coated polyester without oxygen plasma pretreatment and TiO_2 coated polyester substrate pretreated with oxygen plasma within 5 h under UV irradiation, which means that the TiO_2 coated polyester substrates possess bactericidal activities under UV irradiation. Furthermore, it can be seen that TiO_2 coated polyester substrate pretreated with oxygen plasma showed higher bactericidal activity than TiO_2 coated polyester without oxygen plasma pretreatment. This may be due to greater deposition of TiO_2 particles on polyester surface after oxygen plasma treatment and in turn nullify the viable bacteria.

The bactericidal mechanism of TiO_2 coated polyester under UV irradiation is the same as that described in Chapter 4. The reactive oxygen species generated on the irradiated TiO_2 surface decomposed the cell wall and the cell membrane, which resulted in the increase in the permeability of cells, the leakage of

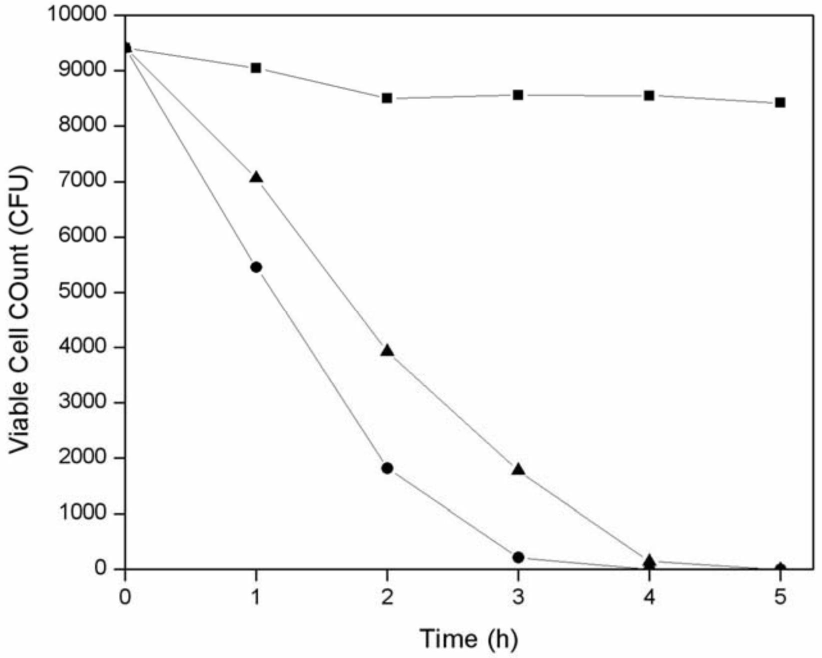

Fig.5-5 Viable *S. aureus* bacterial count as a function of UV irradiation time for oxygen plasma pretreated polyester substrate (■), TiO_2 coated polyester without oxygen plasma pretreatment (▲) and TiO_2 coated polyester with oxygen plasma pretreatment (●).

intracellular molecules and the final death of cells (Huang et al., 2000; Lu et al., 2003). Due to the increase in the roughness and introduction of negative groups COO^-, $-O-O^-$ onto polyester surface, greater deposition of TiO_2 particles on polyester surface with oxygen plasma pretreatment led to a stronger UV absorption as shown in Fig. 5-4, and the increase in the amount of TiO_2 available to participate in the photocatalytic reaction, more oxidizing species can be generated and used to kill the bacterial cells (J. C. Yu et al., 2002) which promotes more efficient oxidation of the bacterial cells when compared with

TiO_2 coated polyester without oxygen plasma pretreatment under UV irradiation. Therefore, TiO_2 coated polyester with oxygen plasma pretreatment showed higher bactericidal activity.

5.5.2 Decomposition activities towards colorant

The decomposition activities of different polyester substrates for the colorant, Neolan Blue 2G, were investigated under UV irradiation (The intensity of UV-A was 0.7–0.8 mW cm^{-2}) as shown in Fig.5-6. The weight of each fabric sample used was 3g. The durability of TiO_2 layers on polyester was evaluated by repeated washing following the AATCC Test Method 61-2003 Test No. 2A. The washing was carried out at 49±2 °C for 45 min, which was equivalent to five times of repeated home washing.

It can be seen that the colorant concentration was reduced more markedly by TiO_2 coated polyester substrate with oxygen plasma pretreatment (Fig.5-6 e) under UV irradiation (UV-A intensity was 1.2–1.3 mW cm^{-2}) compared to that by TiO_2 coated polyester substrate without oxygen plasma pretreatment (Fig.5-6 d). This indicates that TiO_2 coated polyester substrate pretreated with oxygen plasma has higher colorant decomposition activity than TiO_2 coated polyester substrate without oxygen plasma pretreatment. This may be attributed to the increase in the roughness (Carlotti & Mas, 1998) and introduction of negative groups COO^{-}, $-O-O^{-}$ onto polyester surface (Chen, Wang, & Tomiji, 1999) which allow for greater deposition of TiO_2 particles on polyester surface. Under the same UV irradiation, the colorant concentration in contact with only oxygen plasma pretreated polyester substrate without TiO_2 coating remained almost at the same level during UV irradiation (Fig.5-6 a), which means that this type of polyester substrate has no colorant decomposition ability and the dye itself would not be decomposed by UV radiation. It can also be found that the TiO_2 layers on oxygen plasma pretreated polyester substrates after washing (Fig.5-6 c) possess better photocatalytic activity than that of TiO_2 coated polyester substrate without plasma pretreatment (Fig.5-6 b) and of polyester substrate without TiO_2 coating. (Fig.5-6 a). This indicates better adhesion between TiO_2 layers and oxygen plasma pretreated polyester, which is in line with previous studies discussing adhesion improvement after plasma treatment (Carlotti & Mas, 1998; Friedrich et al., 1993; Krump, Šimor, Hudec, Jaššo, & Luyt, 2005; Petasch, Rauchle, Walker, & Elsne, 1995).

The mechanism of degradation of Neolan Blue 2G is same as that of Neolan Blue 2G in Chapter 4. The reactive oxygen species generated on the irradiated TiO_2 surface decomposed the colorant. The increase in the roughness and introduction of negative groups COO^-, $-O-O^-$ onto polyester surface which allowed for greater deposition of TiO_2 particles on polyester surface with oxygen plasma pretreatment resulted in the increase in the amount of TiO_2

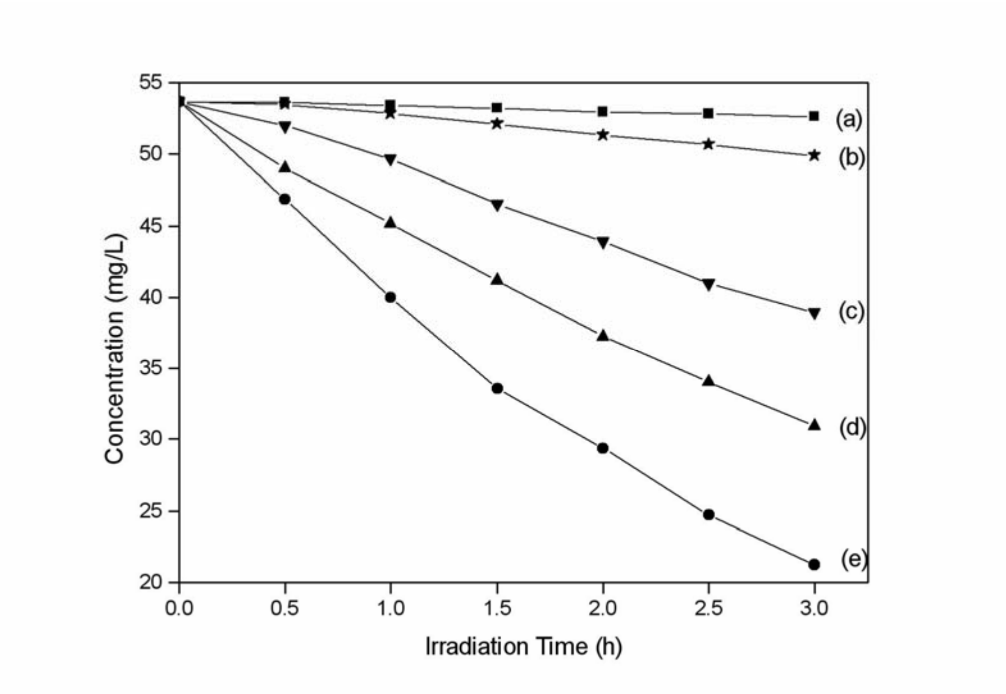

Fig.5-6 Variations in concentration of Neolan Blue 2G in an aqueous solution as a function of UV irradiation time for (a) oxygen plasma pretreated polyester substrate, (b) TiO_2 coated polyester without oxygen plasma pretreatment after washing, (c) TiO_2 coated polyester with oxygen plasma pretreatment after washing, (d) TiO_2 coated polyester without oxygen plasma pretreatment before washing and (e) TiO_2 coated polyester with oxygen plasma pretreatment before washing.

available to participate in the photocatalytic reaction, and thus more reactive oxygen species can be generated on TiO_2 surface on polyester with oxygen plasma pretreatment to promote oxidation of the colorant when compared with TiO_2 coated polyester without oxygen plasma pretreatment under UV irradiation. Therefore, TiO_2 coated polyester with oxygen plasma pretreatment showed higher photocatalytic activity.

5.5.3 Degradation of red wine and coffee stains

Fig.5-7 presents the degradation of red wine and coffee stains on oxygen plasma pretreated white polyester without TiO_2 coating, TiO_2 coated original white polyester substrates and TiO_2 coated white polyester substrates pretreated with oxygen plasma before and after light irradiation in Xenotest Alpha LM light exposure and weathering test instrument. The color, area and shape of stains on oxygen plasma pretreated polyester without TiO_2 coating and TiO_2 coated polyester substrates are different due to the hydrophilic polyester surface by oxygen plasma treatment (Chen, Wang, & Tomiji, 1999) and the hydrophobic titania surface (Rong Wang et al., 1997; Rong Wang et al., 1998; R. Wang, Sakai, Fujishima, Watanabe, & Hashimoto, 1999).

It can be seen that a red wine stain and a concentrated coffee stain on both TiO_2 coated original white polyester substrates (Fig.5-7 (1)b, (2)b) and TiO_2 coated polyester substrates pretreated with oxygen plasma (Fig.5-7 (1)c, (2)c) were discolored significantly after 1h and 5 h of light irradiation respectively. However, the red wine and coffee stains on TiO_2 coated polyester substratespretreated with oxygen plasma were discolored more markedly than those on TiO_2 coated original white polyester substrates after 1h and 5 h of light irradiation, respectively. This indicates that TiO_2 coated polyester substrate pretreated with oxygen plasma has better stain degradation activity than TiO_2 coated polyester substrate without oxygen plasma pretreatment,

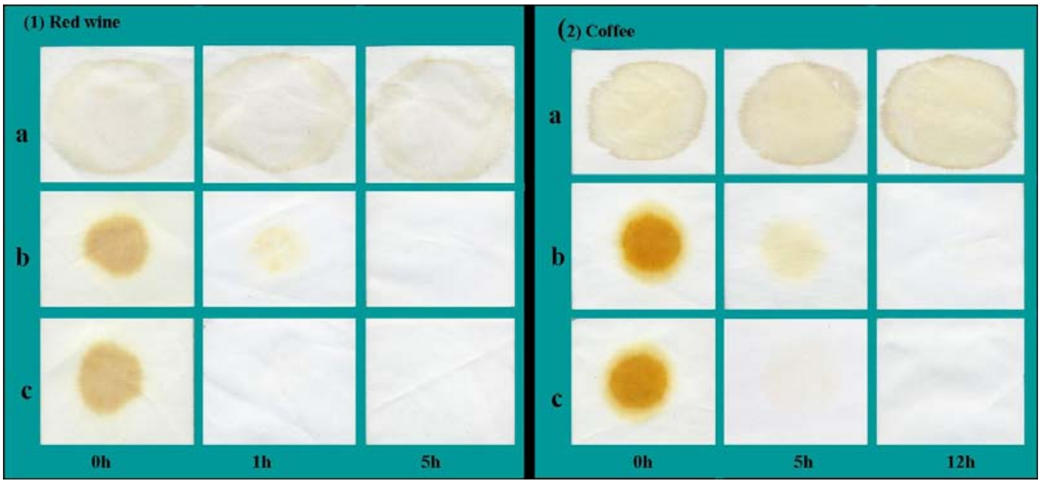

Fig. 5-7 Stain removal test using (1) a red wine stain and (2) a coffee stain. The images shown are the exposed sides of only oxygen plasma pretreated polyester substrates (1a, 2a), titania coated original polyester substrates (1b, 2b) and titania coated polyester substrates pretreated with oxygen plasma (1c, 2c) in Xenotest Alpha LM light exposure and weathering test instrument.

which is in accordance with the results of the colorant decomposition activity shown in Fig.5-6. Furthermore, it can be seen that a complete discoloration of red wine and coffee stains on both TiO_2 coated polyester substrate without oxygen plasma pretreatment and TiO_2 coated polyester substrate with oxygen plasma pretreatment was achieved after 5 h and 12 h of light irradiation respectively. It indicates that TiO_2 layers on polyester substrates can completely discolor red wine and coffee stains after prolonged light irradiation. On the other hand, almost no discoloration of a red wine and a coffee stain on oxygen plasma pretreated polyester without TiO_2 coating (Fig.5-7 (1)a, (2)a) was observed after the light irradiation, which further confirms that polyester substrates without TiO_2 coating have no photocatalytic activity. It is interesting to note that a complete discoloration of red wine and coffee stains on the unexposed sides of titania coated original polyester substrates and TiO_2 coated oxygen plasma pretreated polyester substrate was achieved after 5 h and12 h of light irradiation, respectively.

The mechanism of degradation of red wine and coffee stains on S60 TiO_2 treated polyester fabrics is same as that on TiO_2 treated cotton fabrics described in chapter 4. Red wine and coffee stains were decomposed by the reactive oxygen species generated on the irradiated TiO_2 surface.

5.6 Tearing strength property

Table 5-2 shows the tearing strength of original polyester, oxygen plasma pretreated polyester and TiO_2 coated polyester pretreated with oxygen plasma before and after 20 h of light irradiation in Xenotest Alpha LM light exposure and weathering test instrument.

The tearing strength in warp direction of oxygen plasma pretreated polyester substrates before light irradiation was reduced by 1.67% compared to that of original polyester substrates, which may be attributed to the oxygen plasma treatment causing the tearing strength to drop slightly. And the tearing strength

Table 5-2 Tearing strength study in warp direction

Samples	Tearing Strength (N)		Reduction (%)
	Before light irradiation	After 20 h light irradiation	
Original polyester	13.18	12.55	4.78
Oxygen plasma pretreated polyester	12.96	12.34	4.78
TiO_2 coated polyester	12.24	11.92	2.61

of TiO_2 coated polyester substrates pretreated with oxygen plasma before light irradiation was reduced by 7.13% compared to that of oxygen plasma pretreated polyester. This is could be due to the increase of stiffness after TiO_2 coating. After 20 h of light irradiation, the tearing strength of original polyester, oxygen plasma pretreated polyester and TiO_2 coated polyester substrates were reduced. However, the decrease in both original and oxygen plasma pretreated polyester substrates were 4.78% while the decrease in TiO_2 coated polyester substrates was 2.61%. This suggests that there is no photocatalytic decomposition of the molecular chains of polyester caused by the titania layers. On the contrary, the titania layers reduced the drop of tearing strength due to its ability to absorb UV irradiation. This is agreement with the results of self-cleaning cotton in chapter 4.

5.7 Conclusions

Single-phase anatase coated polyester fibers pretreated with low temperature oxygen plasma showed significant improvement in self-cleaning performance as demonstrated by their bactericidal activities, colorant decomposition and degradation of red wine and coffee stains. The adhesion between TiO_2 layers and polyester substrates was also improved after plasma treatment. The UV absorption of the titania coated polyester was significant enough to promote excellent UV protection to polyester. No photodegradation of the molecular chains of polyester by the titania layers could be observed as demonstrated by a comparison study of the tearing strength of coated polyester fabrics before and after light irradiation.

Chapter 6: Anatase TiO_2/SiO_2 Spherical Nanocomposites and Their Photocatalytic Activities

6.1 Introduction

Titanium dioxide nanocrystallites have become promising photocatalytic materials owing to their ability to catalyze the complete degradation of many organic contaminants and environmental toxins as well as organic stains, dirt etc. In those applications, it is important to improve the efficiency of the photoactive TiO_2-based films. Much work has been conducted on the optimization of the catalytic properties of TiO_2 films by using modified TiO_2 thin films. Parkin and Palgrave (2005) published a systematic review on photocatalytic TiO_2 self-cleaning coatings for the destruction of organic dirt. In Chapter 4 and 5, we investigated the low temperature fabrication of anatase TiO_2 thin films on cotton and polyester, and demonstrated that anatase TiO_2 thin films possess good self-cleaning performance.To further improve the photocatalytic activity of TiO_2 films, the combination of photoactive TiO_2 material with other oxides can be a good strategy.

In most cases, mixed or supported TiO_2 films showed higher photocatalytic activity than pure TiO_2 films. Among them, TiO_2-SiO_2 films have been widely used in industrial applications and most extensively studied. It was reported (Carl Anderson & Bard, 1995; Carl Anderson & Bard, 1997) that a mixed oxide powder of TiO_2 and SiO_2 was a more efficient photocatalyst for the photocatalytic decomposition than that of pure TiO_2 powder. Several other studies (Guo & Dong, 1999; J. Han & Kumacheva, 2001; Hanprasopwattana, Srinivasan, Sault, & Datye, 1996; Hsu, Yu, & Matijevic, 1993) reported the preparation of titania coating on monodisperse silica spheres. Yu *et al.*(2006) also prepared monodispersed anatase TiO_2/SiO_2 composite microspheres by calcining at 400 °C and 600 °C. However, these studies were focused on the preparation of TiO_2 coating on monodispersed SiO_2 spheres, the photocatalytic activity of TiO_2/SiO_2 composite microspheres were not reported. In addition, the temperatures used during the calcining processes were too high for any organic substrates. Zhang *et al*. (2006) reported the poly(divinylbenzene) core/anatase TiO_2 shell hybrid microsphere powder prepared at a low temperature showing high photocatalytic activities. Recently, some work carried out on photocatalysis of TiO_2-SiO_2 nanocomposite thin films on substrates with low thermal resistance. The anatase TiO_2/SiO_2 nanocomposite films on organic polymer substrates were prepared using a sol-gel process followed by a boiling treatment (Atsunori Matsuda et al., 2003; A Matsuda et al., 2003). However, the films were easily leached out from the substrates. Zhou *et al*. (2006)reported the preparation of TiO_2-SiO_2 mixed film on modified PET substrates at 100 °C, and the photocatalytic activity of TiO_2/SiO_2 mixed film was enhanced. The enhancement of photocatalytic activity of the mixed

TiO_2/SiO_2 treated cotton textiles was also reported (Yuranova, Mosteo, Bandata, Laub, & Kiwi, 2006). In that study, the TiO_2-SiO_2 films on the cotton were obtained by immersing the cotton in a mixture of TiO_2 colloid and commercial SiO_2 solution and subsequently followed by thermal treatment at 100°C for 1 h. However, the long treatment time is not feasible in the industrial textile application. In addition, no comparison between the mixture of TiO_2/SiO_2 and TiO_2 was reported.

In this chapter, we extended our previous work in an attempt to further improve the photocatalytic activity of the anatase TiO_2 films. Sol-gel process can offer an attractive means to produce anatase TiO_2–based thin films at a low temperature. The sol-gel process is also advantageous in that it is capable of producing TiO_2–based thin films with high surface areas. In this work, anatase TiO_2/SiO_2 nanocomposites were prepared in an aqueous solution using a sol-gel process at a low temperature. TiO_2/SiO_2 spherical nanocomposites were applied to cotton fabrics from colloidal sol by a simple dip-pad–dry-cure process with a much shorter time duration compared with the process reported before (Yuranova, Mosteo, Bandata, Laub, & Kiwi, 2006). TiO_2/SiO_2 nanocomposite treated the cotton fabrics showed higher photocatalytic activity compared to those treated by TiO_2 only. Consequently, the treated fabrics showed enhanced the self-cleaning performance.

6.2 Preparation of TiO_2/SiO_2 nanocomposites on cotton

6.2.1 Preparation of TiO_2 sols

The TiO_2 sols with different concentrations were prepared as follows. In a typical procedure, 5 ml titanium tetraisopropoxide (Aldrich, 97%) was added dropwise into 100 ml deionized water containing 1 ml nitric acid (Aldrich, 70%) and 10 ml acetic acid (Aldrich, 99.9%) under vigorous stirring. The mixture was heated to 60 °C and kept at that temperature while being vigorously stirred for 16 h (pH=1-2).

6.2.2 Preparation of SiO_2 nanoparticles

Uniform silica with the particle size of around 500 nm was prepared as follows. 100 ml nitric acid aqueous solution (1×10^{-4} M) was charged to a 250 ml one-neck flask, and then the flask with a magnetic stirrer was immersed into a heated water-bath. The solution was heated to 60 ºC, and then 2.5 ml silica precursor methyl-trimethoxysilane (MTMS, Sigma, 98%) was introduced to the solution. After stirring for 1 min, 2.5 ml ammonia (27%) was added to the solution. A milky suspension of silica nanoparticles was obtained (pH=9-11). The suspension was centrifuged to obtain SiO_2 powder.

6.2.3 TiO_2 /SiO_2 nanocomposites

The as-prepared SiO_2 powder above was added to TiO_2 sol and dispersed in an ultrasonic bath for 15 min. The TiO_2/SiO_2 mixture was kept for 12 h to form

SiO_2 supported TiO_2 spherical nanocomposites with a core-shell structure (pH=3-5) (as shown in Scheme 6-1).

6.2.4 Preparation of TiO_2/SiO_2 nanocomposites on cotton

The as-prepared suspension was used to prepare TiO_2/SiO_2 nanocomposites on woven white cotton fabrics. Dipping-padding-neutralizing-drying-curing process of cotton fabrics were repeated 5 times to prepare TiO_2 layers on cotton. For comparison, the TiO_2 sol was also applied to cotton fabric substrate with the same method.

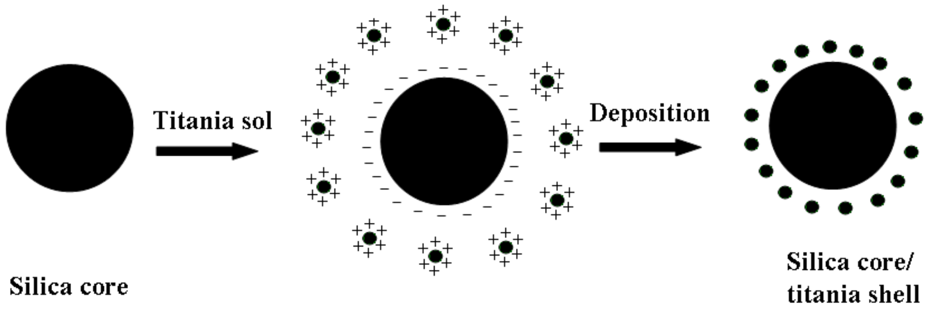

Scheme 6-1 The formation mechanism of TiO_2/SiO_2 nanocomposites with a core-shell structure.

6.3 Characterization of TiO_2/SiO_2 nanocomposites

6.3.1 SEM analysis

Fig.6-1 shows the representative SEM micrographs of the monodispersed spherical SiO_2 nanoparticles, a grainy film of TiO_2 and spherical TiO_2/SiO_2

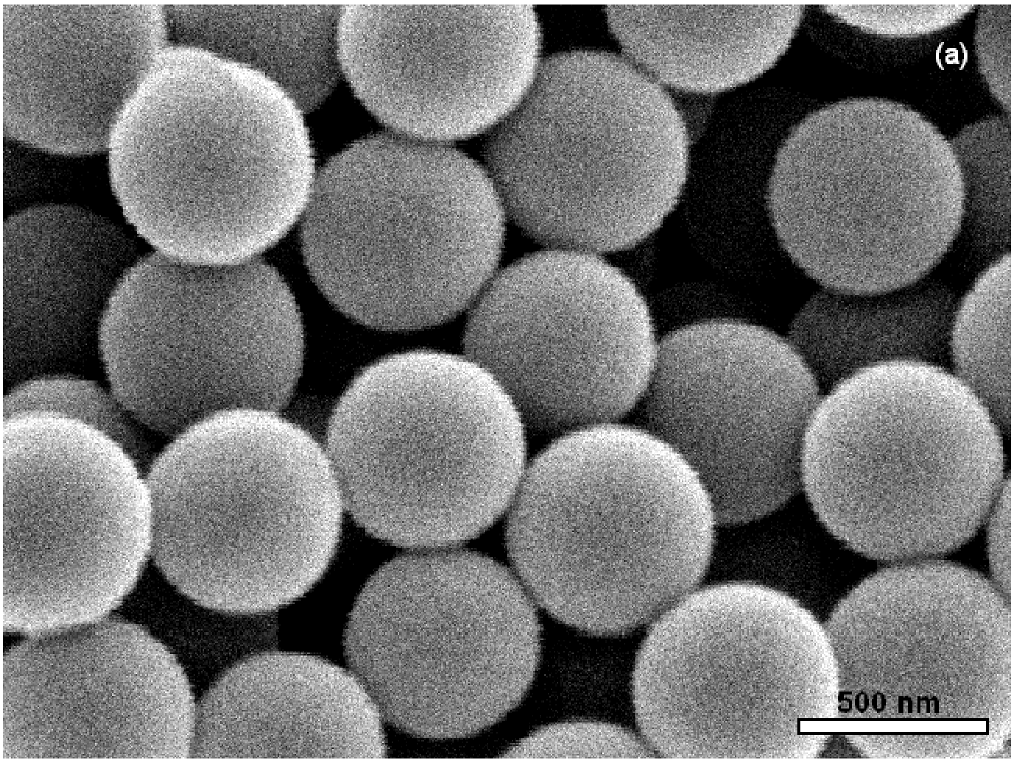

(a)
500 nm

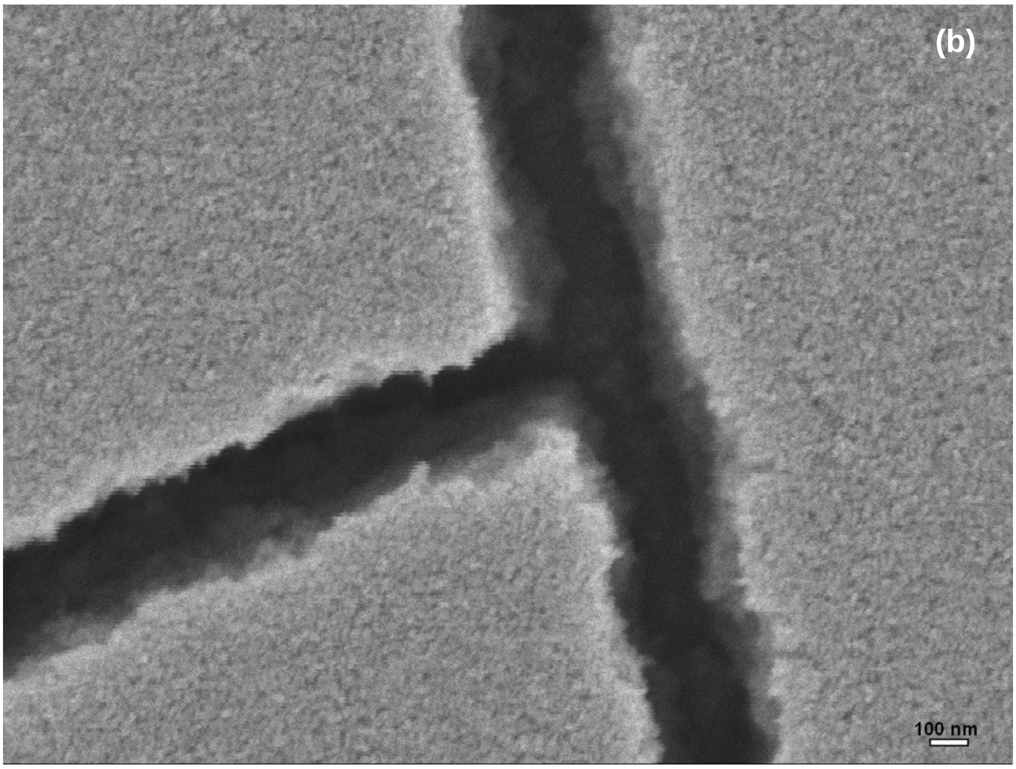

(b)
100 nm

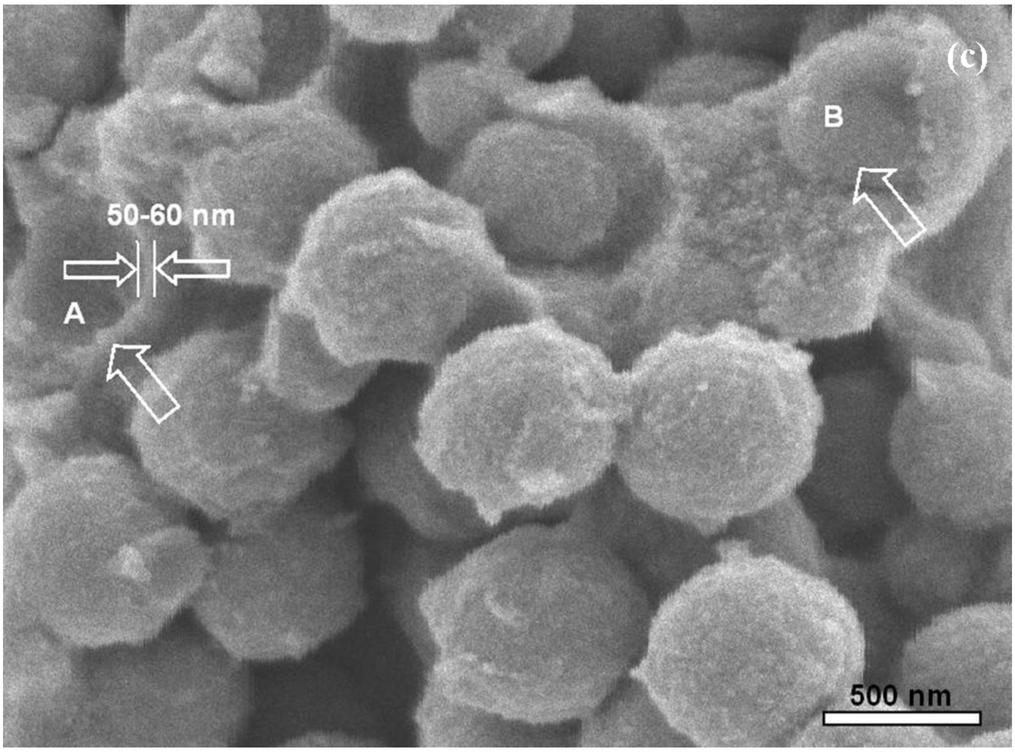

Fig. 6-1 SEM images of (a) SiO_2 nanopartciles (b)TiO_2 film and (c) spherical TiO_2/SiO_2 nanocomposites on silicon wafer (A: TiO_2 shell, B: SiO_2 core).

nanocomposites. It can be seen that the average diameter of the spherical SiO_2 particles is about 500 nm as shown in Fig. 6-1a. A film of TiO_2 was formed on the silicon wafer (as shown in Fig. 6-1b) with a very fine grain size around 4-5 nm according to the characterization in our previous study (Daoud & Xin, 2005). In contrast to the near perfect spherical SiO_2 particles, the TiO_2 deposited SiO_2 particles show a rough surface and less than perfect spherical shape with the average diameter increasing to about 600-620 nm as shown in Fig. 6-1 c. This is clearly attributed to the coating of a TiO_2 layer on spherical SiO_2 particles. The formation mechanism of TiO_2/SiO_2 nanocomposites is considered to be caused by electrostatic deposition. The isoelectric point of TiO_2 nanoparticles was reported to be 5.6 (Larson, Drummond, Chan, & Grieser, 1993), 5.9 (Wiese & Healy, 1975), 6.2 (Yotsumoto & Yoon, 1993), and that of SiO_2 particles ranged from 1.8 (Veeramasuneni, Yalamanchili, & Miller, 1998) to 2.7 (Subramaniam, Yiacoumi, & Tsouris, 2001). As the pH value in this study was 3-5, the TiO_2 would have a positive surface charge density and the SiO_2 particles would have a negative surface charge density. Thus, TiO_2 could be deposited on the surface of SiO_2 particles driven by the electrostatic attraction between TiO_2 and SiO_2.

Fig. 6-2 shows the SEM micrographs of untreated cotton fibres, TiO_2 treated cotton fibres and TiO_2/SiO_2 nanocomposites treated cotton fibres. It can be seen that spherical TiO_2/SiO_2 nanocomposites were deposited on the cotton fibers (as shown in Fig. 6-2 c) in contrast to the fibrillous texture of the pristine cotton fibers (as shown in Fig. 6-2 a) and a flat TiO_2 layer deposited on cotton fibres (as shown in Fig. 6-2 b).

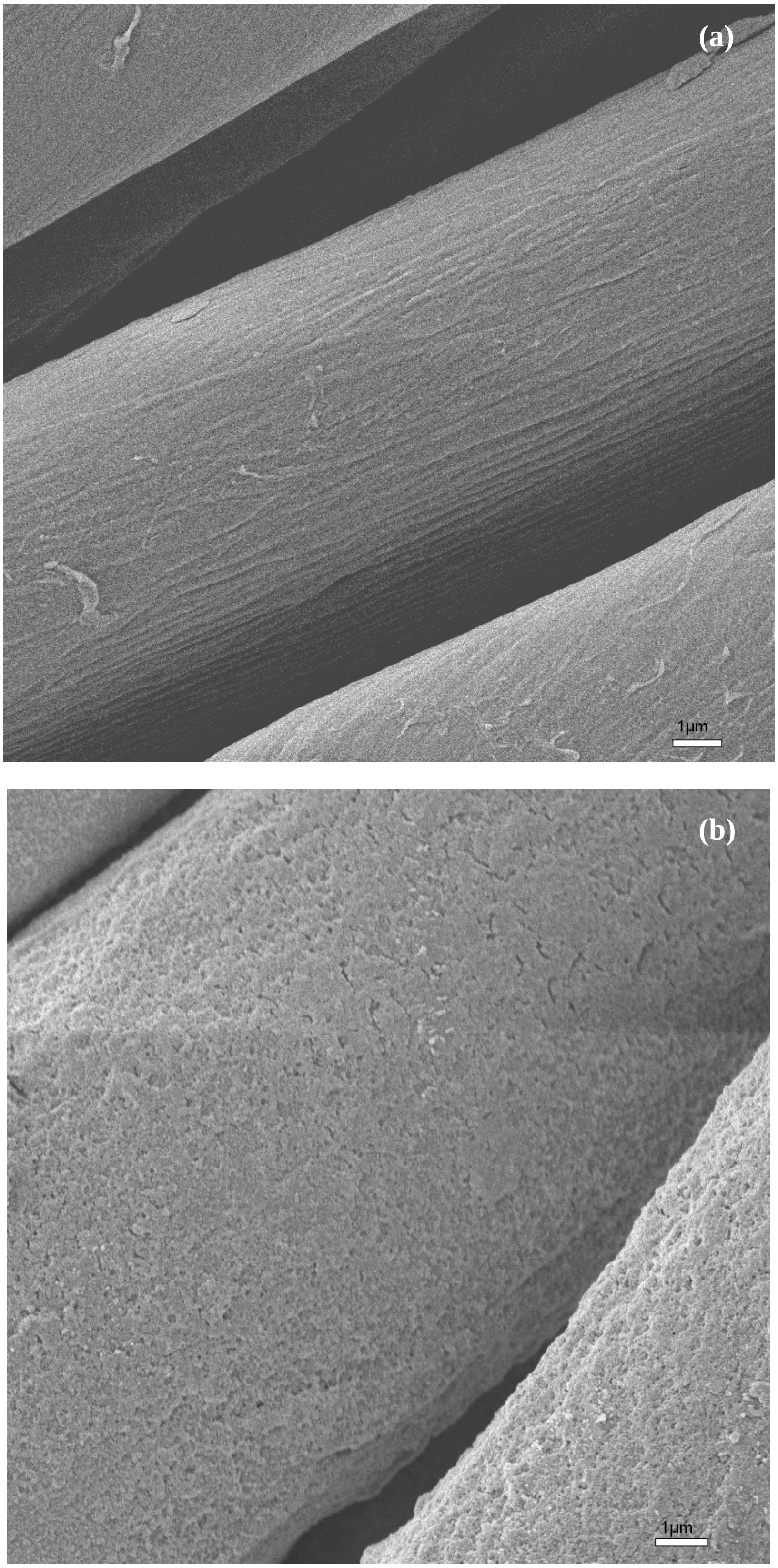
(a)
1μm
(b)
1μm

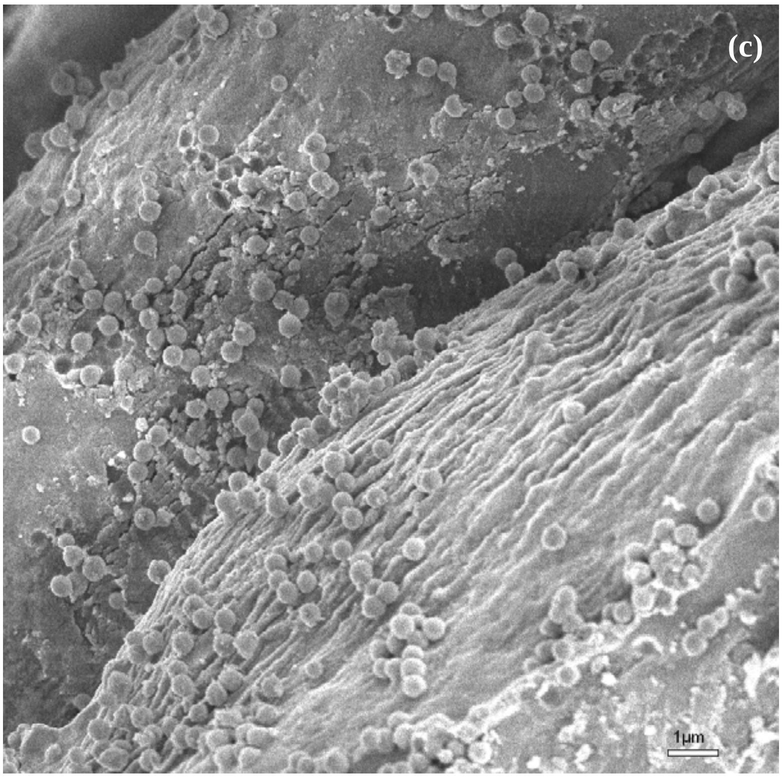

Fig. 6-2 SEM images of (a) untreated cotton fibres, (b) TiO_2 treated cotton fibres and (c) TiO_2/SiO_2 nanocomposite treated cotton fibres.

6.3.2 XRD

Fig. 6-3 shows the XRD patterns of the pure SiO_2, TiO_2 and TiO_2/SiO_2 nanocomposites. No crystal peak is observed in SiO_2 particles (Fig. 6-3a), indicating that the SiO_2 particles are amorphous. Anatase peaks at 25.4°, 38.0° and 48.0° for solid titania particles (Fig. 6-3b) are observed and no traces of brookite or rutile are observed, indicating that single-phase anatase nanocrystallites were formed. Anatase peaks at 25.4°, 38.0° and 48.0° are also observed in the XRD spectra of spherical SiO_2 particles coated with a TiO_2 layer (Fig. 6-3c), which was very similar to that of titania solid particles.

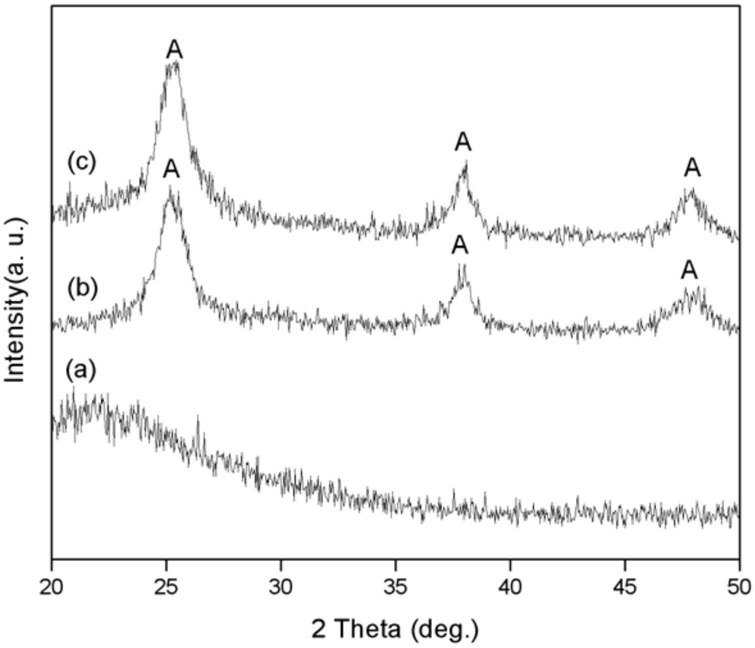

Fig. 6-3 XRD patterns of powder extracted from colloids (a) SiO_2, (b) TiO_2 and (c) TiO_2/SiO_2 nanocomposites (A: anatase).

6.4 Photocatalytic activities

The photocatalytic activities of TiO_2/SiO_2 nanocomposites and only TiO_2 treated cotton fabrics, TiO_2/SiO_2 nanocomposites powder and pure TiO_2 powder were evaluated by the decomposition of Neolan Blue 2G under UV irradiation (The intensity of UV light was 0.7–0.8 mW cm^{-2}) as showed in Fig. 6-4 and Fig. 6-5. The weight of each fabric sample used was 3g.Th

It can be seen from Fig. 6-4 that the dye concentration in the aqueous solution containing the TiO_2/SiO_2 treated cotton fabrics was reduced more than that in the aqueous solution containing TiO_2 treated cotton fabrics under UV irradiation. This result indicates that the TiO_2/SiO_2 treated cotton fabric possesses higher photocatalytic activity than only TiO_2 treated cotton fabrics. Under the same UV irradiation, the dye concentration in the aqueous solution containing untreated cotton fabrics almost kept the same level, which indicates that cotton fabrics possess no photocatalytic activity and the dye itself would not be decomposed by UV radiation. Comparing to the study in Chapter 4, the rate of the dye decomposition reported here is relatively low. This is because of the lower amount of TiO_2 deposited on the fabric surface.

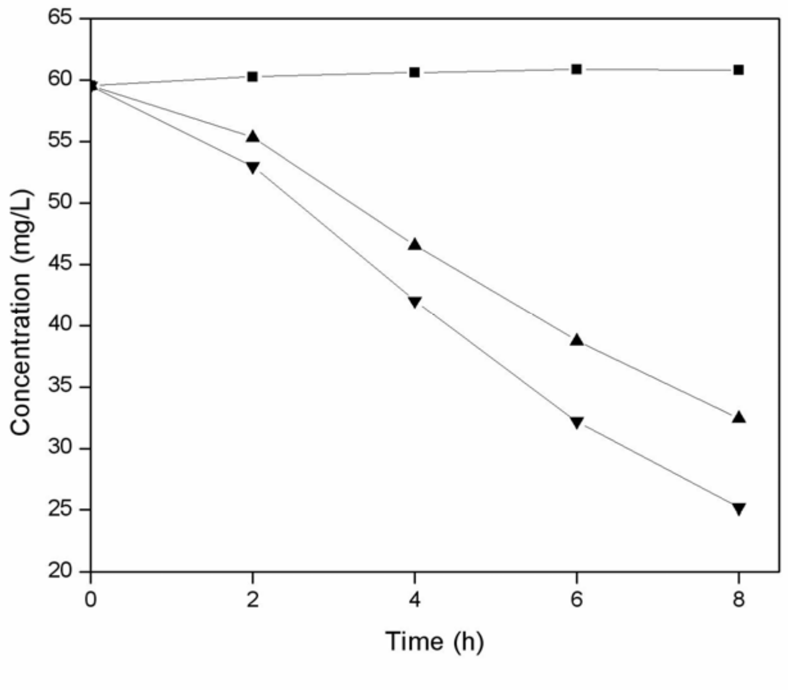

Fig. 6-4 Variations in concentration of Neolan Blue 2G in an aqueous solution as a function of UV irradiation time for different substrates: untreated cotton fabrics (■), TiO_2 treated cotton fabrics (▲) and TiO_2/SiO_2 treated cotton fabrics (▼).

From Fig. 6-5, the dye concentration in the aqueous solution containing the TiO_2/SiO_2 nanocomposite powder was also decreased more than those in the aqueous solutions containing pure TiO_2 powder under UV irradiation where the amount of TiO_2 maintained constant, which further confirmed that TiO_2/SiO_2 nanocomposites possessed higher photocatalytic activities than pure TiO_2. The assessment of photocatalytic activities of treated cotton fabrics and powders was repeated five times and the results were close with an error margin of ±1%. The average results were used in this study.

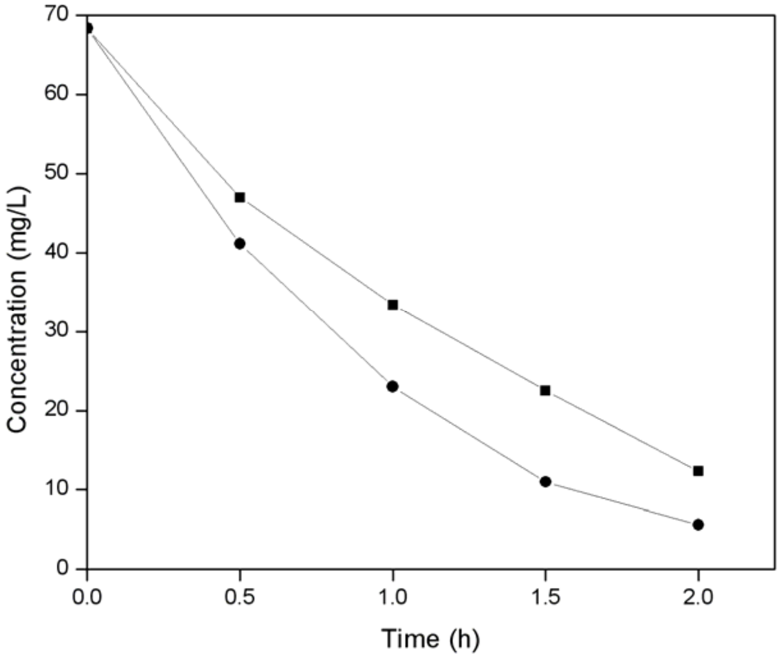

Fig.6-5 Variations in concentration of Neolan Blue 2G in an aqueous solution as a function of UV irradiation time for pure TiO_2 powder (■) and TiO_2/SiO_2 nanocomposite powder (●).

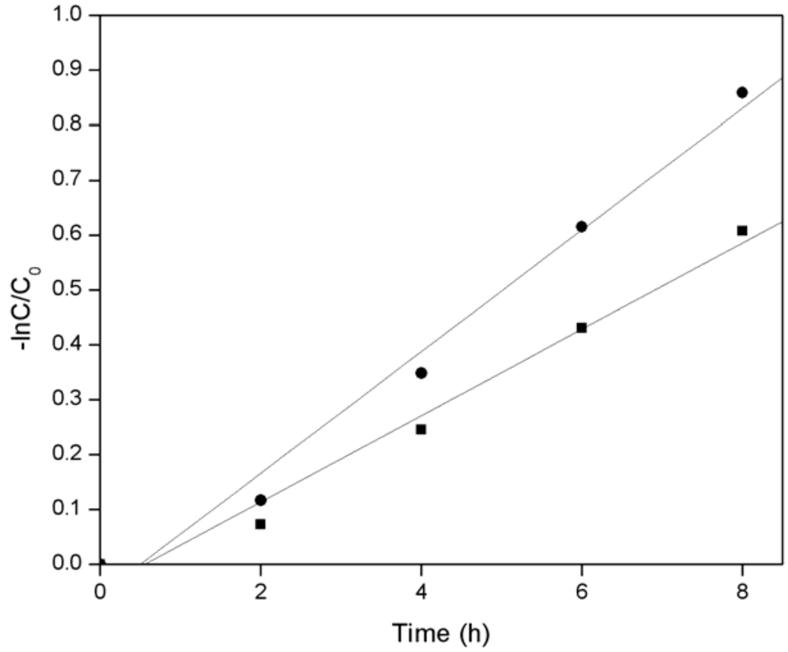

Fig. 6-6 The pseudo-first-order degradation rate constants of Neolan Blue 2G for TiO_2 treated cotton fabrics (■) and TiO_2/SiO_2 nanocomposite treated cotton fabrics (●).

The dye decomposition in the aqueous solution containing pure TiO_2 and TiO_2/SiO_2 nanocomposites treated cotton fabrics under UV irradiation followed a pseudo-first-order kinetic model as shown in Fig. 6-6. Pseudo-first-order reaction kinetic model was shown as equation (1):

$$-\ln C/C_0 = kt, \qquad (1)$$

where C_0 is the initial concentration of dye before UV radiation and after the fabric-dye absorption comes to an equilibrium, C is the concentration at time t, k is the pseudo first-order rate constant. Fig. 6-6 shows the $-\ln C/C_0$ of Neolan Blue 2G versus irradiation time. It is clear that decreasing the dye concentration obeys a linear pattern. Correlation coefficient *R* of linear fitting for TiO_2 is 0.99073, the correlation coefficient *R* for TiO_2/SiO_2 nanocomposites is 0.99206. Rates of the dye decomposition (photocatalytic reaction rate) for pure TiO_2 and TiO_2/SiO_2 nanocomposites are calculated as 0.079±0.006 h^{-1} and 0.111±0.008 h^{-1} respectively. This indicates that TiO_2/SiO_2 nanocomposites possess higher photocatalytic activity than pure TiO_2.

The enhanced photocatalytic activity of the TiO_2/SiO_2 treated cotton fabrics might be attributed to the unique physicochemical properties of TiO_2/SiO_2 nanocomposites which results from the strong interaction of TiO_2 and SiO_2 particles at molecular level, such as the increased specific surface area of TiO_2/SiO_2 nanocomposites (Hong, Lee, Park, & Lee, 2003; Shibata et al., 2006; Yamashita et al., 1996; J. Yu, Zhao, & Cheng, 2006; L. Zhou, Yan, Tian, Zhang, & Anpo, 2006) and the enhanced surface acidity of the nanocomposites (Fu, Clark, Yang, & Anderson, 1996; Guan, Lu, & Yin, 2003; Papp, Soled, Dwight, & Wold, 1994; Shul, Kim, Haam, & Han, 2003). The mechanism of Neolan Blue 2G decomposition is similar to that of Neolan Blue 2G in Chapter 4. As the photodecomposition of the colorant occurs only on the TiO_2/SiO_2 nanocomposite surface, the increase in specific surface area of TiO_2/SiO_2 nanocomposites facilitates more effective adsorption sites which might promote the photocatalytic activity by increasing the concentration of contaminants and reaction intermediates near the TiO_2 relative to the solution concentration of Neolan Blue 2G (Carl Anderson & Bard, 1995; Arai, Tanaka, & Khlaifat, 2006; Minero, Catozzo, & Pelizzetti, 1992; Shul, Kim, Haam, & Han, 2003; Takeda, Ohtani, Torimoto, Kuwabata, & Yoneyama, 1997). The TiO_2 behaves as the photoactive center, i.e., generating hydroxyl radicals under irradiation, while the SiO_2 provides better adsorption sites for Neolan Blue 2G in the vicinity of the TiO_2. This effectively increases the surface concentration of Neolan Blue 2G at or near the TiO_2 sites promoting more efficient oxidation by photogenerated species.

In addition to the increased specific surface area of TiO_2/SiO_2 nanocomposites, mixed metal oxides often generate additional surface acidity over their individual members because of an increase in the polarizability of the hydroxide groups present in the mixed oxide (Nakabayashi, 1992). Amine titration method is a means of determining surface acidity of metal oxides (Papp, Soled, Dwight, & Wold, 1994). N-butylamine titration method in this work showed that the surface acidity of TiO_2/SiO_2 nanocomposite powder was stronger than that of pure TiO_2 powder. Many previous research works reported that the stronger acidity would contribute to the increase in the photocatalytic activity (Fu, Clark, Yang, & Anderson, 1996; Papp, Soled, Dwight, & Wold, 1994). In the TiO_2/SiO_2 nanocomposites, a complex oxide may form at the interfaces due to the existence of Ti–O–Si vibration in the IR spectrum detected from previous works (S. Kim, Park, & Choi, 2004; Liu & Davis, 1994). The presence of the Ti–O–Si vibration band in TiO_2/SiO_2 nanocomposites was confirmed by FT-IR transmission spectra shown in Fig. 6-7. The peak at 946 cm^{-1} in Fig. 6-7(c) corresponds to the vibration of Ti–O–Si. Ti–O–Si bonds enhance surface acidity of the TiO_2/SiO_2 nanocomposites and in turn improve the photocatalytic activity of the TiO_2/SiO_2 nanocomposites fabricated in this study.

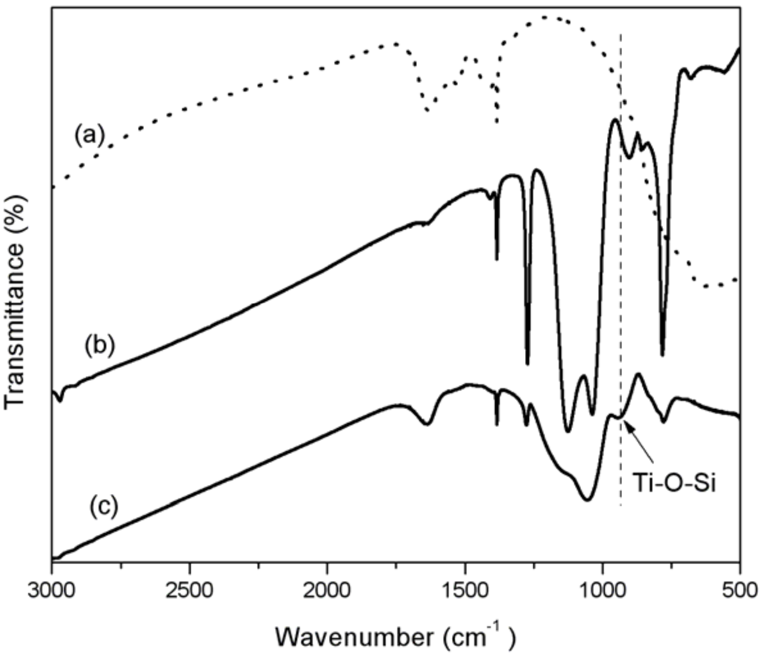

Fig. 6-7 FT-IR spectra of (a) TiO_2, (b) SiO_2 and (c) TiO_2/SiO_2 nanocomposites.

6.5 Conclusions

Anatase TiO_2/SiO_2 spherical nanocomposites with core-shell feature were prepared by a low-temperature sol-gel process. Dye decomposition measurements showed that the anatase TiO_2/SiO_2 treated cotton fabrics possessed higher photocatalytic activity than pure anatase TiO_2 treated cotton fabrics. This enhanced photoactivity was related to the increased specific surface area and the enhanced surface acidity of the TiO_2/SiO_2 nanocomposites. As better self-cleaning performance is related to higher photocatalytic activity, the TiO_2/SiO_2 nanocomposites treated cotton fabrics therefore have better self-cleaning activity than TiO_2 treated fabrics. The anatase TiO_2 /SiO_2 nanocomposites treated cotton fabrics have the high potential in commercial applications of self-cleaning cotton textiles.

Chapter 7: Synthesis of Single-phase Anatase by Aging and its Self-cleaning Properties on Cotton

7.1 Introduction

In sol-gel processes, titania is usually prepared by the hydrolysis and condensation reactions of titanium alkoxides. It is well known that titanium alkoxides hydrolyze vigorously in water and many catalysts, typically various simple acids, e.g., nitric acid (Samuneva, Kazhukharov, Trapalis, & Kranold, 1993), hydrochloric acid (Kamiya, Tanimoto, & Yoko, 1986) and acetic acid (Makishima, Asami, & Wada, 1988), have been applied to lower the reaction rates. Much work has been reported for the preparation of anatase films on low thermal resistant materials using sol-gel process at relatively low temperatures (Daoud & Xin, 2004b; Imai & Hirashima, 1999; Matsuda, Kotani, Kogure, Tatsumisago, & Minami, 2000; Atsunori Matsuda et al., 2003; Matsuda et al., 2005; Shimizu, Imai, Hirashima, & Tsukuma, 1999; Yuranova, Mosteo, Bandata, Laub, & Kiwi, 2006). However, the disadvantages of most processing methods are the use of solvents, corrosive chemicals such as nitric acid and hydrochloric acid, and relatively high temperatures to obtain the anatase films. And some products in these cases are composed of anatase and brookite, not pure anatase. Although aqueous based sol-gel process is more environmentally friendly than the alcohol, the destructive effect of strong acids, used in sol-gel process to keep aqueous sols in the peptized state, on poor acid-resistant materials such as cotton fibers hinders the applications.

The fabrication of photocatalytic anatase films at room temperature or near room temperature not only eliminates the need for high temperature operations, but also broadens their applications to low thermally resistant materials such as biomaterials and textiles. The advantage of room temperature processing is enhanced when the chemicals are sufficiently benign to facilitate the processing in air. Titanium alkoxides as starting materials provide the possibility of obtaining crystalline titania at room temperature. These compounds have the generic formula Ti $(OR)_4$, where R is an alkyl group. The OR groups are electronegative and therefore make titanium highly prone to nucleophilic attack.

Aging is a process in which the gel physical properties can be changed as the result of the following mechanisms: polymerization, coarsening and phase transformation (Brinker & Scherer, 1990).Various studies have shown that the amorphous TiO_2 gels crystallized into anatase by using an aging process in boiling water, in HCl solution at 60 °C, in boiling NH_4OH solution (Hsiang & Lin, 2004, , 2006; D.-S. Seo, Lee, & Kim, 2001; Dong-Seok Seo, Lee, Lee, & Kim, 2001). These reports have mainly focused on the effects of aging on the crystallization, specific surface area, crystallite size, phase transformation and nanocrystallite growth kinetics of TiO_2 powders. However, few studies have reported that anatase nanocrystallites are formed by aging at room temperature and atmospheric pressure and their photocatalytic activities of these nanocrystalline anatase films. In this chapter, anatase sols were developed by hydrolysis and condensation of titanium tetraisopropoxide in water medium followed by aging at room temperature (23°C) using titanium tetraisopropoxide as a starting material and acetic acid as catalysts. TiO_2 thin films were produced on cotton fabrics by a simple dip-pad-dry-cure process. This study was also attempted to discuss the influence of aging on the crystallization of anatase and the self-cleaning activities. The self-cleaning activities of the synthesized TiO_2 thin films on cotton fabrics were evaluated by examining the photodegradation of Neolan Blue 2G as a model photocatalytic reaction and the discoloration of red wine and coffee stains.

7.2 Preparation of TiO_2 sol by aging at room temperature

7.2.1 Preparation of TiO_2 sols

5 ml Titanium tetraisopropoxide (Aldrich, 98%) was added dropwise into 100 ml deionized water containing acetic acid (Aldrich, 99.8%) with pH value 3-4 under vigorous stirring at room temperature (23°C). The mixture was vigorously stirred at room temperature for 24 h. The as-prepared sample is named as A23. Freshly-prepared A23 at room temperature was stored without stirring at room temperature and atmospheric pressure and became transparent within one week. This aged sample is named as TA23. The freshly-prepared A23 and TA23 were used for preparation of TiO_2 powders. Only TA23 was used for preparation of TiO_2 films since precipitation occurs in the

freshly-prepared sol A23.

7.2.2 Preparation of TiO_2 films and solid TiO_2 powders

TA23 was used to prepare TiO_2 thin films on woven white cotton fabrics by a dip-pad-dry-cure process. Solid A23 and TA23 TiO_2 powders were extracted from the corresponding sols by adding adequate amounts of 0.3% sodium carbonate until precipitation occurred. The formed suspensions were centrifuged at 4000 rpm for 5 minutes, followed by removal of the liquid phase. The precipitates were then washed three times with water and finally with acetone twice before being air dried at room temperature overnight.

7.3 Characterization of TiO_2 nanoparticles

7.3.1 XRD spectroscopy

The crystal phase of titania particles and titania films on cotton fabrics were studied by XRD. Fig. 7-1 demonstrates the XRD patterns of titania powders obtained from freshly-prepared A23 and aged transparent TA23. Freshly-prepared A23 at room temperature was precipitated at first. However, it became a transparent sol with slightly blue tint within one week after it stored at room temperature and atmospheric pressure and it was stable without sedimentation and delamination for more than half a year. Freshly-prepared A23 was amorphous phase as shown in Fig. 7-1a. However, after aging, A23 amorphous gel was transformed into single-phase anatase as shown in Fig.7-1b

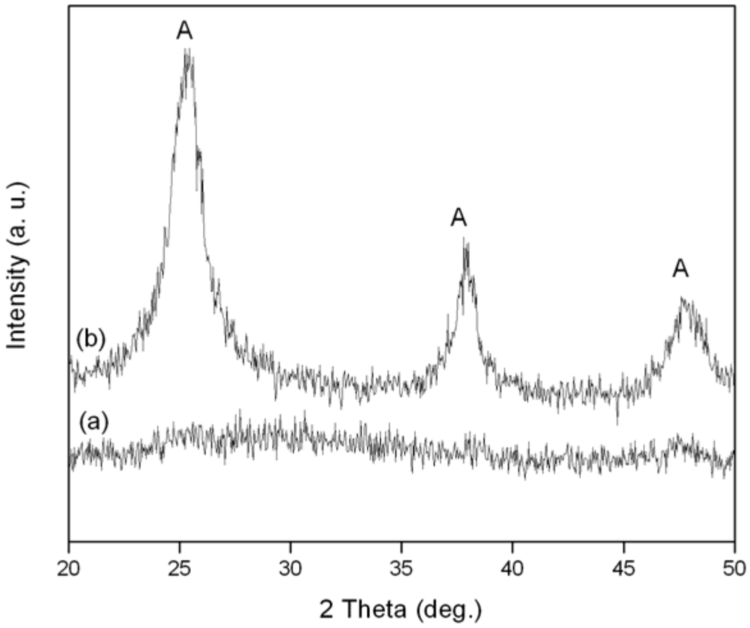

Fig.7-1 XRD patterns of solid powder extracted from (a) freshly- prepared A23 and (b) the aged sample TA23 (A: anatase).

with the anatase peaks at 25.4°, 38.0° and 48.0° observed. The presence of brookite can be qualified by XRD at 27.7°, 31.1° *etc.* (Hengzhong Zhang & Banfield, 2000) and the presence of rutile can be qualified by XRD at 27.5°, 36.0° *etc.* (W. Wang, Gu, Liang, Hamilton, & Wesolowski, 2004). In Fig. 7-1, no traces of brookite or rutile could be found after careful examination of TA23 spectrum curve.

Conventionally, amorphous-anatase transformation may complete in the temperature range from 250 to 400 °C (S.-J. Kim, Park, Jeong, & Park, 1999). Yanagisawa and Ovenstone (1999) studied the crystallization of anatase from amorphous titania using the hydrothermal technique and realized the transformation from amorphous to anatase at temperatures between 120 and 250 °C. It was reported that amorphous titania gels obtained at pH between 2.7 and 5.0 were transformed to titania consisting of anatase and brookite at 40°C for several days (Li, Lee, Song, Lee, & Kim, 2005). In another study by Ding and He (1996), it was reported that amorphous titania was converted into anatase and rutile titania after aging at room temperature for one year. Bischoff and Anderson (1995) investigated the peptization process in the sol-gel preparation of titania and reported that an acidified (nitric or hydrochloric acid) sol peptized at room temperature leads to the formation of a mixture of anatase and rutile; the acidified sol under refluxing at elevated temperatures was a mixture of anatase and brookite. In this study, amorphous titania in aqueous solution transformed into pure anatase after aging at room temperature (23 °C) for only one week. Moreover, sharper anatase peaks with greater intensities for TA23 are observed indicating that better crystallization of anatase occurred in TA23. The single-phase anatase of TA23 obtained by aging at room temperature is similar to that of S60 obtained by heating at 60 °C in Chapter 4.

Fig.7-2 presents the XRD patterns of untreated cotton and aged titania sample TA23 treated cotton. In the profiles, the strong diffraction peaks at 14.9°, 16.6°, 22.8° and 34.7° are originated from cotton substrate. Weak peaks at 25.4°, 38.0° and 48.0° are observed in Fig. 7-2 b, which match well with these

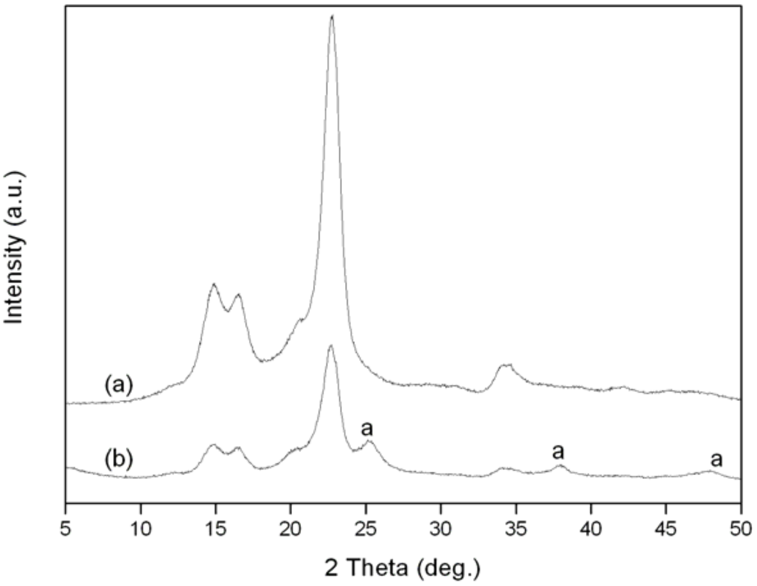

Fig. 7-2 XRD patterns of (a) untreated cotton and (b) aged titania sample TA23 treated cotton (a: anatase).

observed in the anatase phase TiO_2. This further confirmed that nanocrystalline anatase was formed in TA23 with the aging process.

7.3.2 TEM

High resolution TEM confirmed earlier observations of phase and size of crystallites. Fig. 7-3 shows the existence of small nanocrystallites with lattice fringes of 0.356 nm which are characteristic values of the anatase phase. The insets, located on the top left corner of the images, show the corresponding selected area electron diffraction (SAED). Measurement of lattice spacing from the corresponding SAED pattern indicates that the nanocrystals of TA23 were anatase. From Fig.7-3, it can also be seen that the average crystal size of TA23

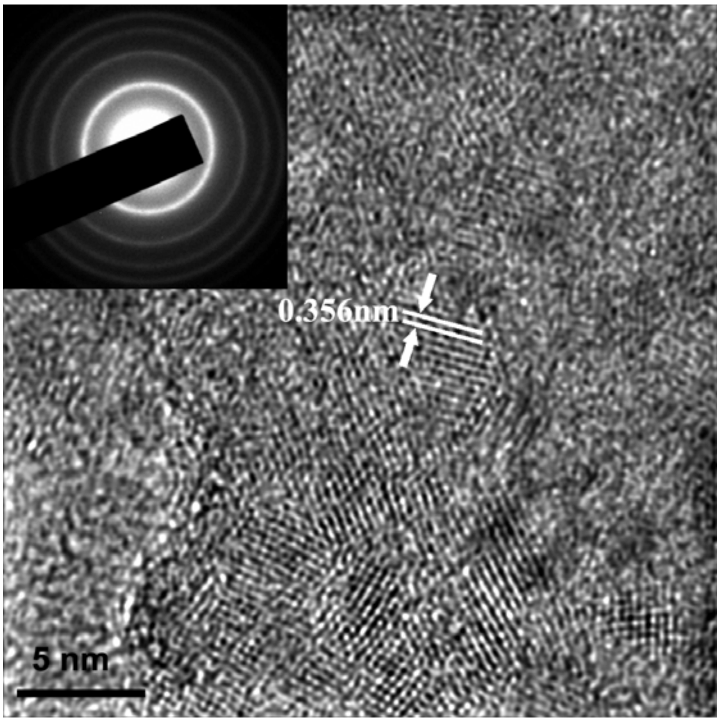

Fig.7-3 High-resolution TEM image of TA23 inset located on the top left corner is the corresponding selected area electron diffraction (SAED).

was 5-7 nm. Sharp and intense Deby-Scherrer rings were observed in Fig. 7-3. Extra effort was devoted to find any traces of the brookite or rutile phase, however nothing could be found. The average crystal size of 5-7 nm and anatase phase of TA23 are similar to those of S60 in Chapter 4.

7.3.3 SEM observations

Fig.7-4 shows the representative SEM micrographs of TiO_2 treated cotton fibres. SEM analysis of TA23 films on cotton fibres in Fig.7-4a shows that TiO_2 layer was formed on cotton fibres. The surface structure of the TA23

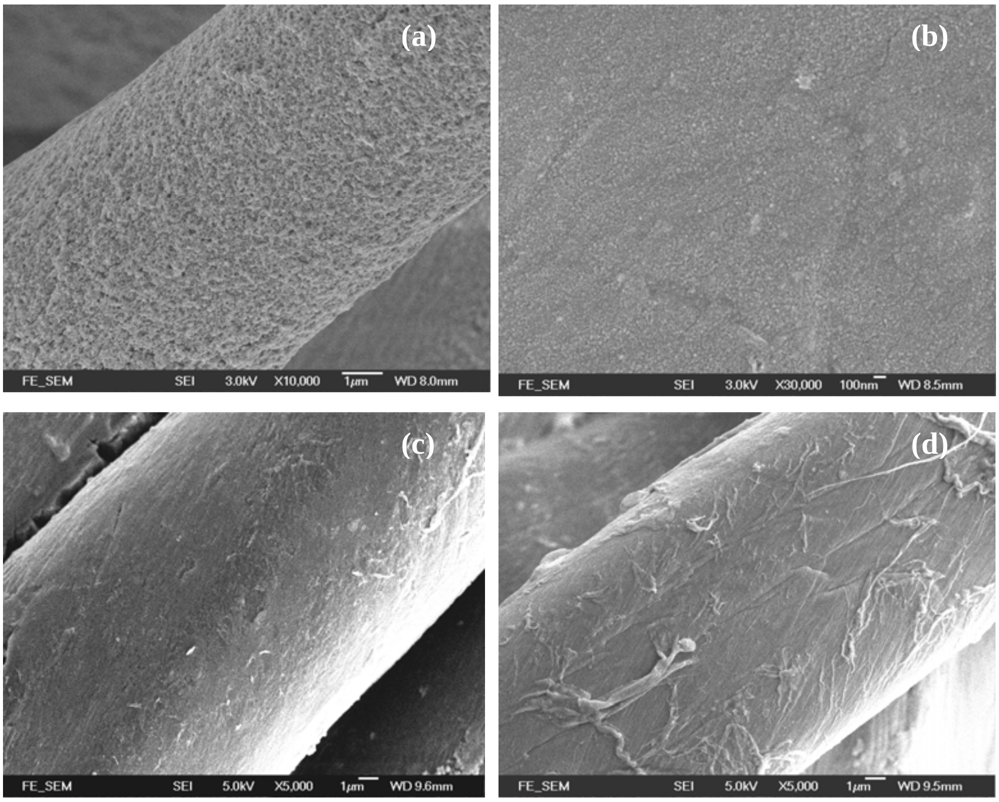

Fig.7-4 SEM images of (a) TA23 treated cotton fiber, (b) TA23 treated cotton fiber at high resolution, (c) TA23 treated cotton fiber after 10 washings and (d) TA23 treated cotton fiber after 20 washings.

treated cotton fibre looks uniform. SEM image at high resolution in Fig. 7-4b shows that the particle size of TA23 on cotton fibre is small. After 10 and 20 washings, the titania films were still observed on cotton fibers as shown in Fig. 7-4 c and Fig. 7-4 d, while the titania films were largely leached out after 20 washings.

7.4 UV absorption

Ultraviolet Protection Factor (UPF) can directly evaluate the UV-absorption

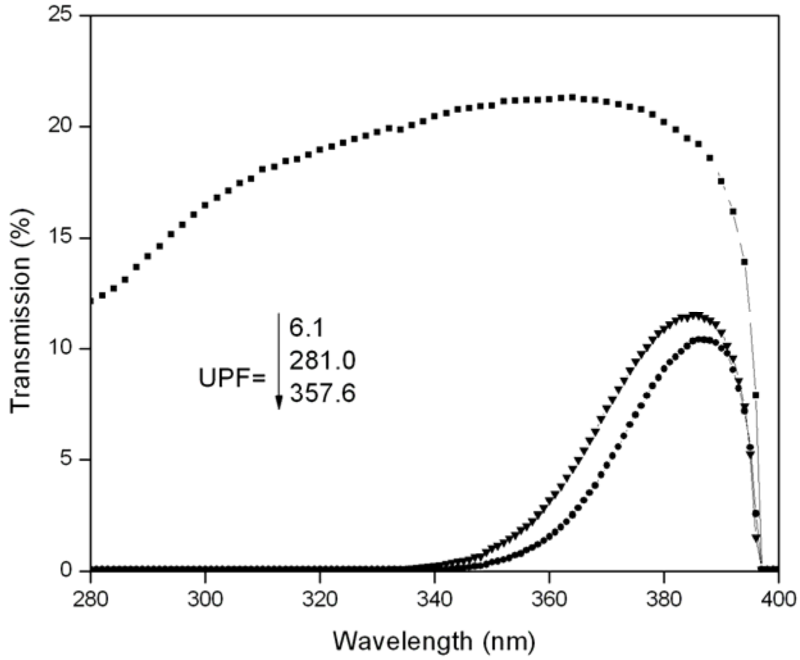

Fig.7-5 UV absorption of untreated cotton (▪), TA23 treated cotton (●) and TA23 treated cotton after 20 washings (▼).

property of the as-prepared products. Strengthened UV absorption is beneficial for UV blocking (Yang, Zhu, & Pan, 2004).The UV absorption study of TA23 treated white cotton fabrics before washing showed a high UPF value of 357.6 according to the Australian/New Zealand Standard, started from a low UPF value of 6.1 for untreated white cotton fabric. After 20 washings, UPF values of TA23 treated cotton fabrics were 281.0, which were lower than that before washing respectively but still much higher than that of untreated white cotton fabric. These high UPF values belong to an excellent protection classification compared to a low and non-ratable UPF rating of 5 for untreated white cotton fabric.

Fig.7-5 also shows that UV transmissions of TA23 treated white cotton fabrics were completely cut off in the UV-B region (280–315 nm) before and after washing. In the UV-A spectral region (315–400 nm), UV transmissions of these treated cotton fabrics were relatively higher, but they remained much lower than that of the untreated cotton fabric. The stronger the UV-absorption, the higher the photocatalytic activity. From the UV-absorption data, it is certain that TA23 treated cotton fabrics should have high photocatalytic activity.

7.5 Self-cleaning performance

7.5.1 Colorant decomposition activities

Self-cleaning effect of TA23 treated white cotton fabrics could be evaluated by the decomposition of the colorant, Neolan Blue 2G, in an aqueous solution under UV light irradiation, as well as S60 treated cotton fabrics in Chapter 4 for comparison (UV intensity was 1.2-1.3 mW/cm^2). The weight of each sample used was 5g. The durability of TA23 film on cotton was investigated by comparing the colorant decomposition activities of TA23 treated cotton fabrics before and after 10 and 20 washings according AATCC Test Method Test No. 2A at 49±2 °C. Fig.7-6 shows the photocatalytic activities of TA23 treated cotton fabrics before and after 10 and 20 washings and S60 treated cotton fabrics.

It can be seen from Fig.7-6d that the colorant concentration under UV

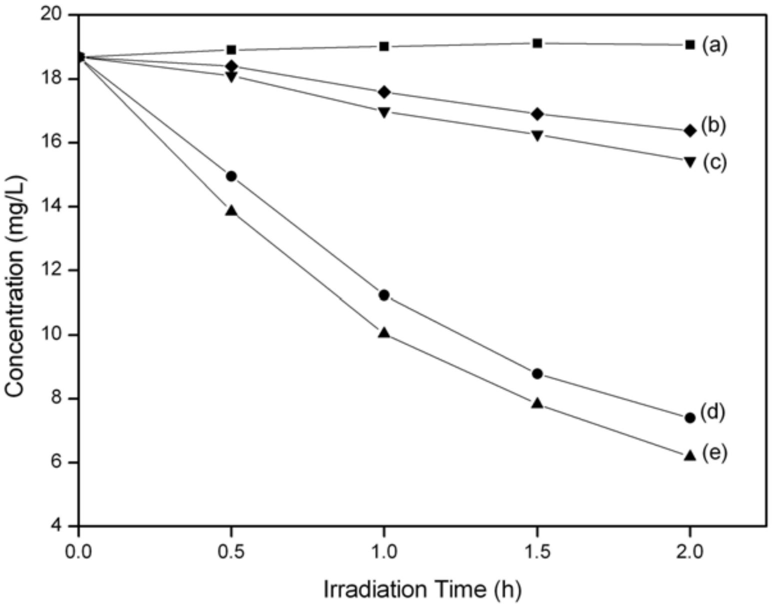

Fig.7-6 Variations in concentration of Neolan Blue 2G in an aqueous solution as a function of UV irradiation time for (a) untreated white cotton, (b) TA23 treated white cotton after 20 washing, (c) TA23 treated white cotton after 10 washing, (d) TA23 treated white cotton before washing, and (e) S60 treated white cotton.

irradiation was reduced remarkably by TA23 treated cotton fabrics before washing, which indicates that TA23 under UV irradiation has high colorant decomposition activity. This may be attributed to single-phase anatase with high crystallinity and small crystal size 5-7 nm of TA23 as shown in XRD and TEM above. It is well known that the photocatalytic activity of titania films is strongly influenced by several factors such as the crystal phase of TiO_2 (Fox & Dulay, 1993; Nishimoto, Ohtani, Kajiwara, & Kagiya, 1985), particle size

(Almquist & Biswas, 2002; Z. Zhang, Wang, Zakaria, & Ying, 1998), surface area (Hengzhong Zhang, Penn, Hamers, & Banfield, 1999) and so on.

The mechanism of Neolan Blue 2G photodegradation under UV irradiation is same as that of Neolan Blue 2G in Chapter 4. The reactive oxygen species such as OH•, O_2^-• $^{\cdot}$generated on TA23 TiO_2 surface decomposed the colorant under UV irradiation. On one hand, TA23 is single-phase anatase TiO_2 which is considered to be the most active photocatalyst. And TA23 anatase TiO_2 with high crystallinity is beneficial for enhancing the photocatalytic activity, since anatase TiO_2 with high crystallinity has relatively little disruption in its electronic band structure and high crystallinity dimishes the e^--h^+ recombination (Yanagisawa & Ovenstone, 1999). On the other hand, TA23 anatase TiO_2 with particle size of 5-7 nm is small enough. Particle size is important for photocatalysis since it directly impacts the specific surface area of a photocatalyst. As the photocatalytic reaction occurs at the TiO_2 surface, the reaction area between the surface of particle and the target materials (that is, the specific surface area) needs to be large for more effective photocatalytic activity. With a smaller particle size, surface area increases which increases available active surface sites and photonic efficiency enhances from a higher surface charge carrier transfer rate in photocatalysis (Z. Zhang, Wang, Zakaria, & Ying, 1998). Therefore, TA23 anatase TiO_2 with high crystallinity and smaller partice size 5-7 nm posseses high photocatalytic activity. Fig. 7-6 also shows that the colorant concentration was reduced slightly more by S60 treated cotton fabrics (Fig. 7-6e) compared to that by TA23 treated cotton fabrics (Fig.7-6d). This means that the photocatalytic activity of TA23 by aging at room temperature is similar to that of S60 by heating method described in Chapter 4.

Although the rates of colorant decomposition of TA23 treated samples were decreased after 10 washings (Fig.7-6c) and after 20 washings (Fig.7-6b) compared to that before washing, they remained much higher than that of untreated cotton substrates. Moreover, the colorant concentration of TA23 treated cotton substrates after 20 washings was reduced a bit more than that after 10 washings. These results suggest good adhesion between TiO_2 and cotton. This might be attributable to the formation of covalent bonding at their interface as a result of dehydration reactions between the cellulosic hydroxyl groups and the hydroxyl groups of titania (Daoud & Xin, 2004a; Daoud, Xin, & Zhang, 2005). It can also be found that under the same UV irradiation, the colorant concentration in contact with only the cotton substrates without TiO_2 films remained almost at the same level during UV irradiation (Fig.7-6a), which means that this type of cotton substrates has no colorant decomposition ability and the dye itself would not be decomposed by UV radiation.

7.5.2 Degradation of red wine and coffee stains

Fig.7-7 and Fig.7-8 present respectively that the degradation of a red wine stain and a coffee stain on untreated cotton and TA23 treated cotton fabrics before and after light irradiation in Xenotest Alpha LM light exposure and weathering test instrument. The color, area and shape of stains on untreated cotton and TiO_2 treated cotton are different. A titania surface (freshly prepared) on is hydrophobic (Rong Wang et al., 1997; Rong Wang et al., 1998) so stains on titania surface spread over a small area and the color of stains becomes more intense, while untreated cotton surface is hydrophilic and the area of stains is larger and the color is lighter.

From Fig. 7-7 and Fig. 7-8, it can be seen that a remarkable discoloration of a red wine stain and a coffee stain on TA23 treated cotton fabrics was observed after 8 h of light irradiation and a complete discoloration was achieved after 20 h of light irradiation. On the other hand, almost no discoloration of red wine and coffee stains on untreated cotton was observed during light irradiation. It means that TA23 layers on cotton fabrics can completely degrade red wine and coffee stains while untreated cotton fabrics have no stain degradation activities for red wine and coffee stains. Furthermore, while significant discoloration of red wine and coffee stains was observed on the exposed side of TA23 treated cotton fabrics after 8 h of light irradiation, the color of the red wine stain and coffee stain on the unexposed side of TA23 treated cotton fabrics could still be

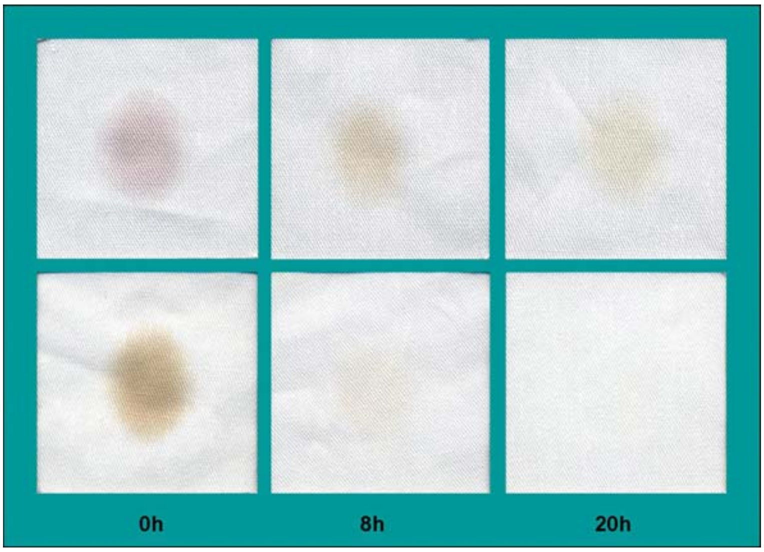

Fig. 7-7 Stain removal test using a red wine stain. The images shown are the exposed side of untreated white cotton (the upper row) and TA23 treated white cotton fabrics (the bottom row) after 0 h, 8 h and 20 h of light irradiation in Xenotest Alpha LM light exposure and weathering test instrument.

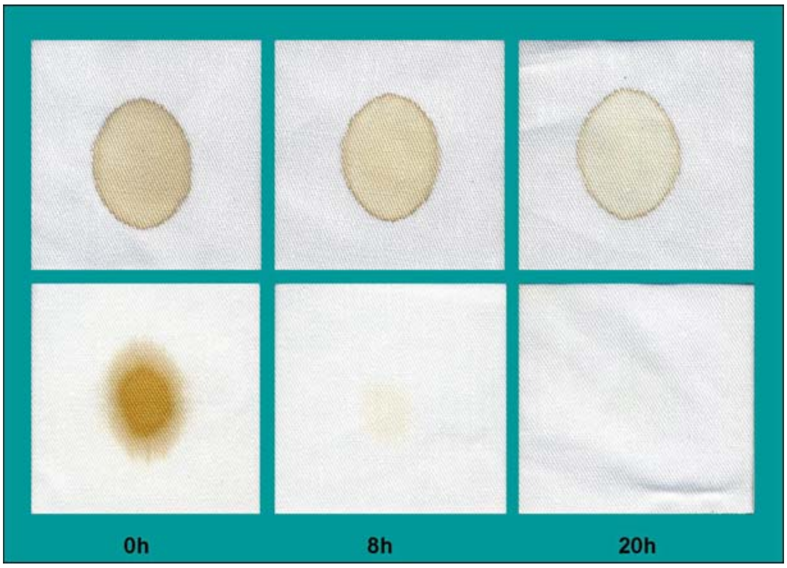

Fig.7-8 Stain removal test using a coffee stain. The images shown are the exposed side of untreated white cotton (the upper row) and TA23 treated white cotton fabrics (the bottom row) after 0 h, 8 h and 20 h of light irradiation in Xenotest Alpha LM light exposure and weathering test instrument.

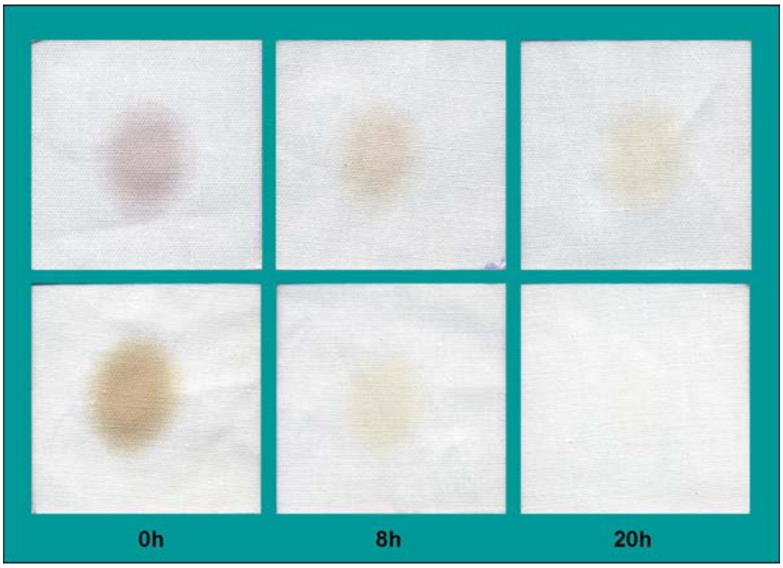

Fig. 7-9 Stain removal test using a red wine stain. The images shown are the unexposed side of untreated white cotton (the upper row) and TA23 treated white cotton fabrics (the bottom row) after 0 h, 8 h and 20 h of light irradiation in Xenotest Alpha LM light exposure and weathering test instrument.

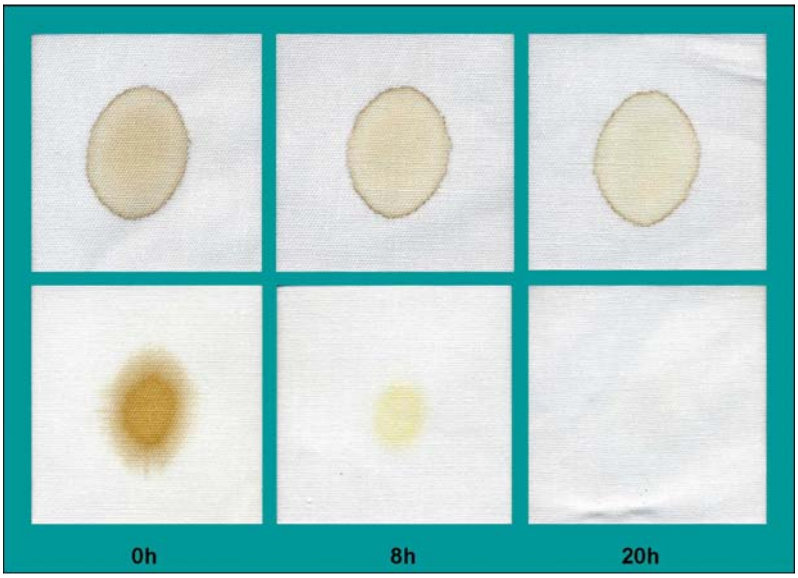

Fig.7-10 Stain removal test using a coffee stain. The images shown are the unexposed side of untreated white cotton (the upper row) and TA23 treated white cotton fabrics (the bottom row) after 0 h, 8 h and 20 h of light irradiation in Xenotest Alpha LM light exposure and weathering test instrument.

observed (Fig. 7-9, 7-10). However, a complete discoloration of all the stains on the unexposed side of TA23 treated cotton fabrics was achieved after 20 h of light irradiation. The degradation activities of a red wine stain and a coffee stain for TA23 by aging at room temperature is similar to those for S60 by heating method in Chapter 4.

The mechanism of degradation of red wine and coffee stains on T23 TiO_2 treated cotton fabrics is same as that described in Chapter 4. The reactive oxygen species generated on the irradiated T23 TiO_2 surface decomposed red wine and coffee stains adsorbed on TiO_2 treated cotton fabrics.

7.6 Tensile Strength

Table 7-1 shows the tensile strength of untreated cotton and TA23 treated cotton before and after 20 h of light irradiation in Xenotest Alpha LM light exposure and weathering test instrument.

The tensile strength in warp direction of TA23 treated cotton fabrics before light irradiation was reduced by 0.75% compared to that of untreated cotton fabrics, This is could be due to the increase of stiffness after TiO_2 coating. After 20 h of light irradiation, the tensile strengths of untreated cotton and TA23 treated cotton fabrics were reduced. However, the decrease in untreated cotton fabrics was 4.50% while the decrease in TA23 treated cotton was 2.26%. This

Table 7-1 Tensile strength study in warp direction

Samples	**Tensile Strength (N)**		**Reduction (%)**
	Before light irradiation	**After 20 h light irradiation**	
Untreated cotton	652.90	623.50	4.50%
A23 after aging treated cotton	648.00	633.37	2.26%

suggests that there is no photocatalytic decomposition of the molecular chains of cotton caused by the TA23 layers. On the contrary, the titania layers reduced the drop of tensile strength due to its ability to absorb UV irradiation. This is agreement with the results of self-cleaning cotton in Chapter 4.

7.7 Conclusions

Nanocrystalline anatase thin films have been prepared on cotton fabrics by a simple sol-gel process in aqueous media followed by aging at room temperature. The aging process at room temperature promotes the crystallization of anatase phase. The cotton fabrics treated by the anatase nanocrystallites after aging at room temperature show significant self-cleaning performance as demonstrated by their colorant decomposition and degradation of a red wine stain and a coffee stain under UV irradiation. The UV absorption by the anatase films was quite substantial, promoting excellent UV protection to the cotton. These thin anatase films have good adhesion to the cotton substrates resulting in high washfastness. No photodegradation of the cellulosic chains of cotton by the anatase films could be observed as demonstrated by a comparison study of the tensile strength of treated cotton fabrics before and after prolonged light irradiation. This study provides an alternative method of the preparation of anatase titania to be used in self-cleaning cotton. The anatase titania prepared have similar photocatalytic power comparing to that prepared by heating method described in chapter 4.

Chapter 8: Visible Light–responsive Iron-doped TiO_2 and its Photocatalytic Activities under UV and Visible light Irradiation

8.1 Introduction

TiO_2 is a promising photocatalyst for the photodegradation of organic dirt. However, due to the wide band-gap energy of TiO_2 (ca. 3.0 eV for rutile and 3.2 eV for anatase), only UV radiation is utilized for the photocatalysis, which is equivalent to a mere 5% of solar spectrum. In addition, the relatively high rate of electron-hole recombination on TiO_2 particles results in low quantum yields, which means a reduced photocatalytic power. The low visible light utilization and low quantum yields limit the application of TiO_2 as a photocatalyst, especially in environments where UV radiation is low, such as ambient lighting environment. Therefore, the development of TiO_2–based photocatalytic self-cleaning system which can utilize visible light and be applicable to low-heat resistant substrates has been very attractive.

A great deal of research has focused on extending the ability of TiO_2 to utilize energy in visible region of the spectrum as well as reducing electron-hole recombination to improve photoactivity by doping TiO_2 with impurities. Selective doping of TiO_2 with transition metal cations has been proven to be an efficient route to improve the photoactivity of TiO_2 while maintaining a good control of the primary particle size to achieve nanoscale configurations of the catalysts (Fuerte et al., 2001; Hoffmann, Martin, Choi, & Bahnemann, 1995; X. Li, Yue, & Kutal, 2003; Yeung et al., 2002). Choi et al.(Choi, Termin, & Hoffmann, 1994a, , 1994b) carried out a systematic study on metal ion doping in quantum-sized (2-4 nm) TiO_2 colloids was prepared by a hydrolysis process, followed by aging for over 1 year. They reported that selectively doped quantum-sized particles had a much greater photoreactivity as measured by their quantum efficiencies for $CHCl_3$ oxidation than their undoped counterparts. Of the 21 metal ion dopants, Fe^{3+} at 0.1-0.5 at % was the most effective dopant in the increase of quantum efficiency. Zhang *et al.* (1998) found that optimal Fe^{3+} dopant concentration for enhancing photocatalytic activity in $CHCl_3$ degradation was dependent on the particle size of TiO_2. Fe^{3+} dopant concentration decreased with increasing particle size of TiO_2. The phase transition of Fe^{3+} doped TiO_2 was studied (Y.-H. Zhang & Reller, 2001), but the photocatalytic activity of Fe^{3+} doped TiO_2 was not reported. In the photocatalytic oxidation of methanol, Fe^{3+} doping at 0.25 or 0.5 at.% in TiO_2 was also found to be highly effective in improving photocatalytic activity (C.-Y. Wang, Böttcher, Bahnemann, & Dohrmann, 2003). Recently, several other studies also reported that Fe^{3+} doped TiO_2 powder with optimal doping concentration exhibited a greatly enhanced photocatalytic activity in the degradation of dyestuff (Feng, Wong, Hu, & Yue, 2004; X. H. Wang, Li, Kamiyama, Moriyoshi, & Ishigaki, 2006; Zhu, Chen, Zhang, Chen, & Anpo, 2006; Zhu, Zheng, He, Zhang, & Anpo, 2004), isopropanol (Colmenares, Aramendia, Marinas, Marinas, & Urbano, 2006) and phenol (Adán, Bahamonde, Fernandez-Garcia, & Martinez-Arias, 2007). It seems that the optimum photocatalytic activities can be achieved upon doping at a relatively level. However, Fe^{3+} doped TiO_2 powders were prepared by combining sol-gel with hydrothermal treatment or post-calcination at 450-564°C (Adán, Bahamonde, Fernandez-Garcia, & Martinez-Arias, 2007; Colmenares, Aramendia, Marinas, Marinas, & Urbano, 2006; Feng, Wong, Hu, & Yue, 2004; Z. Zhang, Wang, Zakaria, & Ying, 1998; Zhu, Chen, Zhang, Chen, & Anpo, 2006; Zhu, Zheng, He, Zhang, & Anpo, 2004) or prepared by plasma oxidative pyrolysis (X. H. Wang, Li, Kamiyama, Moriyoshi, & Ishigaki, 2006). Not only the two preparation processes were too long to be feasible in practical application, but also the temperatures used during the calcining or plasma oxidative pyrolysis processes were too high if substrates with low thermal resistance such as textiles are involved in the processes.

In this chapter, we developed Fe^{3+} doped TiO_2 photocatalytic self-cleaning system to improve the photocatalytic activity of Fe^{3+} doped TiO_2 films under visible light illumination. The synthesis was based on a sol-gel process in an aqueous solution at a low temperature of 60 °C with the addition of Fe^{3+} dopant was designed to reduce the band gap energy and extend the wavelength response range to visible region. The Fe^{3+} dopant with optimal doping level would also provoke a decrease in electron-hole recombination rate (inhibit recombination by increasing the charge separation) and therefore increase the efficiency of the photocatalytic process. This new system was then applied to cotton fabrics in an attempt to achieve a better self-cleaning property comparing to our previous TiO_2 systems in Chapter 4 and Chapter 6 under visible light as well as under another visible light source with no or insignificant amount of UV.

8.2 Synthesis of Fe^{3+} doped TiO_2 sols

The reagents used were titanium tetraisopropoxide (98%, Aldrich,) as TiO_2 source and $Fe(NO_3)_3.9H_2O$ (98%, Aldrich) as the source of dopant. Fe^{3+} doped TiO_2 sols were synthesized as follows. First, a predetermined amount of $Fe(NO_3)_3.9H_2O$ was dissolved in 100 ml deionized water containing 0.7 ml nitric acid (70%, Aldrich) and 10 ml acetic acid (99.8%, Aldrich). The weight ratio of Fe^{3+} to TiO_2 was controlled to be between 0.1-5.0 wt%. Then 10 ml titanium tetraisopropoxide (TTIP) was added dropwise into $Fe(NO_3)_3 .9H_2O$ aqueous solution under vigorous stirring. The mixtures were heated to 60 °C and kept at that temperature while being stirred for 16 h. The prepared Fe^{3+} doped TiO_2 sols were named as 0.1% Fe^{3+}-TiO_2, 0.25% Fe^{3+}-TiO_2, 0.5% Fe^{3+}-TiO_2, 1.0% Fe^{3+}-TiO_2, 2.0% Fe^{3+}-TiO_2 and 5.0% Fe^{3+}-TiO_2 respectively.

8.3 Characterization of Fe^{3+} doped TiO_2 nanoparticles

8.3.1 XRD spectroscopy

Fig.8-1 shows the XRD patterns of pure TiO_2 and Fe^{3+} doped TiO_2. It can be seen that all samples exhibit the patterns associated to the crystalline anatase phase. Any other crystalline phase containing Fe could not be observed. With Fe-doping concentration increasing, the peak intensities of anatase slightly decrease and the width of (101) plane diffraction peak of anatase (2θ=25.4°) becomes broader. This indicates that the larger the amount of Fe-doping, the poorer the crystallization of the TiO_2 particles, and the smaller the crystallite size of TiO_2. Since the radius of Fe^{3+} is 0.64Å, which is slightly smaller than 0.77 Å for channels along the *c*-axis in pure TiO_2 and the radius of Ti^{4+} (0.68 Å) in the TiO_2 lattice (Egerton, Harris, John Lawson, Mile, & Rowlands, 2001), it is possible that Fe^{3+} diffuses along the *c*-axis and substitutes Ti^{4+} in the TiO_2 lattice. Due to the different atomic sizes of Fe^{3+} and Ti^{4+}, some extent of distortion is introduced into the crystal lattice of TiO_2. Thus comparing with the XRD pattern of pure TiO_2, pattern peaks weakening were observed in those of Fe^{3+} doped TiO_2. On the other hand, as a result of crystal lattice distortion, the crystallite growth of Fe^{3+} doped TiO_2 grains is restrained, which resulted in a slight broadening in XRD peaks.

It is worth to note that iron oxides or Fe_xTiO_y phases are not found in the patterns of XRD, which is in accord with the reports published previously(C.-Y.

Wang, Böttcher, Bahnemann, & Dohrmann, 2003; M. Zhou, Yu, & Cheng, 2006; M. Zhou, Yu, Cheng, & Yu, 2005). One possible reason is that the concentration of Fe- doping is so low that it can not be detected by XRD. The other is that the radius of Fe^{3+} and Ti^{4+} are very close and all the iron ions maybe insert into the structure of titanium, and substitutes Ti^{4+} in the TiO_2 lattice (C.-Y. Wang, Böttcher, Bahnemann, & Dohrmann, 2003). These results support that the current doping procedure allows uniform distribution of the dopants, forming stable solid solutions within TiO_2.

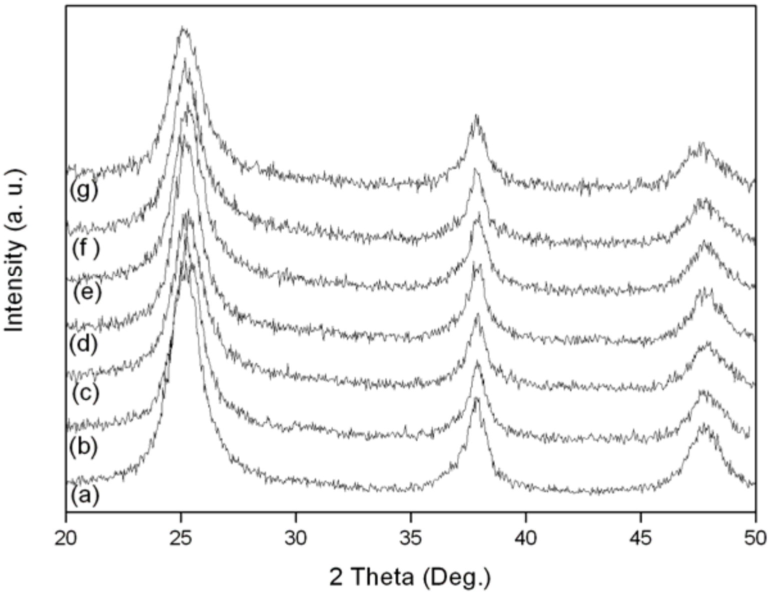

Fig. 8-1 XRD patterns of solid powder extracted from (a) pure TiO_2, (b) 0.1% Fe^{3+}-TiO_2, (c) 0.25% Fe^{3+}-TiO_2, (d) 0.5% Fe^{3+}-TiO_2, (e) 1.0% Fe^{3+}-TiO_2, (f) 2.0% Fe^{3+}-TiO_2 and (g) 5.0% Fe^{3+}-$TiO_{2.}$

8.3.2 TEM

Fig. 8-2 shows HRTEM images of 0.25 wt.% Fe^{3+} doped TiO_2 nanoparticles.

0.25 wt.% Fe^{3+} doped TiO_2 nanoparticles were well dispersed with narrow size distribution as shown in Fig.8-2a. Fig.8-2b shows the selected area electron diffraction (SAED). Measurements of lattice spacing from the corresponding SAED pattern shown in Fig. 8-2b indicated that the nanocrystals are anatase. The nanocrystals observed in Fig.8-2c have a lattice fringe of 0.35 nm that corresponds to the 101 lattice plane and a diameter of 4-7 nm which is smaller than pure TiO_2 (S60) in Chapter 4. This indicated that the particle growth becomes restrained upon iron doping.

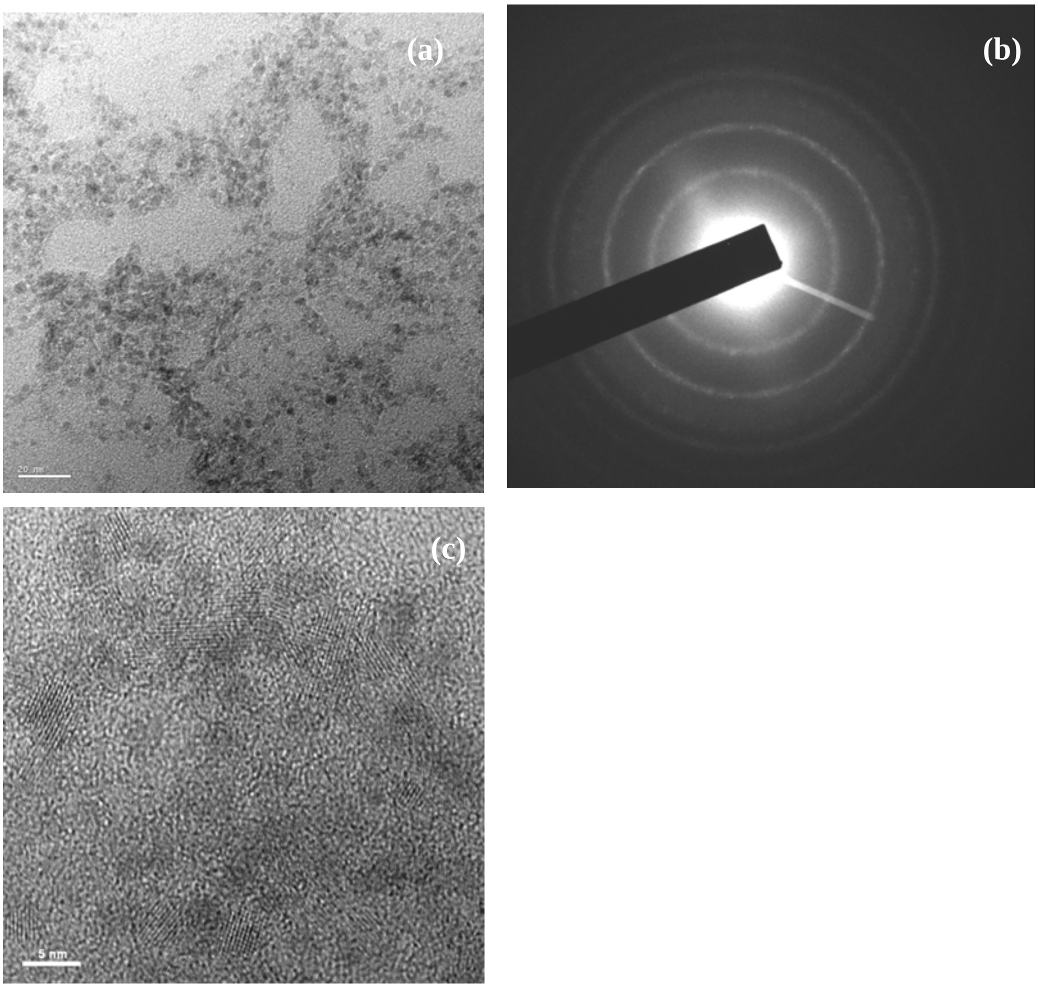

Fig. 8-2 HRTEM micrographs of 0.25 wt.% Fe^{3+} doped TiO_2 (a) at low resolution, (b) selected area electron diffraction and (c) at high resolution.

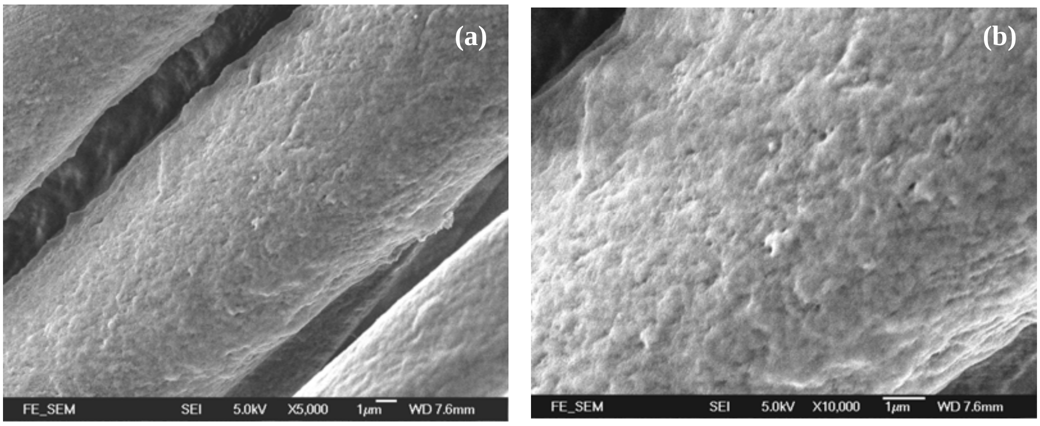

Fig. 8-3 SEM images of (a) 0.25 wt.% Fe^{3+} doped TiO_2 treated cotton fibers at low magnification and (b) 0.25 wt.% Fe^{3+} doped TiO_2 treated cotton fibers at higher magnification.

8.3.3 SEM

SEM micrographs of 0.25wt.% Fe^{3+} doped TiO_2 treated cotton fibers in Fig. 8-3a showed that a uniform continuous layer was formed on cotton fibers. A higher magnification SEM image (Fig. 8-3b) revealed that the surface structure is grainy.

8.4 Photocatalytic activities

The photocatalytic activities of pure TiO_2 treated cotton fabric and various amount of Fe^{3+} doped TiO_2 treated cotton fabrics for Neolan Blue 2G decomposition under UV irradiation (Philips TLD 18W/08, UV intensity is 0.8-0.9 mW/cm^2) and under visible light illumination (Philips TLD 18W/54 Daylight, Ev=6562 lx, x=3207, y=3539) are revealed in Fig.8-4 and Fig.8-5

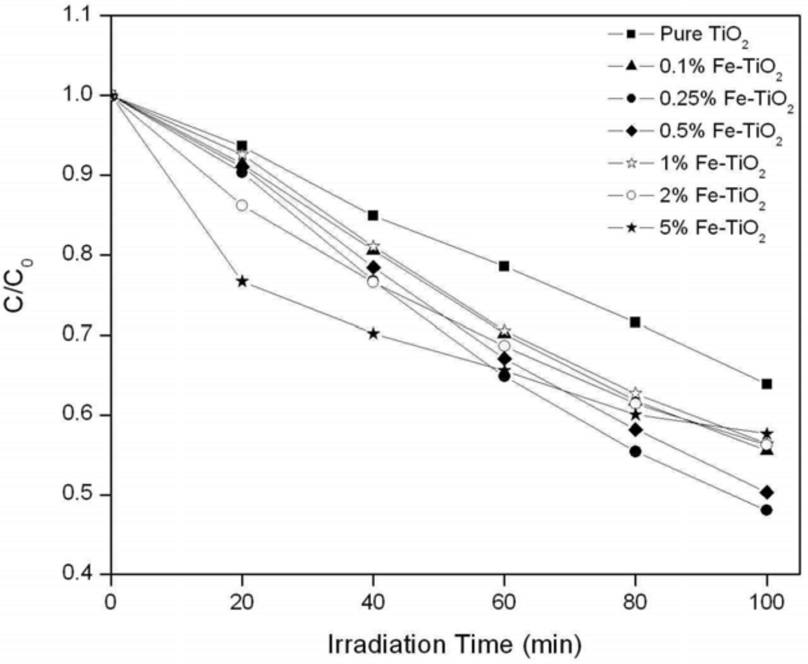

Fig.8-4 Photodecomposition of Neolan Blue 2G in an aqueous solution as a function of UV irradiation time for different substrates: pure TiO_2 (■), 0.1 % Fe^{3+}-TiO_2 (▲), 0.25% Fe^{3+}-TiO_2, (●), 0.5% Fe^{3+}-TiO_2 (◆), 1.0% Fe^{3+}-TiO_2 (☆), 2.0% Fe^{3+}-TiO_2 (○), and 5.0% Fe^{3+}-TiO_2 (★) treated cotton fabrics.

respectively. In Fig.8-4 and Fig.8-5, C_0 is the initial concentration of dye before UV radiation and after the fabric-dye absorption comes to an equilibrium, C is the concentration at irradiation time t.

It can be seen from Fig. 8-4 that all of the colorant concentrations decrease more rapidly for all of Fe^{3+} doped TiO_2 treated cotton fabrics than that for pure TiO_2 treated cotton fabric. This indicates that all of Fe^{3+} doped TiO_2 treated cotton fabrics have higher photocatalytic activities than pure TiO_2 treated

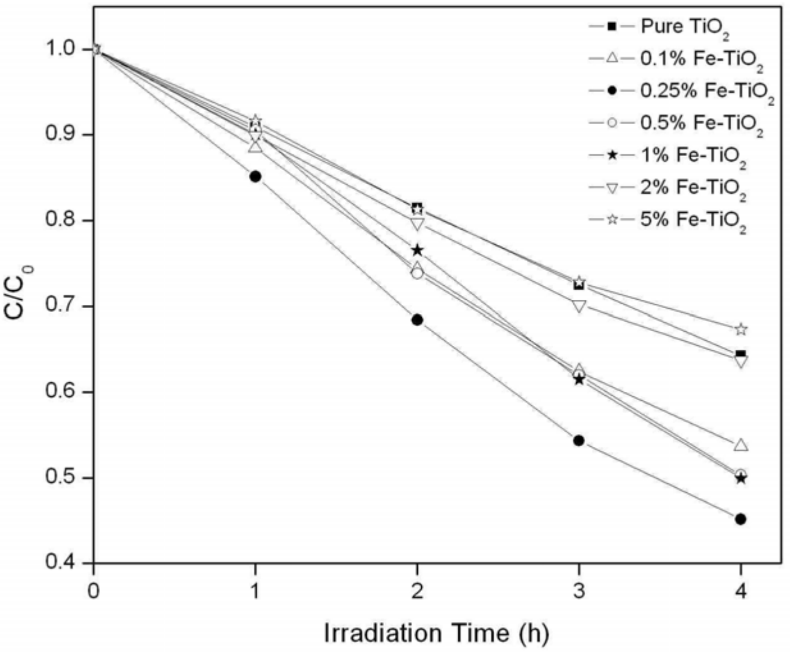

Fig.8-5 Photodecomposition of Neolan Blue 2G in an aqueous solution as a function of visible light illumination time for different substrates: pure TiO_2 (■), 0.1% Fe^{3+}-TiO_2 (△), 0.25% Fe^{3+}-TiO_2 (●), 0.5% Fe^{3+}-TiO_2 (○), 1.0% Fe^{3+}-TiO_2 (★), 2.0% Fe^{3+}-TiO_2 (▽), and 5.0% Fe^{3+}-TiO_2 (☆) treated cotton fabrics.

cotton fabric during 100 min UV irradiation. It is obvious in Fig.8-5 that the colorant concentration for each sample decreases much more slowly under visible light illumination than under UV irradiation respectively. The colorant concentration for from 0.1 to 2.0 wt.% Fe^{3+} doped TiO_2 treated cotton fabrics reduces more quickly than that for pure TiO_2 treated cotton fabric respectively, but the concentration for 5.0 wt.% Fe^{3+} doped TiO_2 treated cotton fabric decreases most slowly and even more slowly than that for pure TiO_2 treated cotton fabric at 4h visible light illumination. This shows that pure TiO_2 and Fe^{3+} doped TiO_2 are more photoactive under UV irradiation than under visible light illumination and overloaded Fe^{3+} retards the photocatalytic decomposition.

As can be readily seen in Fig.8-4 and Fig.8-5, the colorant concentration for Fe^{3+} doped TiO_2 treated cotton fabrics decreases faster as Fe^{3+} doping level increased from 0.1 to 0.25 wt.% and the colorant concentration reduces most rapidly for 0.25 wt.% Fe^{3+} doped TiO_2 treated cotton fabrics under both UV and visible light irradiation. With further increasing Fe^{3+} doping concentration, the difference was observed. In Fig.8-4, during the first 40 min UV irradiation, the decrease in the colorant concentration for 2.0 wt.% and 5.0 wt.% Fe^{3+} doped TiO_2 treated cotton fabrics is more than those with other doping levels and the decrease for 5.0 wt.% Fe^{3+} doped TiO_2 treated cotton fabric is the most. However, with UV irradiation time increasing, the decreases in colorant concentration for 2.0 wt.% and 5.0 wt.% Fe^{3+} doped TiO_2 treated cotton fabrics under UV irradiation are slower. At 100 min UV irradiation, the decrease in colorant concentration for 5.0 wt.% Fe^{3+} doped TiO_2 treated cotton fabric is the slowest among all doping levels, only higher than that for pure TiO_2 treated cotton fabric. This shows that higher amount of Fe^{3+} doped TiO_2 has higher photocatalytic activities under UV irradiation in the initial photocatalytic degradation and higher Fe^{3+} doping level retards photocatalytic degradation of the colorant under longer UV irradiation.

In Fig.8-5, as Fe^{3+} doping level increases beyond 0.25 wt.%, the colorant concentration reduces more and more slowly with the increasing Fe^{3+} concentration under visible light illumination. This indicates that photocatalytic activity of Fe^{3+} doped TiO_2 decreases more and more with increasing Fe^{3+} doping concentration up to 0.25 wt.% under visible light illumination. The results also indicate that the optimal Fe^{3+} doping level is 0.25 wt.% with the highest photocatalytic activity.

The photocatalytic mechanism of Fe^{3+} doped TiO_2 under UV and visible light irradiation was proposed previously(Choi, Termin, & Hoffmann, 1994b; Hung, Fu, Tseng, Chu, & Ko, 2007; C.-Y. Wang, Böttcher, Bahnemann, & Dohrmann, 2003; M. Zhou, Yu, & Cheng, 2006; M. Zhou, Yu, Cheng, & Yu, 2005; Zhu, Chen, Zhang, Chen, & Anpo, 2006; Zhu, Zheng, He, Zhang, & Anpo, 2004). When Fe^{3+} doped TiO_2 is exposed to UV light and visible light, the excited holes (h^+) and excited electrons (e^-) are generated that will migrate to the surface. The photocatalytic activity of Fe^{3+} doped TiO_2 with lower doping level was enhanced compared to that of undoped TiO_2. The beneficial effect of Fe^{3+} may be explained by considering the efficient separation of photoexcited electrons and holes. Fe^{3+} with lower doping level can act as photogenerated hole trappers and photogenerated electron trappers (Choi, Termin, & Hoffmann, 1994b; Zhu, Chen, Zhang, Chen, & Anpo, 2006; Zhu, Zheng, He, Zhang, & Anpo, 2004). It can not be excluded that Fe^{3+} in the TiO_2 lattice could act as recombination centers for electron-hole pair. When the dopant concentration is too high, the recombination rate will increase and compete with the redox processes as the distance between trapping sites decreases.

The photocatalytic activities of Fe^{3+} doped TiO_2 under UV and visible light irradiation in Fig. 8-4 and Fig.8-5 can be explained as follows. Firstly, Fe^{3+} can enhance the intensity of absorption in the UV-Visible light region and make a red shift in the band gap transition of Fe-doped TiO_2 samples as showed in Fig.8-6. It is apparent from Fig. 8-6 that the UV-Vis diffuse reflectance spectrum of 0.25 wt.% Fe doped TiO_2 shows a stronger absorption in the UV-visible light region and an obvious red shift in the band gap transition compared to that of pure TiO_2. The enhanced absorption in the visible region associated with the presence of iron ions may be attributed to a charge transfer transition between the d electrons of iron ions and the TiO_2 conduction or valence band (Zhu, Zheng, He, Zhang, & Anpo, 2004). The absorption edges shifting toward longer wavelengths for 0.25 wt.% Fe^{3+} doped TiO_2 should certainly mean a decrease in the band gap energy of TiO_2 (M. Zhou, Yu, & Cheng, 2006). This can induce more photo-generated electrons and holes to participate in the photocatalytic reaction. Increased light absorption in the visible region possibly could lead to better photocatalytic activities, especially under visible light irradiation. Secondly, Fe^{3+} ions can also serve as a mediator of the transfer of interfacial charge at an appropriate doping concentration. In our study, the optimal dopant concentration is 0.25 wt.%. At lower concentrations than the optimal value (0.25 wt.%), the photocatalytic activities increase with the increasing Fe^{3+}concentration because a small amount of Fe^{3+} ions can trap both holes and electrons to achieve better effective inhibition for the hole and electron recombination (C.-Y. Wang, Böttcher, Bahnemann, & Dohrmann, 2003; M. Zhou, Yu, Cheng, & Yu, 2005). But excessive Fe^{3+} ions are detrimental. Above the optimal concentration, Fe^{3+} ions become recombination center and cause the decrease in the photocatalytic activity (Feng, Wong, Hu, & Yue, 2004; Hung, Fu, Tseng, Chu, & Ko, 2007; M. Zhou, Yu, & Cheng, 2006) .

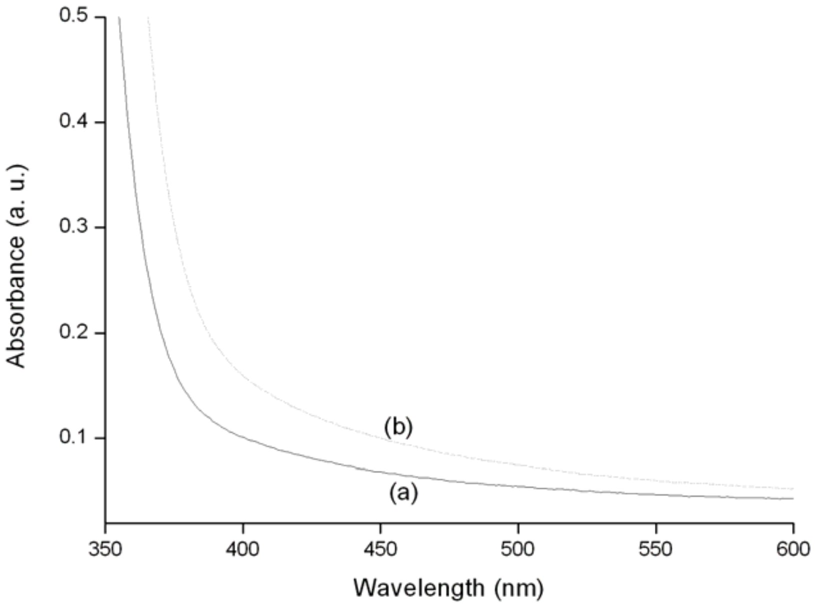

Fig. 8-6 UV-Vis diffuse reflectance spectra of (a) pure TiO_2 and (b) 0.25 wt.% Fe^{3+} doped TiO_2 nanoparticles.

8.5 Conclusions

Visible light-responsive Fe^{3+} doped TiO_2 was successfully synthesized by a sol-gel process at a low temperature of 60°C. The Fe^{3+} doped TiO_2 showed a strong absorption in the UV-Visible light region and a red shift in the band gap transition. The results in the study showed that the Fe^{3+} dopant did not change the crystal structure of TiO_2, but significantly affect their photocatalytic activity. The XRD patterns and TEM images showed that the nanocrystals of Fe^{3+} doped TiO_2 were single-phase anatase same as that of undoped $TiO_{2.}$ A small amount of Fe^{3+} doping could clearly enhance the photocatalytic activity of TiO_2. The UV activity was higher than the visible light activity. 0.25 wt.% Fe^{3+} dopant was optimum for both UV and visible light irradiation. However, overloading Fe^{3+} decreased the photocatalytic activity under both UV and visible light irradiation. The results could be explained by the balance of excited electron/hole trapped by the doped Fe^{3+} and their charges recombination on the doped Fe^{3+} level.

Chapter 9: Conclusions and Suggestions for Future Research

9.1 Conclusions

Photocatalysis self-cleaning function can provide high added value to both consumers and the textile and apparel industry. It is also beneficial to the cleaner and ‘greener’ environment with the reduced needs for laundering. Among various metal oxide photocatalysts, titanium dioxide (TiO_2) is one of the most promising photocatalytic materials due to its high oxidizing ability, nontoxicity, long term stability and low cost.TiO_2 nanoparticles are catalysts that help to chemically break down organic materials, requiring only sunlight to trigger the reaction. TiO_2 treated textiles could lead to self-cleaning fabrics that tackle organic dirt, environmental pollutants and harmful microorganisms. For maximum activity of TiO_2 treated textiles, TiO_2 nanoparticles should have anatase crystal structure, which was difficult to achieve previously with a low processing temperature. This research work was aimed to study the preparation of anatase TiO_2–based photocatalytic self-cleaning system at a low temperature and their self-cleaning performance on cotton and polyester under UV or visible light irradiation. Six objectives were identified in Chapter 1 and the following sections summarize the extent to which these objectives are achieved.

9.1.1 Fabrication of anatase titania nanoparticles and their application to cotton fabrics

Chapter 4 describes the development of anatase TiO_2 nanoparticles at low temperatures and the investigation of their application to cotton fabrics. The experimental results reported in Chapter 4 reveal that the formation of nanocrystalline anatase TiO_2 strongly depends on the acid catalysts and reaction temperatures using a sol-gel method in acidic deionized water. When only nitric acid used as catalysts, amorphous titania was formed at room temperature since almost no peak could be observed in XRD. And predominantly anatase with a small amount of brookite was formed at 60°C as anatase peaks at 25.4°, 38.0°, 48.0° and brookite peaks at 27.7°, 31.1°, 37.6°, 42.6° and 48.3° in XRD.

When using nitric acid and acetic acid as catalysts, predominantly amorphous TiO_2 with a very small content of anatase crystallites were obtained at room temperature since broad weak anatase-associated peaks were observed at 25.4° in XRD. On the other hand, single-phase anatase TiO_2 was achieved at both 40 and 60°C. The addition of organic acetic acid in a HNO_3-contained aqueous solution may benefit the formation of pure anatase phase at low temperatures. And the average size of as-synthesized anatase crystallites increased when the reaction temperatures increased from room temperature to 60°C.

Due to the highest crystallinity of anantase TiO_2 formed at 60°C as demonstrated by its sharpest anatase peaks with greatest intensities from the XRD study, anantase TiO_2 formed at 60°C possessed the strongest photocatalytic activity. The TiO_2 anatase treated cotton fabrics showed significant self-cleaning performance as demonstrated by their bactericidal activities, colorant decomposition and degradation of red wine and coffee stains under UV irradiation. The UV absorption by the titania film was quite substantial, promoting excellent UV protection to the cotton. No photodegradation of the cellulosic chains of cotton by the titania film could be observed as demonstrated by a comparison study of the tearing strength of treated cotton fabrics before and after prolonged solar-simulated light irradiation.

9.1.2 The application of anatase titania to polyester fabrics

In Chapter 5, the application of single-phase anatase TiO_2 to polyester fabrics was investigated as well as the low temperature plasma (LTP) pretreatment of polyester surface to improve the bondability of TiO_2 on polyester fiber and self-cleaning performance of polyester fibers. Single-phase anatase TiO_2 prepared by an aqueous sol-gel process at 60°C was applied to polyester fibers that were treated with low temperature plasma. This process not only functionalizes polyester, but also enhances its adhesion to the anatase. Oxygen was chosen as the LTP gas. The discharge power, pressure and gas flow rate were 100 W, 6 Pa and 15scc/min, respectively. The exposure time was 10 min. 100W discharge power and 10 min treatment time are enough for the surface structure modification.

The surface morphological changes of polyester fibers before and after plasma treatment, and of plasma-treated fibers before and after anatase coating were characterized by SEM. The results showed that the surface etching process occurred on the surface of oxygen plasma pretreated fiber. Granules, micro-craters and ripple-like structures of sub-micrometer size are observed on the oxygen plasma pretreated surface. The removal of the surface layers leads to an increase in the roughness and the roughness of this surface is far more accentuated than that of the original fiber surface. And the surface structure of the TiO_2-coated polyester filament pretreated with oxygen plasma indicated the formation of TiO_2 layers.

Anatase TiO_2 coated polyester fibers pretreated with low temperature oxygen plasma showed significant improvement in self-cleaning performance as demonstrated by their bactericidal activities, colorant decomposition and degradation of red wine and coffee stains under UV irradiation. The adhesion between TiO_2 layers and polyester substrates was also improved after plasma treatment, which was studied by comparing the ability of dye decomposition under UV irradiation. The UV absorption of the titania coated polyester was significant enough to promote excellent UV protection to polyester. No photodegradation of the molecular chains of polyester by the titania layers could be observed as demonstrated by a comparison study of the tearing strength of coated polyester fabrics before and after light irradiation.

9.1.3 Preparation of anatase TiO_2/SiO_2 spherical nanocomposites and their photoctalytic activities

To further improve the photocatalytic activity of TiO_2 films, the combination of photoactive TiO_2 with SiO_2 has been investigated in Chapter 6. Anatase TiO_2/SiO_2 spherical nanocomposites with core-shell feature were prepared by a sol-gel process at 60°C. The structural properties of these as-prepared nanocomposites were characterized with SEM and XRD. The results showed that the average diameter of the spherical SiO_2 particles was about 500 nm and the TiO_2 deposited SiO_2 particles showed a rough surface and less than perfect spherical shape with the average diameter increasing to about 600-620 nm, which indicated that TiO_2 nanoparticles were deposited on the surface of SiO_2 spheres. The formation mechanism of TiO_2/SiO_2 nanocomposites is considered to be caused by electrostatic deposition.

Dye decomposition measurements under UV irradiation showed that the anatase TiO_2/SiO_2 treated cotton fabrics possessed higher photocatalytic activity than pure anatase TiO_2 treated cotton fabrics. This enhanced photoactivity was related to the increased specific surface area and the enhanced surface acidity of the TiO_2/SiO_2 nanocomposites. The dye decomposition in the aqueous solution containing pure TiO_2 and TiO_2/SiO_2 nanocomposites under UV irradiation followed a pseudo-first-order kinetic model. Correlation coefficient R of linear fitting for TiO_2 is 0.99073, the correlation coefficient R for TiO_2/SiO_2 nanocomposites is 0.99206. Rates of the dye decomposition (photocatalytic reaction rate) for pure TiO_2 and TiO_2/SiO_2 nanocomposites are calculated as $0.079\pm0.006\ h^{-1}$ and $0.111\pm0.008\ h^{-1}$ respectively.

9.1.4 Synthesis of single-phase anatase by aging and its self-cleaning properties on cotton

In Chapter 7, the study is for the synthesis of single-phase anatase TiO_2 by a sol-gel process in an aqueous media using only acetic acid as catalysts followed by aging at room temperature, and its self-cleaning properties on cotton. This study further optimizes the preparation of self-cleaning cotton in potential commercialization in the textile industry. The experimental results display that the aging process at room temperature promotes the crystallization of anatase phase. Freshly-prepared TiO_2 was amorphous phase as demonstrated in XRD. However, after aging at room temperature and atmospheric pressure for a few days, the amorphous gels were transformed to single-phase anatase TiO_2 since only anatase peaks at 25.4°, 38.0° and 48.0° were observed in XRD.

High resolution TEM confirmed the nanocrystals after aging were single-phase anatase TiO_2 and the average crystal size of nanocrystallites after aging was 5-7 nm.

The cotton fabrics treated by the anatase nanocrystallites after aging at room temperature showed significant self-cleaning performance as demonstrated by their colorant decomposition and degradation of a red wine stain and a coffee stain under UV irradiation. These thin anatase films had good adhesion to the cotton substrates resulting in excellent washfastness. No photodegradation of the cellulosic chains of cotton by the anatase films could be observed as demonstrated by a comparison study of the tensile strength of treated cotton fabrics before and after prolonged light irradiation.

9.1.5 Visible light–responsive iron-doped TiO_2 and its photocatalytic activities under UV and visible light irradiation

To further enhance photocatalytic activity of TiO_2–based self-cleaning system, Chapter 8 reports the development of visible light-responsive Fe^{3+} doped anatase TiO_2 and its photocatalytic activities under UV and visible light irradiation. Fe^{3+} doped anatase TiO_2 was obtained by a sol-gel process using nitric acid and acetic acid as catalysts at a low temperature of 60°C. The results demonstrated that various amount of Fe^{3+} doped anatase TiO_2 exhibited only patterns assigned to the crystalline anatase phase in XRD, and any other crystalline phase containing Fe could not be observed. Moreover, with Fe-doping concentration increasing, the poorer the crystallization of the TiO_2 particles, and the smaller the crystallite size of TiO_2 because the peak intensities of anatase slightly decrease and the width of (101) plane diffraction peak of anatase (2θ=25.4°) becomes broader in XRD. High resolution TEM confirmed the nanocrystallites of optimal 0.25% Fe^{3+} doping level were single-phase anatase TiO_2 and the average crystal size of the nanocrystallites was 4-7 nm. The results in the study showed that the Fe^{3+} dopant does not change the crystal structure of TiO_2, but significantly affect their photocatalytic activity. The crystallites of Fe^{3+} doped TiO_2 was anatase phase as those of pure TiO_2.

The Fe^{3+} doped anataseTiO_2 showed a strong absorption in the UV-Visible light region and a red shift in the band gap transition. A small amount of Fe^{3+} doping could obviously enhance the photocatalytic activity of TiO_2. The UV activity was higher than the visible light activity. 0.25 wt.% Fe^{3+} dopant was optimum for both UV and visible light irradiation. However, overloading Fe^{3+} decreased the photocatalytic activity for both UV and visible light irradiation. The results could be explained by the balance of excited electron/hole trapped by the doped Fe^{3+} and their charges recombination on the doped Fe^{3+} level.

9.2 Suggestions for future work

In this project, the major effects of acid catalysts, reaction temperatures, TiO_2/SiO_2 nanocomposites, Fe^{3+} doping level on the formation of anatase TiO_2 and their photocatalytic activities of these TiO_2 treated cotton and polyester have been studied. Some recommendations are suggested for future investigation.

Development of other transition metal ions and nonmetal doped TiO_2

While TiO_2 treated textiles will be desired to decompose dirt under sunlight irradiation, their ability to decompose organic contaminants and to kill the bacteria, fungi, or germs, under ordinary room light irradiation from various types of indoor light fixtures such as fluorescent lamps will be more desirable. To achieve this, anionic N, S, P, C doped TiO_2 and metal cation Ag, Cu, Mn, Au doped TiO_2, etc. could be investigated. The study of these kinds of dopants will be helpful and valuable for developing more effective photocatalysts in UV-visible light region and further enhancing photocatalytic activities under visible light illumination.

Test of other organic stains, unpleasant odor and noxious gases

Besides bacteria, colorant, coffee and red wine stains, other organic stains, unpleasant odor and noxious gases, such as curry stains, smoke, formaldehyde, could be explored to test self-cleaning properties of TiO_2 treated fabrics. This will be beneficial to the understanding of the stains in our ordinary life, of which TiO_2 treated fabrics can decompose, and hence to promote the use of self-cleaning technology in apparel and textiles.

Exploration of the method to maintain tearing strength of fabrics

In this project, the TiO_2 films on fabrics were prepared by a dipping–padding-neutralizing-drying-curing process. NH_3 gas was used in neutralization step. The tearing strength of TiO_2 treated fabrics was reduced compared to original fabrics due to acid from acidic TiO_2 sol and the increase of stiffness. However, NH_3 gas may not completely neutralize acid before drying. Then the residual acid on fabrics may damage cellulosic fabrics such as cotton and reduce the tearing strength of TiO_2 treated cotton. Therefore, other neutralization steps should be explored to decrease the damage to cellulosic fabrics. Moreover, other neutralization steps may be easy to do and more environmentally friendly. Adding pH adjustment agents to TiO_2 sol before padding or using alkali solution in neutralization step should be a good choice. On the other hand, in order to maintain the tearing strength of TiO_2 treated fabrics, appropriate softener should be used to decrease the stiffness of these fabrics.

Improvement of washfastness of TiO_2 films on textile materials

Durability of TiO_2 films is a particular requirement for textiles because they are subject to frequent washing and hence good washfastness is essential for the practical application of TiO_2 in textiles. Appropriate binders should be used to promote adhesion between TiO_2 films and textile materials.

Potential application of TiO_2 on other textile materials

TiO_2 -based self-cleaning system applied to other textile substrates such as silk, wool, linen should be studied. This will be useful for extending their utilization in the textile and apparel industry and offering added value to the products. Studies of the appropriate application conditions, finish durability, mechanical properties and the fabric hand should be explored.

References

Abidi, N., Hequet, E., Tarimala, S., & Dai, L. L. (2007). Cotton fabric surface modification for improved UV radiation protection using sol–gel process. *Journal of Applied Polymer Science, 104*(1), 111-117.

Adán, C., Bahamonde, A., Fernandez-Garcia, M., & Martinez-Arias, A. (2007). Structure and activity of nanosized iron-doped anatase TiO_2 catalysts for phenol photocatalytic degradation. *Applied Catalysis B: Environmental 72*(1-2), 11-17.

Almquist, C. B., & Biswas, P. (2002). Role of synthesis method and particle size of nanostructured TiO_2 on its photoactivity. *Journal of Catalysis, 212*(2), 145-156.

Anderson, C., & Bard, A. J. (1995). An improved photocatalyst of TiO_2/SiO_2 prepared by a sol–gel synthesis. *Journal of Physical Chemistry, 99*(24), 9882-9885.

Anderson, C., & Bard, A. J. (1997). Improved photocatalytic activity and characterization of mixed TiO_2/SiO_2 and TiO_2/Al_2O_3 materials. *Journal of Physical Chemistry B, 101*(14), 2611-2616.

Anpo, M., Shima, T., Kodama, S., & Kubokawa, Y. (1987). Photocatalytic hydrogenation of propyne with water on small-particle TiO_2: Size quantization effects and reaction intermediates. *Journal of Physical Chemistry B, 91*(16), 4305-4310.

Arai, Y., Tanaka, K., & Khlaifat, A. L. (2006). Photocatalysis of SiO_2-loaded

TiO_2. *Journal of Molecular Catalysis A: Chemical, 243*(1), 85-88.

Arnal, P., Corriu, R. J. P., Leclercq, D., Mutin, P. H., & Vioux, A. (1996). Preparation of anatase, brookite and rutile at low temperature by non-hydrolytic sol–gel methods. *Journal of Materials Chemistry, 6*(12), 1925-1932.

Aruna, S. T., & Patil, K. C. (1996). Synthesis and properties of nanosize titania. *Journal of Materials Synthetic Processing, 4*(3), 175-179.

Bacsa, R. R. R., & Grätzel, M. (1996). Rutile formation in hydrothermally crystallised nanosized titania. *Journal of the American Ceramic Society, 79*(8), 2185-2188.

Bartlett, J. R., & Woolfrey, J. L. (1992). Peptization of Hydrous Titania. In L. L. Hench & J. K. West (Eds.), *Chemical Processing of Advanced Materials* (pp. 247-256). New York: John Wiley &Sons.

Bischoff, B. L., & Anderson, M. A. (1995). Peptization process in the sol-gel preparation of porous anatase (TiO_2). *Chemistry of Materials, 7*(10), 1772-1778.

Bozzi, A., Yuranova, T., Guasaquillo, I., Laub, D., & Kiwi, J. (2005). Self-cleaning of modified cotton textiles by TiO_2 at low temperatures under daylight irradiation. *Journal of Photochemistry and Photobiology A: Chemistry, 174*(2), 156-164.

Bozzi, A., Yuranova, T., & Kiwi, J. (2005). Self-cleaning of wool-polyamide and polyester textiles by TiO_2-rutile modification under daylight irradiation at ambient temperature. *Journal of Photochemistry and Photobiology A: Chemistry, 172*(1), 27-34.

Brinker, C. J., & Scherer, G. W. (1990). *Sol–gel Science: The physics and Chemistry of Sol- Gel Processing*. San Diego: Academic Press.

Cao, L., Huang, A., Spiess, F.-J., & Suib, S. L. (1999). Gas-state oxidation of 1- butane using nanoscale TiO_2 photocatalysis. *Journal of Catalysis, 188*(1), 48-57.

Carlotti, S., & Mas, A. (1998). Improvement of adhesion of PET fibers to rubber by argon-oxygen plasma treatment. *Journal of Applied Polymer Science, 69*(12), 2321-2330.

Cermenati, L., Pichat, P., Guillard, C., & Albini, A. (1997). Probing the TiO_2 photocatalytic mechanisms in water purification by use of quinoline, phot-fenton generated OH* radicals and superoxide dismutase. *Journal of Physical Chemistry B, 101*(14), 2650-2658.

Chen, J.-R., Wang, X.-Y., & Tomiji, W. (1999). Wettability of poly(ethylene terephthalate) film treated with low-temperature plasma and their surface analysis by ESCA. *Journal of Applied Polymer Science, 72*(10), 1327-1333.

Choi, W., Termin, A., & Hoffmann, M. R. (1994a). Effects of metal-Ion dopants on the photocatalytic reactivity of quantum-sized TiO_2 particles. *Angewandte Chemie-International Edition, 33*(10), 1091-1092.

Choi, W., Termin, A., & Hoffmann, M. R. (1994b). The role of metal ion dopants in quantum-sized TiO_2: correlation between photoreactivity and charge carrier recombination dynamics. *Journal of Physical Chemistry, 98*(51), 13669-13679.

Colmenares, J. C., Aramendia, M. A., Marinas, A., Marinas, J. M., & Urbano, F. J. (2006). Synthesis, characterization and photocatalytic activity of different metal doped titania systems. *Applied Catalysis A: General, 306*, 120-127.

Daoud, W. A., Leung, S. K., Tung, W. S., Xin, J. H., Cheuk, K., & Qi, K. (2008). Self-cleaning keratins. *Chemistry of Materials, 20*(4), 1242-1244.

Daoud, W. A., & Xin, J. H. (2004a). Low temperature sol-gel processed photocatalytic titania coating. *Journal of Sol-Gel Science and Technology, 29*(1), 25-29.

Daoud, W. A., & Xin, J. H. (2004b). Nucleation and growth of anatase crystallites on cotton fabrics at low temperatures. *Journal of the American Ceramic Society, 87*(5), 953-955.

Daoud, W. A., & Xin, J. H. (2005). Synthesis of single-phase anatase nanocrystallites at near room temperatures. *Chemical Communications,*(16), 2110-2112.

Daoud, W. A., Xin, J. H., & Zhang, Y.-H. (2005). Surface functionalization of cellulose fibers with titanium dioxide nanoparticles and their combined bactericidal activities. *Surface Science, 599*(1-3), 69-75.

Daoud, W. A., Xin, J. H., Zhang, Y.-H., & Qi, K. (2005). Surface characterization of thin titania films prepared at low temperatures. *Journal of Non-Crystalline Solids, 351*(16-17), 1486-1490.

Ding, X.-Z., & He, Y.-Z. (1996). Study of the room temperature aging effect on structural evolution of gel-derived nanocrystalline titania powders. *Journal of Materials Science Letters, 15*(4), 320-322.

Edelson, L. H., & Glaeser, A. M. (1988). Role of particle substructure in the sintering of monosized titania. *Journal of the American Ceramic Society, 71*(4), 225-235.

Egerton, T. A., Harris, E., John Lawson, E., Mile, B., & Rowlands, C. C. (2001). An EPR study of diffusion of iron into rutile. *Physical Chemistry Chemical Physics, 3*(3), 497-504.

Feng, J., Wong, R. S. K., Hu, X., & Yue, P. L. (2004). Discoloration and mineralization of Orange II by using Fe^{3+}-doped TiO_2 and bentonite clay-based Fe nanocatalysts. *Catalysis Today, 98*(3), 441-446.

Fernandez, A., Lassaletta, G., Jimenez, V. M., Justo, A., Gonzales-Elipe, A. R., Herrmann, J. M., et al. (1995). Preparation and characterization of TiO_2 photocatalysts supported on various rigid supports (glass, quartz and stainless steel). Comparative studies of potocatalytic activity in water purification. *Applied Catalysis B: Environmental, 7*(1-2), 49-63.

Fox, M. A., & Dulay, M. T. (1993). Heterogeneous photocatalysis. *Chemical Reviews, 93*(1), 341-357.

Friedrich, J. F., Rohrer, P., Saur, W., Gross, T., Lippitz, A., & Unger, W. (1993). Improvement in polymer adhesivity by low and normal pressure plasma surface modification. *Surface Coatings and Technology, 59*(1-3), 371-378.

Fu, X., Clark, L. A., Yang, Q., & Anderson, M. A. (1996). Enhanced photocatalytic performance of titania-based binary metal oxides: TiO_2/SiO_2 and TiO_2/ZrO_2. *Environmental Science and Technology, 30*(2), 647-653.

Fujishima, A., Hashimoto, K., & Watanabe, T. (1999). *TiO_2 Photocatalysis: Fundamentals and Applications*. Tokyo: BKC

Fujishima, A., Rao, T. N., & Tryk, D. A. (2000). Titanium dioxide photocatalysis. *Journal of Photochemistry and Photobiology C, 1*(1), 1-21.

Ganesh, R., Boardman, G. D., & Michelsen, D. (1994). Fate of azo dyes in sludges. *Water Research 28*(6), 1367-1376.

Gopal, M., Chan, W. J. M., & De, J. L. C. (1997). Room temperature synthesis of crystalline metal oxides. *Journal of Materials Science, 32*(22), 6001-6008.

Guan, K., Lu, B., & Yin, Y. (2003). Enhanced effect and mechanism of SiO_2 addition in super-hydrophilic property of TiO_2 films. *Surface and Coatings Technology, 173*(2-3), 219-223.

Guo, X.-C., & Dong, P. (1999). Multistep coating of thick titania layers on monodisperse silica nanospheres. *Langmuir, 15*(17), 5535-5540.

Hagfeldt, A., & Gräetzel, M. (1995). Light-induced redox reactions in nanocrystalline systems. *Chemical Reviews, 95*(1), 49-68.

Han, J., & Kumacheva, E. (2001). Monodispersed silica-titanyl sulfate microspheres. *Langmuir, 17*(25), 7912-7917.

Han, K., & Yu, M. (2006). Study of the preparation and properties of UV-blocking fabrics of a PET/TiO_2 nanocomposite prepared by in situ polycondensation. *Journal of Applied Polymer Science 100*(2), 1588-1593.

Hanprasopwattana, A., Srinivasan, S., Sault, A. G., & Datye, A. K. (1996). Titania coatings on monodisperse silica spheres (characterization using 2-propanol dehydration and TEM). *Langmuir, 12*(13), 3173-3179.

Heller, A. (1995). Chemistry and applications of photocatalytic oxidation of thin organic film. *Accounts of Chemical Research, 28*(12), 503-508.

Hoffmann, M. R., Martin, S. T., Choi, W., & Bahnemann, D. W. (1995). Environmental applications of semiconductor photocatalysis. *Chemical Reviews, 95*(1), 69-96.

Hong, S.-S., Lee, M. S., Park, S. S., & Lee, G.-D. (2003). Synthesis of nanosized TiO_2/SiO_2 particles in the microemulsion and their photocatalytic activity on the decomposition of p-nitrophenol. *Catalysis Today, 87*(1-4), 99-105.

Hsiang, H.-I., & Lin, S.-C. (2004). Effects of aging on the phase transformation and sintering properties of TiO_2 gels. *Materials Science & Engineering A: Structural Materials: Properties, Microstructure and Processing A, 380*(1-2), 67-72.

Hsiang, H.-I., & Lin, S.-C. (2006). Effects of aging on the kinetics of nanocrystalline anatase crystallite growth. *Materials Chemistry and Physics, 95*(2-3), 275-279.

Hsu, W. P., Yu, R., & Matijevic, E. (1993). Paper whiteners: I. Titania coated silica. *Journal of Colloid and Interface Science, 156*(1), 56-65.

Hu, Y., & Yuan, C. (2005). Low-temperature preparation of photocatalytic thin films from anatase sols. *Journal of Crystal Growth, 274*(3-4), 563-568.

Huang, Z., Maness, P.-C., Blake, D. M., Wolfrum, E. J., Smolinski, S. L., & Jacoby, W. A. (2000). Bactericidal mode of titanium dioxide photocatalysis. *Journal of Photochemistry and Photobiology A: Chemistry 130*(2-3), 163-170.

Hung, W.-C., Fu, S.-H., Tseng, J.-J., Chu, H., & Ko, T.-H. (2007). Study on photocatalytic degradation of gaseous dichloromethane using pure and iron ion-doped TiO_2 prepared by the sol-gel method. *Chemosphere, 66*(11), 2142-2151.

Ibusuki, T., & Takeuchi, K. (1986). Toluene oxidation on UV-irradiated titanium dioxide with and without O_2, NO_2 or H_2O at ambient temperature. *Atmospheric Environment, 20*(9), 1711-1715.

Imai, H., & Hirashima, H. (1999). Preparation of porous anatase coating from sol-gel-derived titanium dioxide and titanium dioxide-silica by water-vapor exposure. *Journal of the American Ceramic Society, 82*(9), 2301-2304.

Inagaki, N., Narushim, K., Tuchida, N., & Miyazaki, K. (2004). Surface characterization of plasma-modified poly(ethylene terephthalate) film surfaces. *Journal of Polymer Science Part B: Polymer Physics, 42*(20), 3727-3740.

Inagaki, N., Tasaka, S., & Shimada, S. (2000). Comparative studies on surface modification of poly(Ethylene Terephthalate) by remote and direct argon plasmas. *Journal of Applied Polymer Science, Volume Date 2001, 79*(5), 808-815.

Jacoby, W. A., Maness, P. C., Wolfrum, E. J., Blake, D. M., & Fennell, J. A. (1998). Mineralization of bacterial cell mass on a photocatalytic surface in air. *Environmental Science and Technology, 32*(17), 2650-2653.

Jalava, J.-P., Heikkilae, L., Hovi, O., Laiho, R., Hiltunen, E., Hakanen, A., et al. (1998). Structural investigation of hydrous TiO_2 precipitates and their aging products by X-ray diffraction, atomic force microscopy and transmission electron microscopy. *Industrial & Engineering Chemistry Research, 37*(4), 1317-1323.

Kamiya, K., Tanimoto, K., & Yoko, T. (1986). Preparation of titanium dioxide fibers by hydrolysis and polycondensation of titanium tetraisopropoxide. *Journal of Materials Science Letters, 5*(4), 402-404.

Karakitsou, K. E., & Verykios, X. E. (1993). Effects of altervalent cation doping of TiO_2 on its performance as a photocatalyst for water cleavage. *Journal of Physical Chemistry, 97*(6), 1184-1189.

Kato, K., Tsuzuki, A., Taoda, H., Torii, Y., Kato, T., & Butsugan, Y. (1994). Crystal structures of TiO_2 thin coatings prepared from the alkoxide solution via the dip-coating technique affecting the photocatalytic decomposition of aqueous acetic acid. *Journal of Materials Science, 29*(22), 5911-5915.

Kesselman, J. M., Shreve, O., Hoffmann, M. R., & Lewis, N. S. (1994). Flux-matching conditions at TiO_2 photoelectrodes: Is interfacial electron transfer to O_2 rate-limiting in the TiO_2-catalyzed photochemical degradation of organics? *Journal of Physical Chemistry, 98*(50), 13385-13395.

Kikuchi, Y., Sunada, K., Iyoda, T., Hashimoto, K., & Fujishima, A. (1997). Photocatalytic bactericidal effect of TiO_2 thin films: dynamic view of the active oxygen species responsible for the effect. *Journal of Photochemistry and Photobiology A: Chemistry, 106*(1-3), 51-56.

Kim, S.-J., Park, S.-D., Jeong, Y. H., & Park, S. (1999). Homogeneous precipitation of TiO_2 ultrafine powders from aqueous $TiOCl_2$ solution. *Journal of the American Ceramic Society, 82*(4), 927-932.

Kim, S., Park, H., & Choi, W. (2004). Comparative study of homogeneous and heterogeneous photocatalytic redox reactions: $PW_{12}O_{40}^{3-}$ vs. TiO_2.

Journal of Physical Chemistry B, 108(20), 6402-6411.

Kinloch, A. (1987). *Adhesion and Adhesives*. New York: Chapman and Hall.

Kormann, C., Bahnemann, D. W., & Hoffmann, M. R. (1988). Preparation and characterization of quantum-size titanium dioxide. *Journal of Physical Chemistry, 92*(18), 5196-5201.

Kraeutler, B., & Bard, A. J. (1978). Heterogeneous photocatalytic synthesis of methane from acetic acid - new Kolbe reaction pathway. *Journal of the American Chemical Society, 100*(7), 2239-2245.

Krump, H., Šimor, M., Hudec, I., Jaššo, M., & Luyt, A. S. (2005). Adhesion strength study between plasma treated polyester fibres and a rubber matrix. *Applied Surface Science*, *240*(1-4), 268-274.

Larson, I., Drummond, C. J., Chan, D. Y. C., & Grieser, F. (1993). Direct force measurements between titanium dioxide surfaces. *Journal of the American Chemical Society*, *115*(25), 11885 - 11890.

Legrini, O., Oliveros, E., & Braun, A. M. (1993). Photochemical processes for water treatment. *Chemical Reviews, 93*(2), 671-698.

Li, Y., Lee, N.-H., Song, J. S., Lee, E. G., & Kim, S.-J. (2005). Synthesis and photocatalytic properties of nano bi-crystalline titania of anatase and brookite by hydrolyzing $TiOCl_2$ aqueous solution at low temperatures. *Research on Chemical Intermediates, 31*(4-6), 309-318.

Linsebigler, A. L., Lu, G., & Yates, J. T., Jr. (1995). Photocatalysis on TiO_2 surfaces: principles, mechanisms, and selected results. *Chemical*

Reviews, 95(3), 735-758.

Liu, Z., & Davis, R. J. (1994). Investigation of the structure of microporous Ti-Si mixed oxides by X-ray, UV reflectance, FT-Raman, and FT-IR spectroscopies. *Journal of Physical Chemistry, 98*(4), 1253-1261.

Livage, J., & Henry, M. (1988). A Predictive Model for Inorganic Polymerization Reactions. In J. D. Mackenzie & D. R. Ulrich (Eds.), *Ultrastructure Processing of Advanced Ceramics* (pp. 183-195). New York: John Wiley & Sons.

Livage, J., Henry, M., & Sanchez, C. (1988). Sol-gel chemistry of transition metal alkoxides. *Progress in Solid State Chemistry, 18*(4), 259-341.

Lu, Z.-X., Zhou, L., Zhang, Z.-L., Shi, W.-L., Xie, Z.-X., Xie, H.-Y., et al. (2003). Cell damage induced by photocatalysis of TiO_2 thin films. *Langmuir 19*(21), 8765-8768.

Luo, H., Wang, C., & Yan, Y. (2003). Synthesis of mesostructured titania with controlled crystalline framework. *Chemistry of Materials, 15*(20), 3841-3846.

Makishima, A., Asami, M., & Wada, K. (1988). Preparation of cerium dioxide-titanium dioxide coatings by the sol-gel process. *Journal of Non-Crystalline Solids, 100*(1-3), 321-324.

Maness, P.-C., Smolinski, S., Blake, D. M., Huang, Z., Wolfrum, E. J., & Jacoby, W. A. (1999). Bactericidal activity of photocatalytic TiO_2 reaction: toward an understanding of its killing mechanism. *Applied* *and Environmental Microbiology, 65*(9), 4094-4098.

Matsuda, A., Kotani, Y., Kogure, T., Tatsumisago, M., & Minami, T. (2000). Transparent anatase nanocomposite films by the sol–gel process at low temperatures. *Journal of the American Ceramic Society, 83*(1), 229 - 231.

Matsuda, A., Matoda, T., Kogure, T., Tadanaga, K., Minami, T., & Tatsumisago, M. (2003). Formation of anatase nanocrystals-precipitated silica coatings on plastic substrates by the sol-gel process with hot water treatment. *Journal of Sol-Gel Science and Technology, 27*(1), 61-69.

Matsuda, A., Matoda, T., Kotani, Y., Kogure, T., Tatsumisago, M., & Minami, T. (2003). Evaluation of photocatalytic activity of transparent anatase nanocrystals-dispersed silica films prepared by the sol-gel process with hot water treatment. *Journal of Sol-Gel Science and Technology, 26*(1-3), 517-521.

Matsuda, A., Matoda, T., Tadanaga, K., Minami, T., Tatsumisago, M., & Kogure, T. (2005). Lowering of preparation temperatures of anatase nanocrystals-dispersed coatings via sol–gel process with hot water treatment. *Journal of the American Ceramic Society, 88*(6), 1421-1426.

Matsunaga, T., Tomoda, R., Nakajima, T., Nakamura, N., & Komine, T. (1988). Continuous-sterilization system that uses photosemiconductor powders. *Applied and Environmental Microbiology 54*(6), 1330-1333.

Matsunaga, T., Tomoda, R., Nakajima, T., & Wake, H. (1985).

Photoelectrochemical sterilization of microbial cells by semiconductor powders. *FEMS Microbiology Letters 29*(1-2), 211-214.

Meilert, K. T., Laub, D., & Kiwi, J. (2005). Photocatalytic self-cleaning of modified cotton textiles by TiO_2 clusters attached by chemical spacers. *Journal of Molecular Catalysis A, 237*(1-2), 101-108.

Mills, A., & Le Hunte, S. (1997). An overview of semiconductor photocatalysis. *Journal of Photochemistry and Photobiology A: Chemistry, 108*(1), 1-35.

Mills, A., & Lee, S.-K. (2002). A web-based overview of semiconductor photochemistry-based current commercial applications. *Journal of Photochemistry and Photobiology A: Chemistry, 152*(1-3), 233-247.

Mills, A., Lepre, A., Elliott, N., Bhopal, S., Parkin, I. P., & O'Neill, S. A. (2003). Characterisation of the photocatalyst Pilkington ActivTM: a reference film photocatalyst. *Journal of photochemistry and Photobiology A: Chemistry, 160*(3), 213-224.

Mills G., & Hoffman, M. R. (1993). Photocatalytic degradation of pentachlorophenol on TiO2 particles: Identification of intermediates and mechanism of reaction. *Environmental Science and Technology, 27,* 1681-1689.

Minero, C., Catozzo, F., & Pelizzetti, E. (1992). Role of adsorption in photocatalyzed reactions of organic molecules in aqueous titania suspensions. *Langmuir, 8*(2), 481-486.

Nagame, S., Oku, T., Kambara, M., & Konishi, K. (1989). Antibacterial effects of the powdered semiconductor TiO_2 on the viability of oral micro-organisms. *Journal of Dental Ressearch, 68*(Special Issue), 1696-1697.

Nakabayashi, H. (1992). Properties of acid sites on titania-silica and titania-alumina mixed oxides measured by infrared spectroscopy. *Bulletin of the Chemical Society of Japan, 65*(3), 914-916.

Navio, J. A., Cerrillos, C., Marchena, F. J., Pablos, F., & Pradera, M. A. (1996). Photoassisted degradation of n-butyltin chlorides in air-equilibrated aqueous TiO_2 suepensions. *Langmuir, 12*(8), 2007-2014.

Neely, A. N., & Maley, M. P. (2000). Survival of enterococci and staphylococci on hospital fabrics and plastic. *Journal of Clinical Microbiology, 38*(2), 724-726.

Negishi, N., Iyoda, T., Hashimoto, K., & Fujishima, A. (1995). Preparation of transparent TiO_2 thin film photocatalyst and its photocatalytic activity. *Chemistry Letters,*(9), 841-842.

Nishimoto, S., Ohtani, B., Kajiwara, H., & Kagiya, T. (1985). Correlation of the crystal structure of titanium dioxide prepared from titanium tetra-2-propoxide with the photocatalytic activity for redox reactions in aqueous propan-2-ol and silver salt solutions. *Journal of the Chemical Society, Faraday Transactions 1: Physical Chemistry in Condensed Phases, 81*(1), 61-68.

Nosaka, Y., Koenuma, K., Ushida, K., & Kira, A. (1996). Reaction mechanism of the decomposition of acetic acid on illuminated TiO_2 powder studied by means of in situ electron spin resonance measurements. *Langmuir, 12*(3), 736-738.

Ohtani, B., Ogawa, Y., & Nishimoto, S.-i. (1997). Photocatalytic activity of amorphous-anatase mixture of titanium(IV) oxide particles suspended in aqueous solutions. *Journal of physical chemistry B, 101*(19), 3746 - 3752.

Papp, J., Soled, S., Dwight, K., & Wold, A. (1994). Surface acidity and photocatalytic activity of TiO_2, WO_3/TiO_2, and MoO_3/TiO_2 photocatalysts. *Chemistry of Materials, 6*(4), 496-500.

Park, S. E., Joo, H., & Kang, J. W. (2004). Effect of impurities in TiO_2 thin films on trichloroethylene conversion. *Solar Energy Materials and Solar Cells, 83*(1), 39-53.

Parkin, I. P., & Palgrave, R. G. (2005). Self-cleaning coatings. *Journal of Materials Chemistry, 15*(17), 1689-1695.

Paz, Y., Luo, Z., Rabenberg, L., & Heller, A. (1995). Photooxidative self-cleaning transparent titanium dioxide films on glass. *Journal of Materials Research, 10*(11), 2842-2848.

Peblow, M. (2004, 07 June). Clothes launder own fabric. *Nature News*.

Pelizzetti, E., Minero, C., & Vincenti, M. (1994). *Technologies for Environmental Cleanup: Toxic and Hazardous Waster Management*

(Avogadro A. and Ragaini R. C. ed.). Dordrecht: Kluwer Academic

Peral, J., Domenech, X., & Ollis, D. F. (1997). Hetergeneous photocatalysis for purification, decontamination and deodorization of air. *Journal of Chemical Technology and Biotechnology, 70*(2), 117-140.

Petasch, W., Rauchle, E., Walker, M., & Elsne, P. (1995). Improvement of the adhesion of low-energy polymers by a short-time plasma treatment. *Surface Coatings and Technology, 74-75*(1-3, Pt. 2), 682-688.

Pottier, A., Chanéac, C., Tronc, E., Mazerolles, L., & Jolivet, J.-P. (2001). Synthesis of brookite TiO_2 nanoparticles by thermolysis of $TiCl_4$ in strongly acidic aqueous media. *Journal of Materials Chemistry, 11*(4), 1116-1121.

Prairie, M. R., Evans, L. R., Stange, B. M., & Martinez, S. L. (1993). An investigation of photocatalysis for the treatment of water contaminated with metals and organic chemicals. *Environmental Science and Technology, 27*(9), 1776-1782.

Saito, T., Iwase, T., & Morioka, T. (1992). Mode of photocatalytic bactericidal action of powdered semiconductor TiO_2 on mutans streptococci. *Journal of Photochemistry and Photobiology B: Biology 14*(4), 369-379.

Samuneva, B., Kazhukharov, V., Trapalis, C., & Kranold, R. S. (1993). Sol-gel processing of titanium-containing thin coatings. Part I. Preparation and structure. *Journal of Materials Science, 28*(9), 2353-2360.

Schiavello, M., & Sclafani, A. (1989). Thermodynamic and Kinetic Aspect in Photocatalysis In N. Serpone & E. Pelizetti (Eds.), *Photocatalysis: Fundamentals and Applications* (pp. 159-173). New York: John Wiley & Sons.

Sclafani, A., & Herrman, J. M. (1996). Comparison of the photoelectronic and photocatalytic activities of various anatase and rutile forms of titania in pure liquid organic phases and in aqueous solutions. *Journal of Physical Chemistry, 100*(32), 13655-13661.

Seo, D.-S., Lee, J.-K., & Kim, H. (2001). Synthesis of TiO_2 nanocrystalline powder by aging at low temperature. *Journal of Crystal Growth, 233*(1-2), 298-302.

Seo, D.-S., Lee, J.-K., Lee, E.-G., & Kim, H. (2001). Effect of aging agents on the formation of TiO_2 nanocrystalline powder. *Materials Letters, 51*(2), 115-119.

Shibata, H., Ohkubo, T., Kohno, H., Rangsunvigit, P., Sakai, H., & Abe, M. (2006). Preparation and photocatalytic activity of titania particulate film with mesostructured silica as binder. *Journal of Photochemistry and Photobiology A: Chemistry, 181*(2-3), 357-362.

Shimizu, K., Imai, H., Hirashima, H., & Tsukuma, K. (1999). Low-temperature synthesis of anatase thin films on glass and organic substrates by direct deposition from aqueous solutions. *Thin Solid Films, 351*(1,2), 220-224.

Shukla, S., & Seal, S. (2003). Sol-Gel-Derived Oxide and Sulfide Nanoparticles. In M.-I. Baraton (Ed.), *Synthesis, Functionalization and Surface Treatment of Nanoparticles* (pp. 31-49). Stevenson Ranch: American Scientific.

Shul, Y. G., Kim, H. J., Haam, S. J., & Han, H. S. (2003). Photocatalytic characteristics of TiO_2 supported on SiO_2. *Research on Chemical Intermediates, 29*(7-9), 849-859.

Sjogren, J. C., & Sierka, R. A. (1994). Inactivation of phage MS2 by iron-aided titanium dioxide photocatalysis. *Applied Environmental Microbiology, 60*(1), 344-347.

Sopyan, I., Watanabe, M., Murasawa, S., Hashimoto, K., & Fujishima, A. (1996). A film-type photocatalyst incorporating highly active TiO_2 powder and fluororesin binder: photocatalytic activity and long-term stability. *Journal of Electroanalytical Chemistry, 415*(1-2), 183-186.

Soria, J., Conesa, J. C., Augugliaro, V., Palmisano, L., Schiavello, M., & Sclafani, A. (1991). Dinitrogen photoreaction to ammonia over titanium dioxide powders doped with ferric ions. *Journal of Physical Chemistry, 95*(1), 274-282.

Subramaniam, K., Yiacoumi, S., & Tsouris, C. (2001). Copper uptake by inorganic particles — equilibrium, kinetics, and particle interactions: experimental. *Colloids and Surfaces A: Physicochemical and Engineering Aspects, 177*(2-3), 133-146.

Subramanian, V., Wolf, E. E., & Kamat, P. V. (2004). Catalysis with TiO_2/gold nanocomposites: Effect of metal particle size on the fermi level equilibration. *Journal of the American Chemical Society, 126*(15), 4943-4950.

Sun, B., & Smirniotis, P. G. (2003). Interaction of anatase and rutile TiO_2 particles in aqueous photooxidation. *Catalysis Today, 88*(1-2), 49-59.

Sunada, K., Kikuchi, Y., Hashimoto, K., & Fujishima, A. (1998). Bactericidal and detoxification effects of TiO_2 thin film photocatalysts. *Environmental Science and Technology, 32*(5), 726-728.

Sunada, K., Watanabe, T., & Hashimoto, K. (2003). Studies on photokilling of bacteria on TiO_2 thin film. *Journal of Photochemistry and Photobiology A: Chemistry, 156*(1-3), 227-233.

Tada, H., Kokubu, A., Iwasaki, M., & Ito, S. (2004). Deactivation of the TiO_2 photocatalyst by coupling with WO_3 and the electrochemically assisted high photocatalytic activity of WO_3. *Langmuir, 20*(11), 4665-4670.

Takeda, N., Ohtani, M., Torimoto, T., Kuwabata, S., & Yoneyama, H. (1997). Evaluation of diffusibility of adsorbed propionaldehyde on titanium dioxide-loaded adsorbent photocatalyst films from its photodecomposition rate. *Journal of Physical Chemistry B, 101*(14), 2644-2649.

Terabe, K., Kato, K., Miyazaki, H., Yamaguchi, S., Imai, A., & Iguchi, Y. (1994). Microstructure and crystallization behavior of TiO_2 precursor prepared by the sol-gel method using metal alkoxide. *Journal of Materials Science, 29*(6), 1617-1622.

Tung, W. S., & Daoud, W. A. (2008). Photocatalytic formulations for protein fibers: Experimental analysis of the effect of preparation on compatibility and photocatalytic activities. *Journal of Colloid and Interface Science, 326*(1), 283-288.

Veeramasuneni, S., Yalamanchili, M. R., & Miller, J. D. (1998). Interactions between dissimilar surfaces in high ionic strength solutions as determined by atomic force microscopy. *Colloids and Surfaces A: Physicochemical and Engineering Aspects, 131*(1-3), 77-87.

Wang, C.-Y., Böttcher, C., Bahnemann, D. W., & Dohrmann, J. K. (2003). A comparative study of nanometer sized Fe(III)-doped TiO_2 photocatalysts: synthesis, characterization and activity. *Journal of Materials Chemistry, 13*(9), 2322-2329.

Wang, Q. J., Moss, S. C., Shalz, M. L., Glaeser, A. M., Zandbergen, H. W., & Zschack, P. (1991). X-ray Study of Alkoxide Derived Amorphous TiO_2 Powder. In P. Jena, S. N. Khanna & B. K. Rao (Eds.), *Physics and Chemistry of Finite systems: From Clusters to Crystals, Vol. II NATO ASI Series* (pp. 1287-1294). Dordrecht: Kluwer Academic

Wang, R., Hashimoto, K., Fujishima, A., Chikuni, M., Kojima, E., Kitamura, A., et al. (1997). Light-induced amphiphilic surfaces. *Nature, 388*(6641), 431-432.

Wang, R., Hashimoto, K., Fujishima, A., Chikuni, M., Kojima, E., Kitamura, A., et al. (1998). Photogeneration of highly amphiphilic TiO_2 surfaces. *Advanced Materials, 10*(2), 135-138.

Wang, R., Sakai, N., Fujishima, A., Watanabe, T., & Hashimoto, K. (1999). Studies of surface wettability conversion on TiO_2 single-crystal surfaces. *Journal of Physical Chemistry B, 103*(12), 2188-2194.

Wang, W., Gu, B., Liang, L., Hamilton, W. A., & Wesolowski, D. J. (2004). Synthesis of rutile (α-TiO_2) nanocrystals with controlled size and shape by low-temperature hydrolysis: effects of solvent composition. *Journal of Physical Chemistry B, 108*(39), 14789-14792.

Wang, X. H., Li, J.-G., Kamiyama, H., Moriyoshi, Y., & Ishigaki, T. (2006). Wavelength-sensitive photocatalytic degradation of methyl orange in aqueous suspension over iron(III)-doped TiO2 nanopowders under UV and visible light irradiation. *Journal of Physical Chemistry B, 110*(13), 6804-6809.

Wiese, G. R., & Healy, T. W. (1975). Coagulation and electrokinetic behavior of TiO_2 and Al_2O_3 colloidal dispersions. *Journal of Colloid And Interface Science, 51*(3), 427-433

Wright, J. D., & Sommerdijk, N. A. J. M. (2001). *Sol- Gel Materials: Chemistry and Applications*. Australia: Gordon and Breach Science.

Xia, B., Li, W., Zhang, B., & Xie, Y. (1999). Low temperature vapour-phase preparation of TiO_2 nanopowders. *Journal of Materials Science, 34*(14), 3505-3511.

Xin, J. H., Daoud, W. A., & Kong, Y. Y. (2004). A new approach to UV-blocking treatment for cotton fabrics. *Textile Research Journal, 74*(2), 97-100.

Yamashita, H., Ichihashi, Y., Harada, M., Stewart, G., Fox, M. A., & Anpo, M. (1996). Photocatalytic degradation of 1-octanol on anchored titanium oxide and on TiO_2 powder catalysts. *Journal of Catalysis, 158*(1), 97-101.

Yanagisawa, K., & Ovenstone, J. (1999). Crystallization of anatase from amorphous titania using the hydrothermal technique: effects of starting material and temperature. *Journal of Physical Chemistry B, 103*(37), 7781-7787.

Yang, H., Zhu, S., & Pan, N. (2004). Studying the mechanisms of titanium dioxide as ultraviolet-blocking additive for films and fabrics by an improved scheme. *Journal of Applied Polymer Science, 92*(5), 3201-3210.

Yip, Y. W. (2003). *UV excimer laser and low temperature plasma treatments of polyamide materials.* The Hong Kong Polytechnic University, Hong Kong.

Yotsumoto, H., & Yoon, R.-H. (1993). Application of extended DLVO theory: I. Stability of rutile suspensions. *Journal of Colloid and Interface Science, 157*(2), 426-433.

Yu, J., Zhao, L., & Cheng, B. (2006). Facile preparation of monodispersed SiO_2/TiO_2 composite microspheres with high surface area. *Materials Chemistry and Physics, 96*(2-3), 311-316.

Yu, J. C., Tang, H. Y., Yu, J., Chan, H. C., Zhang, L., Xie, Y., et al. (2002). Bactericidal and photocatalytic activities of TiO_2 thin films prepared by sol-gel and reverse micelle methods. *Journal of Photochemistry and Photobiology A: Chemistry, 153*(1-3), 211-219.

Yu, J. C., Yu, J., Ho, W., & Zhang, L. (2001). Preparation of highly photocatalytic active nano-sized TiO_2 particles via ultrasonic irradiation. *Chemical communications,*(19), 1942-1943.

Yuranova, T., Mosteo, R., Bandata, J., Laub, D., & Kiwi, J. (2006). Self-cleaning cotton textiles surfaces modified by photoactive SiO_2/TiO_2 coating. *Journal of Molecular Catalysis A: Chemical, 244*(1-2), 160-167.

Zhang, H., & Banfield, J. F. (2000). Understanding polymorphic phase transformation behavior during growth of nanocrystalline aggregates: insights from TiO_2. *Journal of Physical Chemistry B, 104*(15), 3481-3487.

Zhang, H., Penn, R. L., Hamers, R. J., & Banfield, J. F. (1999). Enhanced adsorption of molecules on surfaces of nanocrystalline particles. *Journal of Physical Chemistry B, 103*(22), 4656-4662.

Zhang, L., & Mou, J. (2001). *Nano-materials and Nano-structure*. Beijing:

Science Press.

Zhang, L. X., Liu, P., & Su, Z. X. (2006). A low temperature preparation and photocatalytical activities of PDVB@TiO_2 hybrid microspheres. *Journal of Materials Science, 41*(21), 7218-7224.

Zhang, Y.-H., & Reller, A. (2001). Nanocrystalline iron-doped mesoporous titania and its phase transition. *Journal of Materials Chemistry, 11*(10), 2537-2541.

Zhang, Y., Xiong, G., Yao, N., Yang, W., & Fu, X. (2001). Preparation of titania-based catalysts for formaldehyde photocatalytic oxidation from $TiCl_4$ by the sol-gel method. *Catalysis Today, 68*(1-3), 89-95.

Zhang, Z., Wang, C.-C., Zakaria, R., & Ying, J. Y. (1998). Role of particle size in nanocrystalline TiO_2-based photocatalysts. *Journal of Physical Chemistry B, 102*(52), 10871-10878.

Zheng, Y., Shi, E., Chen, Z., Li, W., & Hu, X. (2001). Influence of solution concentration on the hydrothermal preparation of titania crystallites. *Journal of Materials Chemistry, 11*(5), 1547-1551.

Zhou, J., Liu, S., Qi, J., & Zhang, L. (2006). Structure and properties of composite films prepared from cellulose and nanocrystalline titanium dioxide particles. *Journal of Applied Polymer Science, 101*(6), 3600-3608.

Zhou, L., Yan, S., Tian, B., Zhang, J., & Anpo, M. (2006). Preparation of TiO_2–SiO_2 film with high photocatalytic activity on PET substrate.

Materials Letters, 60(3), 396-399.

Zhou, M., Yu, J., & Cheng, B. (2006). Effects of Fe-doping on the photocatalytic activity of mesoporous TiO_2 powders prepared by an ultrasonic method. *Journal of Hazardous Materials, 137*(3), 1838-1847.

Zhou, M., Yu, J., Cheng, B., & Yu, H. (2005). Preparation and photocatalytic activity of Fe-doped mesoporous titanium dioxide nanocrystalline photocatalysts. *Materials Chemistry and Physics, 93*(1), 159-163.

Zhu, J., Chen, F., Zhang, J., Chen, H., & Anpo, M. (2006). Fe^{3+}-TiO_2 photocatalysts prepared by combining sol-gel method with hydrothermal treatment and their characterization. *Journal of Photochemistry and Photobiology A: Chemistry, 180*(1-2), 196-204.

Zhu, J., Zheng, W., He, B., Zhang, J., & Anpo, M. (2004). Characterization of Fe-TiO_2 photocatalysts synthesized by hydrothermal method and their photocatalytic reactivity for photodegradation of XRG dye diluted in water. *Journal of Molecular Catalysis A: Chemical, 216*(1), 35-43.

`